

**Measuring ligand concentration where
it matters: Assessing the “micro
pharmacokinetic/pharmacodynamics”
of adenosine receptor ligands**

Jack Andrew Michael Lochray, MPharmacol (Hons)

**Thesis submitted to the University of Nottingham
for the degree of Doctor of Philosophy**

September 2021

Abstract

The methods used to determine fundamental pharmacological parameters almost exclusively assume that the concentration of drug in the local environment of the target receptor is equal to the concentration of drug that has been added to the system. It has, however, recently been shown that, dependent upon their physicochemical properties, β 2-adrenoceptor ligands can interact directly with phospholipids, increasing their local concentration and directly influencing the measured association rate constant at the receptor. This local concentrating effect also been demonstrated directly using a fluorescent β 2-ligand with fluorescence correlation spectroscopy (FCS).

In this study we expand these early observations by investigating multiple ligands at a different G protein-coupled receptor, the adenosine A2a receptor. In particular, we probe the importance of physicochemical properties on membrane interaction and observed pharmacology by utilising eight fluorescent adenosine receptor ligands with identical pharmacophores (xanthine amine congener (XAC)), but varying fluorophores and linker regions to modulate their properties. These ligands were assessed for kinetic binding profiles, phospholipid affinity, and local concentrations above cell membranes.

The binding kinetics of the eight fluorescent ligands was assessed by measuring the time resolved fluorescence energy transfer (TR-FRET) between the terbium-labelled A2a receptor and fluorescent ligand over time. From this series, three ligands with distinct kinetic profiles were chosen for analysis by FCS (XACXBY, $k_{on}=24100\pm 6860 \text{ min}^{-1}\text{mM}^{-1}$; CA200645, $k_{on}=1330\pm 175 \text{ min}^{-1}\text{mM}^{-1}$; AV075 $k_{on}=791\pm 36.4 \text{ min}^{-1}\text{mM}^{-1}$), where their local concentration was measured at distances 2-200 μm above live CHO cells. The concentration of all ligands was higher close to the cells, with XAC-X-BY630 having the highest concentration at 2 μm above the membrane ($1024.6\pm 347.4 \text{ nM}$) compared to CA200645 ($62.3\pm 9.5 \text{ nM}$) and AV075 ($111.3\pm 30.1 \text{ nM}$). This was consistent

XACXBY displaying the fastest association rate and supports previous observations.

These studies were then extended to investigate the kinetics and phospholipid interaction of 57 commercially available compounds known to bind at least one adenosine receptor. Binding kinetics were measured at all four adenosine receptors using a competition association assay, and phospholipid affinity (K_{IAM}) was assessed in an Immobilised Artificial Membrane High Performance Liquid Chromatography assay. In this cohort, there was a statistically significant relationship between k_{on} and K_{IAM} ($p=0.03$), but surprisingly a better correlation with k_{off} ($p=0.0012$), which may suggest that hydrophobic interactions are important for modulating dissociation rate in this receptor family.

In general, the data in this study support the hypothesis that lipophilic ligands have a greater concentration in the local receptor environment close to the cell membrane, which may in turn influence observed pharmacological parameters. This reinforces the importance of considering “micro pharmacokinetics/pharmacodynamics” when determining the pharmacology of novel receptor ligands.

Acknowledgments

Firstly, I would like to say a massive thank you to my supervisors Steven Charlton and Stephen Briddon for your unrelenting support and patience. I would also like to thank the people who got me started in the lab and were available to help at a moment's notice throughout my PhD: David Sykes, Karolina Gherbi, and Liz Rosethorne.

I am extremely grateful to the BBSRC for funding my PhD, as well as everyone at the University involved with the doctoral training program or the department of Life Sciences.

I would also like to thank Marleen Groenen and June McCulloch for everything you have done round the lab, Rick Proudman for keeping me safe, Tim Self and the SLIM team for maintaining the microscopes, George for always giving me a grilling when I needed one, Barrie Kellam and Lee Hibbert for helping me set up an HPLC machine in your lab, and everyone at Excellerate Biosciences for making me feel welcome during my PIP.

The Cell Signalling group was genuinely an amazing place to work, and I don't want to list names and risk forgetting people absolutely everyone there during my time was great.

Finally I'd like to thank my partner Melissa, my friends outside of work, and my family for always supporting me.

Contents

Chapter 1- Introduction	7
1.1 Adenosine receptors as therapeutic targets.	7
1.2 Quantifying ligand-receptor pharmacology	10
1.3 Aims and objectives	16
Chapter 2- Materials and methods.	18
2.1 Materials	18
2.2 Methods	22
Chapter 3- Characterising the receptor-ligand kinetic binding properties of a series of adenosine receptor compounds using time-resolved Förster resonance energy transfer (TR-FRET)	34
3.1 Introduction	34
3.2 Results	36
3.3 Discussion	61
Chapter 4- Characterising the physicochemical properties of a series of adenosine receptor compounds using in silico approaches and immobilised artificial membrane high performance liquid chromatography (IAM-HPLC).	66
4.1 Introduction	66
4.2 Results	73
4.3 Discussion	88
Chapter 5- Investigating the local concentration of fluorescent ligands using Fluorescence Correlation Spectroscopy (FCS).	93
5.1 Introduction	93
5.2 Results	95
5.3 Discussion	103
Chapter 6- General discussion: Understanding the relationships between kinetics, physicochemical properties, and local concentration of drugs.	107
6.1 Introduction	107
6.2 Combining results of previous chapters, with discussion.	108

6.3 General concluding discussion.	117
6.4 Future Directions	119
Chapter 7- References	120
Chapter 8- Appendix	138

Chapter 1 – Introduction

1.1 Adenosine receptors as therapeutic targets

The purine nucleoside adenosine forms part of nucleic acids DNA and RNA as well as the units of biological energy transfer ATP and ADP. Furthermore, adenosine can act as an autocrine signalling molecule, released under conditions of cell stress and hypoxia, to activate cell surface adenosine receptors. Adenosine receptors, consisting of four distinct subtypes (A1, A2a, A2b and A3), are members of the G protein-coupled receptor (GPCR) superfamily, which are the target of a third of all small molecule drugs (Santos et al., 2016). Adenosine receptors can nominally be split into two sub-families. The A1 and A3 adenosine receptors inhibit adenylate cyclase through $G_{ai/o}$ family of G proteins, leading to reduced conversion of ATP to cAMP, and a decrease in cellular levels of cAMP. Conversely the A2a and A2b receptors couple to the G_{as} family of G proteins, stimulating adenylate cyclase activity and increase cellular levels of cAMP.

All four adenosine receptors are widely expressed throughout the body and have diverse functions in both physiological and pathophysiological contexts (Sheth et al., 2014). As such, they have been proposed as drug targets for many diseases including, but not limited to, heart disease, sleep disorders, inflammatory diseases, neurodegenerative disorders and cancer (Chen et al., 2013; Allard et al., 2017). The only currently approved adenosine receptor specific drug in Europe is Regadenoson (Chen et al., 2013). This drug acts as a vasodilator by selectively agonising A2a adenosine receptors and is used in stress testing (Gupta and Bajaj, 2017). Istradefylline, an adenosine A2a antagonist, is approved in Japan and USA for use in treating Parkinson's disease (Jenner et al., 2021).

As GPCRs, the adenosine receptors consist of seven transmembrane domains, three intracellular and three extracellular loops, and an

intracellular and extracellular C- and N-terminus respectively. There is an 80-95% homology between receptors with multiple published crystal structures of A1 and A2a receptors (Jaakola et al., 2008; Franco et al., 2021). This high homology allows for predicted structures of A2b and A3 receptors to be formed. Notably, the A2a receptor substantially longer C-terminus of 122 amino acids compared to 30-40 amino acids for the other three adenosine receptors (Borea et al., 2018). The available crystal structures locate the orthosteric binding pocket of adenosine receptors to be in the extracellular cluster, with key residues in the extracellular loops important for ligand binding (Jaakola et al., 2008; Liu et al., 2012). Currently there is no evidence or indication that suggesting that ligands laterally diffuse through the membrane to reach the orthosteric binding pocket as there is for the cannabinoid and sphingosine-1-phosphate receptors (Szlenk et al., 2019).

The A2 adenosine receptors have attracted particular attention as oncological drug targets due to their involvement with some of the hallmarks of cancer such as immune evasion, angiogenesis and metastasis (Hanahan et al., 2011; Allard et al., 2017). Both A2a and A2b receptors have been shown to be overexpressed in certain cancers (Sepúlveda et al., 2016; Ma et al., 2017). ATP released during cell stress induces inflammation via activation of P2 receptors. Adenosine, a metabolite of ATP, can subsequently act as an anti-inflammatory off switch (Ohta and Sitkovsky, 2001). One of many immunosuppressive strategies employed by tumours to remain unharmed by the immune system is to have high concentrations of adenosine in the tumour microenvironment (Allard et al., 2016). Activation of A2 adenosine receptors, and subsequent increases in cAMP levels, in T cells leads to activation of type I protein kinase A (PKA) that is present in lipid rafts around T cell receptors (TCRs). Type I PKA phosphorylates C-terminal Src kinase (Csk), which then inhibits Src family tyrosine kinases Lck and Fyn, and ultimately inhibits TCR function (Mosenden and Taskén, 2011). Increases in cAMP can also regulate cell functions through cAMP response element binding protein

(CREB), nuclear factor-kappaB (NF-kappaB), nuclear factor of activated T cells (NFAT) stimulated activator protein-1 (AP-1), Epac and Rap1 (Jimenez et al., 2001; Cheng et al., 2008; Sands and Palmer, 2008; Vang et al., 2013). Using selective agonists, A2a adenosine receptor signalling has been shown to reduce the secretion of pro-inflammatory cytokines interleukin 2 (IL-2) and tumour necrosis factor alpha (TNF- α) in type 1/2 cytotoxic T cells (Tc1/2). The proliferation of type 1 helper T cells (Th1) and Tc1 cells was also shown to be inhibited by the agonists *in vivo* (Erdmann et al., 2005). Activation of A2 adenosine receptors has also been shown to promote T regulator cells (Zarek et al., 2008) and inhibit natural killer cells (Beavis et al., 2013).

Adenosine and adenosine receptors are abundant in the central nervous system (CNS) and the later are targets or potential targets in the treatment for Alzheimer's disease, Parkinson's disease, epilepsy, sleep disorders and cerebral ischemia (Choudhury et al., 2019; Liu et al., 2019). In Alzheimer's disease often A1 receptors have a lower than normal expression and A2a receptors have a higher than normal expression leading to cholinergic system dysfunction. Novel drugs are in clinical trials with the aim of addressing these imbalances in Alzheimer's disease patients. The role of adenosine receptors, and potential mechanism of action behind the benefit of the A2a antagonist istradefylline, in Parkinson's disease is not entirely understood. However, it is believed A2a receptors in the striatum co-localize with dopamine D2 receptors with activation of the former having a negative allosteric modulatory effect on the later (Cieślak et al., 2008).

Angiogenesis, the formation of new blood vessels, is essential to the grow of tumours allowing the delivery of oxygen and nutrients while removing waste, as well as providing the avenue for metastasis to occur (Nishida et al., 2006). The pro-angiogenic protein vascular endothelial growth factor (VEGF) is upregulated by both A2a (Leibovich et al., 2002) and A2b adenosine receptor activation (Feoktistov et al., 2003). Additionally, the anti-angiogenic protein thrombospondin 1 (TSP-1) has been shown to be downregulated by A2 adenosine receptor

signalling (Desai et al., 2005; Ernens et al., 2015). Similarly, knockdown and pharmacological inhibition of A2 adenosine receptors leads to reduced metastasis in *in vitro* and *in vivo* models (Cekic et al., 2012; Beavis et al., 2013; Zhou et al., 2017).

In contrast to previously discussed research, some studies have indicated that some roles of the A2b adenosine receptor could be anti-cancerous, and thus a blockade of the receptor could be detrimental to patients. Although the A2b adenosine receptor normally couples $G_{\alpha s}$ G proteins, it is pleotropic in nature and can in some instances couple $G_{\alpha q}$. In dendritic cells A2b adenosine receptor activation has been shown to induce proinflammatory IL-6 release and subsequent T helper 17 cell activation via $G_{\alpha q}$ coupling independently of cAMP (Wilson et al., 2011). However, $G_{\alpha q}$ coupling through A2b receptors has also been linked to increases in angiogenic factors (Feoktistov et al., 2002). Additionally, A2b receptors may promote the activity of p53, the most important tumour suppressor protein in cancer (Long et al., 2013).

The importance of adenosine receptors in human disease has resulted in a large number of drug discovery programmes being initiated to discover both agonists and antagonists at these receptors. The next section will discuss the importance of accurate assessment of ligand pharmacology at G protein-coupled receptors.

1.2 Quantifying ligand-receptor pharmacology

Pharmacodynamics (the effect of drugs on the body) and pharmacokinetics (the effect of the body on the drug including absorption, distribution, metabolism, and excretion) are the two main disciplines making up pharmacology. Ultimately these two elements are combined to build PK/PD models that allow the prediction of clinical dose levels and frequency. A critical step in the utilisation of PK/PD models is to quantify the pharmacological properties of novel ligands in a system-independent manner so that these can be used to scale to potency and efficacy in the clinic. In order to achieve this, mathematical

models are built that describe the interaction of ligand and receptor. These are then used with biological data to estimate system-independent, fully scalable parameters.

The affinity and kinetics of a drug binding to its target receptor are almost exclusively calculated using equations that assume the interacting molecules are homogeneously distributed in a solvent, with the concentration of drug available to bind target being equal to that in the bulk aqueous phase. While this assumption applies well to soluble enzymes, it is less satisfactory for membrane-associated targets (e.g., GPCRs) where the protein is embedded in a phospholipid bilayer. This is because the inclusion of phospholipid adds an additional amphiphilic compartment into which drugs may partition, depending on their physicochemical properties.

1.2.1 The membrane as a second drug compartment

It has long been proposed that the phospholipid bilayer in which the receptors reside can interact with drugs acting as a second compartment for drugs to diffuse into (McCloskey and Poo, 1986; Sargent and Schwyzer, 1986), or through concentrating drugs at the interface with water through electrostatic interactions (Avdeef et al., 1998). It is important to note that cell membranes are not just a homogenous lipophilic pool, but they are defined structures comprising a bilayer of phospholipids and cholesterol with charged head groups and many integral proteins and carbohydrates. Therefore, membrane affinity and interaction will likely be high for lipophilic compounds, but also potentially for compounds that can interact with for example the phospholipid head group through charge or steric interactions. It is known that the composition of the membrane can affect receptor pharmacology through essentially allosteric modulation of receptors (Seddon et al., 2009; Desai and Miller, 2018; Li et al., 2018). Therefore it is also conceivable that the composition of membrane could affect micro PK/PD depending on the interactions between ligands and given constituents of the membrane in a given location. The membrane also

acts as the point of attachment for the extracellular matrix – a 3d structure surrounding cells made up collagen, enzymes, glycoproteins and more – which equally could interact with certain ligands more than others (Theocharis et al., 2016).

Our group has for the first time quantified the concentration of a fluorescently labelled drug at varying distances above and in a cell membrane using fluorescence correlation spectroscopy (FCS) (Gherbi et al., 2015). A fluorescent derivative of propranolol was shown to be 20-fold more concentrated 2 μm above β_2 -adrenoceptor expressing Chinese hamster ovary (CHO) cells compared to the bulk aqueous phase. This was partially reversed by the presence of antagonist or absence of receptor suggesting both the membrane and receptor were contributing the higher local concentration of ligand.

It is therefore possible that the physicochemical properties of ligands could be distorting observed pharmacological parameters i.e., more lipophilic/basic ligands could be concentrating around receptors in assays resulting in higher affinity and quicker association rates being observed.

1.2.2 Ligand-receptor binding from the membrane compartment

The diffusion micro PK model, originally describing long acting β_2 -agonists, suggests that lipophilic ligands can embed in the membrane and slowly leak out into the immediate vicinity of the receptor and/or diffuse laterally into the receptor (Anderson, 1993; Anderson et al., 1994b; Johnson, 2001). The crystal structure of the sphingosine-1-phosphate (S1P) receptor suggests extracellular ligand access is occluded and ligands enter by lateral diffusion (Hanson et al., 2012). 2D lateral diffusion, as opposed to extracellular 3D diffusion, has been suggested to increase ligand binding with the reduction in dimensionality providing an effectively shorter random path to the receptor. However, the 2D lateral diffusion would likely be significantly slower (McCloskey and Poo, 1986). Furthermore, the membrane has

been proposed to act as catalyst by anchoring some drugs at the receptor while allowing them to bind the active site (Coleman et al., 1996).

In addition to thinking of the whole body as the biological system concerned, a growing interest is being placed in thinking about more local phenomena referred to as “micro” pharmacokinetics/pharmacodynamics (micro PK/PD) (Vauquelin, 2015). Whereas pharmacodynamics and pharmacokinetics are often regarded as disparate disciplines, micro PK and PD are perhaps more interlinked. Micro PD mechanisms includes how a drugs residence time can be increased through multiple conformational adjustments such as that described by the induced fit model. Here, a drug binds to receptor forming an intermediate complex that is isomerized to a more stable complex creating an additional step to be reverse for dissociation (Dror et al., 2011; Vauquelin, 2015). Additionally, bivalent ligands (where one ligand binds to two distinct sites simultaneously) must undergo multiple unbinding steps increasing its residence time (Vauquelin, 2013; Vauquelin et al., 2014).

1.2.3 Limited diffusion and drug rebinding

In addition to physicochemical interactions, the physical barriers associated with some physiological compartments (e.g., synapses) may restrict drug diffusion away from the receptor-compartment, promoting drug “rebinding”.

The accumulation of drug near receptor and/or the reduced diffusion of drug away from receptor caused by micro-anatomical properties can allow for individual drug molecules to rebind the same or nearby receptors multiple times before being cleared from the system. Similarly to long residence time, rebinding could allow for a drug to sustain efficacy after it has been effectively cleared from the bulk phase away from the receptor (Vauquelin and Charlton, 2010). This phenomena is likely driven by fast association rates (Vauquelin and Charlton, 2010). The diffusion of drugs in physiological contexts will likely be reduced,

for example, in synapses and interstitial spaces where little stirring of the water filled cavity occurs promoting rebinding (Coombs and Goldstein, 2004). Evidence exists to support this notion where brain slices of radioligand treated mice showed increased dissociation of radioligand in the presence unlabelled antagonist (preventing rebinding) when intact but not when homogenised (Sadée et al., 1982). Mathematical models incorporating rebinding in specific geometric shapes, such as synapses, into ligand kinetics have been proposed and reviewed (Goldstein and Dembo, 1995; Coombs and Goldstein, 2004; Vauquelin and Charlton, 2010). Additionally, the extracellular matrices (ECM) surrounding cells could act as another microanatomical structure to limited diffusion (Dityatev et al., 2006). Rebinding to nearby receptors has also been suggested to be increased by the fact receptors tend to cluster together (Andrews, 2005). Therefore the context in which GPCRs are expressed is likely to influence micro PK/PD as appreciated in a recent paper exploring a rebinding model to explain extrapyramidal side effects of antipsychotics of D2 receptor targeting drugs in synapses (Sykes et al., 2017). Finally, a particular form of rebinding is apparent with bivalent ligands (where one ligand binds to two distinct sites simultaneously) must undergo multiple unbinding steps increasing its residence time (Vauquelin, 2013; Vauquelin et al., 2014).

1.2.4 Experimental methods for measuring variations in local ligand concentrations

As previously mentioned, our group previous used FCS to measure the local ligand concentration of one fluorescently labelled beta receptor antagonist above cell membranes (Gherbi et al., 2018). In short, FCS involves a laser being focussed through a high numerical aperture microscope objective lens with a pinhole positioned in the confocal plane creating a detection volume of $\sim 0.2\text{fL}$. Fluorescent species diffusing through the volume are excited and emit photons that are

detected in a single photon-counting device over time. Fluctuations in fluorescent intensity above and below an average intensity over time are analysed using autocorrelation. The autocorrelation analysis works by taking the size of a fluctuation (δI) at a given time (t) and comparing it to the size of a fluctuation at a later time ($t+\tau$), all normalised to the average intensity (I) squared. Repeating this for many values of τ (e.g. 0.1 μ s to 1s) gives the autocorrelation function $G(\tau)$. Plotting this graphically with $G(\tau)$ on the Y-axis and time on the x-axis, the y-intercept ($G(0)$) is equal to the reciprocal of the average number of fluorescent species in the volume ($1/N$), and the time corresponding to the mid-point of the decay curve is equal to the average time a fluorescent species spends in the volume (dwell time (τ_D)). These values are obtained during analysis using non-linear curve fitting adapted to an appropriate biophysical model, for example if the fluorescent species is diffusing in 2 dimensions (e.g., in a cell membrane) or in 3 dimensions (e.g., in solution), or if multiple components are present of vastly different masses/diffusion speeds (e.g., a freely diffusing small molecule fluorescent ligand and ligand bound to a protein).

With the volume defined by a calibration using a standard compound (e.g., Cy5) at the start of every experiment, the concentration and diffusion coefficient (D) of the fluorescent species in a given position can be calculated from N and τ_D , respectively.

1.2.5 The principle of “micro PK/PD”

The interplay of drug concentration and receptor binding at a local, subcellular level can clearly be very different from that assumed using whole-body exposure levels, and as such need to be considered separately from standard PK/PD modelling. We have therefore coined the phrase “micro PK/PD” to describe the events at a molecular level (Sykes et al, 2014; Vauquelin, 2015). Our group has previously shown that association rates and affinity values of a series of β 2-adrenoceptor

ligands, but not dissociation rates, were affected by local concentration estimated using phospholipid membrane partition coefficients (K_{IAM}) (Sykes et al., 2014). However, if the local concentration was accounted for, the new k_{on} values remained relatively constant and the K_d values correlated strongly to the k_{off} values. This was perhaps the first clear example of “micro PK/PD”, but clearly more research is required into the interplay of compound physicochemical properties, local ligand concentrations and observed receptor pharmacology.

1.3 Aims and objectives

The goal of this study was to expand upon our initial observation that local drug concentrations can be significantly different from those nominally added by using a larger cohort of compounds to examine the influence of physicochemical properties on local ligand concentrations and observed receptor pharmacology. We also aimed to determine whether these observations were common across receptor subtypes by examining the effects across members of the adenosine receptor family. Our objectives were as follows:

1. Probe the importance of physicochemical properties on membrane interaction and observed pharmacology by utilising eight fluorescent adenosine receptor ligands with identical pharmacophores (xanthine amine congener (XAC)), but varying fluorophores and linker regions to modulate their properties. These ligands were to be assessed to determine kinetic binding profiles, phospholipid affinity, and local concentrations above cell membranes.
2. Extend these studies to investigate the kinetics and phospholipid interaction of 57 commercially available compounds known to bind at least one adenosine receptor. Binding kinetics were to be measured at all four adenosine receptors using a competition association assay, and phospholipid affinity (K_{IAM}) was to be assessed in an

Immobilised Artificial Membrane High Performance Liquid
Chromatography assay

3. Compare the data from the above studies to assess the global relationship between local ligand concentrations and observed receptor pharmacology.

Chapter 2 – Material and Methods

2.1 Materials

Chinese Hamster Ovary (CHO) cells (herein referred to as wild type (WT) when not transiently or stably transfected) were purchased from Sigma Aldrich (Gillingham, UK). Dulbecco's modified Eagle's medium (DMEM), foetal bovine serum (FBS), phosphate buffered saline (PBS), and trypsin were purchased from Sigma-Aldrich (Gillingham, UK). SNAP-Surface Alexa Fluor 488 was purchased from New England Biolabs (NEB; Ipswich, MA, USA). Nunc Labtek 8-well cover-glass plates (155411) and all other cell culture plasticware were purchased from Thermo-Fisher Scientific (Loughborough, UK). Unless otherwise stated, all other cell culture reagents were purchased from Sigma Aldrich (Gillingham, UK). pcDNA3.1 (+) encoding for N-terminally SNAP-tagged A1, A2a, A2b, or A3 receptors were constructed and kindly provided by Nick Groenewoud (University of Nottingham).

Commercially available unlabelled adenosine receptor compounds were sourced from the companies listed in Table 2.1. Compounds were made up according to manufacturers' recommendations. In general, this involved adding DMSO to powdered compound to achieve the maximum possible concentration for which the compound soluble, sonicating for 5mins, aliquoting to minimise freeze-thaw cycles, and freezing at -20°C.

Compound	Vendor
(±)-5'-Chloro-5'-deoxy-ENBA	Tocris Bioscience (Bristol, UK)
2-Chloroadenosine (2-CADO)	Tocris Bioscience (Bristol, UK)
2'-MeCCPA	Tocris Bioscience (Bristol, UK)
8-(3-Chlorolstyryl)caffeine (CSC)	Tocris Bioscience (Bristol, UK)
8-Cyclopentyl-1,3-dimethylxanthine (8-CPT, CPX)	Sigma Aldrich (Gillingham, UK)
Adenosine	Sigma Aldrich (Gillingham, UK)
ANR 94	Tocris Bioscience (Bristol, UK)
BAY 60-6583	Tocris Bioscience (Bristol, UK)
caffeine	Sigma Aldrich (Gillingham, UK)
Capadenoson (BAY 68-4986)	Insight Biotechnology (Wembley, UK)
CCPA (2-Chloro-N6-cyclopentyladenosine)	Tocris Bioscience (Bristol, UK)
CGH 2466	Tocris Bioscience (Bristol, UK)
CGS 15943	Tocris Bioscience (Bristol, UK)
CGS-21680	Sigma Aldrich (Gillingham, UK)
CI-IB-MECA (CF102)	Sigma Aldrich (Gillingham, UK)
Cordycepin (3'-Deoxyadenosine)	Tocris Bioscience (Bristol, UK)
CPA (N6-Cyclopentyladenosine)	Sigma Aldrich (Gillingham, UK)
CV 1808 (2-Phenylamino Adenosine) (2-PAA)	Tocris Bioscience (Bristol, UK)
DMPX (3,7-Dimethyl-1-propargylxanthine)	Sigma Aldrich (Gillingham, UK)
DPCPX (PD-116,948)	Sigma Aldrich (Gillingham, UK)
Enprofylline (3-Propylxanthine)	Cayman Chemical Company (Michigan, USA)
GR 79236	Tocris Bioscience (Bristol, UK)
GS 6201 (CVT 6883)	Tocris Bioscience (Bristol, UK)
HEMADO	Tocris Bioscience (Bristol, UK)
IB-MECA (CF101)	Tocris Bioscience (Bristol, UK)
Istradefylline (KW-6002)	Tocris Bioscience (Bristol, UK)
KW-3902	Sigma Aldrich (Gillingham, UK)
LUF 5834	Sigma Aldrich (Gillingham, UK)
MRE 3008F20	Tocris Bioscience (Bristol, UK)
MRS 1191	Sigma Aldrich (Gillingham, UK)
MRS 1220	Tocris Bioscience (Bristol, UK)
MRS 1334	Tocris Bioscience (Bristol, UK)
MRS 1523	Santa Cruz Biotechnology (Texas, USA)
MRS 1706	Tocris Bioscience (Bristol, UK)
MRS 1754	Sigma Aldrich (Gillingham, UK)
MRS 3777 hemioxalate	Sigma Aldrich (Gillingham, UK)
MRS 5698	Tocris Bioscience (Bristol, UK)
N6-(2-Phenylisopropyl)adenosine (R-PIA)	Sigma Aldrich (Gillingham, UK)
NECA	Sigma Aldrich (Gillingham, UK)

PQ-69	Tocris Bioscience (Bristol, UK)
Preladenant (SCH 420814)	Insight Biotechnology (Wembley, UK)
PSB 0788	Tocris Bioscience (Bristol, UK)
PSB 10 hydrochloride	Tocris Bioscience (Bristol, UK)
PSB 11 hydrochloride	Sigma Aldrich (Gillingham, UK)
PSB 1115	Tocris Bioscience (Bristol, UK)
PSB 36	Tocris Bioscience (Bristol, UK)
PSB 603	Tocris Bioscience (Bristol, UK)
Regadenoson (Lexiscan; CVT-3146)	Sigma Aldrich (Gillingham, UK)
resveratrol	Tocris Bioscience (Bristol, UK)
SCH-442,416	Tocris Bioscience (Bristol, UK)
SCH-58261	Sigma Aldrich (Gillingham, UK)
SDZ WAG 994	Tocris Bioscience (Bristol, UK)
SLV320	Sigma Aldrich (Gillingham, UK)
Theophylline	Tocris Bioscience (Bristol, UK)
Tozadenant (SYN115)	Adooq Bioscience (California, USA)
VUF 5574	Tocris Bioscience (Bristol, UK)
XAC	Tocris Bioscience (Bristol, UK)
ZM-241,385	Sigma Aldrich (Gillingham, UK)

Table 2.1 List of unlabelled adenosine receptor compounds and their vendors.

The eight fluorescent compounds were synthesised by Andrea Vernall (University of Nottingham). Compounds were made up from powder in DMSO, sonicated for 5 mins, aliquoted, and frozen in dark conditions.

Compound	AKA	Structure
XAC-X-BY630	XAC-X-BY	
XAC---BY630	Ca200645	
XAC-ser-tyr-X-BY630	AV041	
XAC-ala-tyr-X-BY630	AV069	
XAC-ala-ser-X-BY630	AV074	
XAC-asn-ala-X-BY630	AV075	
XAC-ser-tyr-BYFL	AV050	

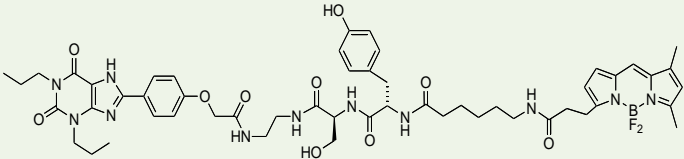
XAC-ser-tyr-X-BYFL	AV051	
--------------------	-------	--

Table 2.2. List of fluorescently labelled adenosine receptor compounds and their linker region and fluorophore with structures.

All phenone-based compounds used as standard in the IAM-HPLC experiments were sourced from Sigma Aldrich (Gillingham, UK). Compounds arrived in liquid form and were stored according to manufacturers' instructions to be diluted on the day of experiments.

2.2 Methods

2.2.1 Cell culture and transfection

Cells were cultured at 37°C in a humidified 5% CO₂/95% air atmosphere in DMEM supplemented with 10%v/v FBS and 2mM L-glutamine (complete media). Cells were routinely passaged when at around 80-90% confluency at a split ratio of between 1:2 and 1:25 with cells roughly doubling in number every 24hours. During passaging, the adherent cells were gently washed with warmed PBS, then incubated with 2mls of trypsin-EDTA solution for 5-10mins before being detached with gentle knocking of the flask if required. The trypsin was neutralised with about 10mls of complete media and the solution containing cells pelleted by centrifugation for 5 mins at 1000 rpm. The pellet was resuspended in complete media and seeded as appropriate.

2.2.2 Membrane preparation

For kinetic binding experiments membrane preparations were used instead of whole cells in order to achieve a single phase of binding. For this, a batch of several flasks of adherent cells were transiently transfected with the appropriate plasmid containing the receptor of choice. The plasmid was diluted to a concentration of 1 µg/ µl then diluted 1:50 in Optimum. Polyethylenimine (PEI), also at 1 µg/ µl, was diluted in a separate container in Optimum at a 3:50 ratio. The two

solutions were combined for 20mins at room temperature before 2.5mls of the solution was added to cells in 22.5mls of media in a 175cm² flask. The cells were then incubated as normal for 24hours.

After 24 hours, with the cells now expressing the SNAP-tagged receptor, the cells were labelled with SNAP-Lumi4-Terbium(Tb) labelling reagent from CisBio (Codolet, France). Media was aspirated from cells and the cells washed twice with PBS and once with Tag-lite labelling Buffer (LabMed) (CisBio, Codolet, France). Cells were then incubated for 1 hour at 37°C in 10mls of labelling reagent. The labelling agent was carefully removed and frozen for repeated use. Cells were washed in PBS and incubated for 10mins with Hank's Based Enzyme Free Cell Dissociation Solution Sigma-Aldrich (Gillingham, UK) before being scraped, pelleted as above and frozen.

The frozen pellet was thawed and processed into homogenised membranes ready for use in assays. The thawed pellet was resuspended in 10mls of cold buffer B (10mM HEPES and 10mM EDTA at pH7.4) and homogenised with 8 x 1 second bursts using an ultra-turrax homogeniser. A further 10mls of buffer B was added and the solution transferred to ultra-fast centrifugation tubes and spun at 22,000 g using a JA25.5 rotor for 30mins at 4°C. The supernatant was discarded, the pellet resuspended in 20mls of buffer B and spun again as before. The pellet was then resuspended in 1ml of cold buffer C (10mM HEPES and 0.1mM EDTA at pH7.4) and frozen at -80°C. The protein concentration was determined by a standard bicinchoninic acid (BCA) assay.

2.2.3 TR-FRET Kinetic assays

The kinetic binding assays in this thesis can be thought of as one of two modes. The fluorescent compounds were screened in a 'global fit mode' where the observed association of several concentrations of ligand are measured \pm a single high concentration of competitor to determine non-specific and specific binding. Alternatively, for the unlabelled compounds a single concentration of a fluorescent tracer is

used in competition with increasing concentrations of the unlabelled compound i.e., 'competition mode'. Other than the ligands present and the analysis, the rest of the assay protocol is the same.

The assay used 384-well white opaque OptiPlates (Perkin Elmer, Massachusetts, USA) and was read in a PheraStar plate reader (BMG Labtech, Ortenburg, Germany). The buffer used was HBSS supplemented with 5mM HEPES, 0.02%w/v pluronic acid, and 100 µg/ml saponin, as well as 1.5%v/v DMSO consistently in all solutions to avoid problems when solutions mix such as compounds becoming less soluble. All experiments took place at room temperature.

In the 'global fit' mode the total assay well volume was 40 µl consisting of:

- 10 µl of buffer or buffer containing 10µM of unlabelled XAC to block all receptors and allow for non-specific binding to be measured.

- 20 µl of fluorescent ligand at 2 times the final assay concentration serially diluted in Eppendorf tubes.

- 10 µl of membrane diluted such that 10 µl contains 1 µg of protein (pre-incubated for 30mins pre-assay with Guanosine 5'-[β,γ-imido]triphosphate trisodium salt hydrate (Gpp(NH)p) sourced from Sigma Aldrich (Gillingham, UK)). This was added last to the well by injectors built into the PheraStar and started the reaction.

In the 'competition mode' the total assay well volume was 40.2 µl consisting of:

- 200nl of unlabelled compound was stamped out into the plates by a Mosquito LV liquid handling robot (SPT Labtech, Hertfordshire, UK).

The Mosquito also completed the serial dilutions. A DMSO only and a non-specific binding control were also present on each row.

- 20 µl of buffer. The fluorescent intensity (excitation 620nm, emission 665nm) was checked at this point to see if any compounds had intrinsic fluorescent properties.

- 10 µl of fluorescent tracer at a single concentration was then added to each well. The plate was spun and fluorescent intensity checked again

to see if the compounds were quenching or potentiating the signal from the tracer, and to check for any addition errors.

-10 µl of membrane was added as per the 'global fit' mode. Fluorescent intensity was again checked after completion of the read as some compounds appear to cause unusual fluorescent effects in the presence of the membrane.

	c1	c2	c3	c4	c5	c6	c7	c8	c9	c10	c11	c12	c13	c14	c15	c16	c17	c18	c19	c20	c21	c22	c23	c24
a	dmsc	dmsc	dmsc	dmsc	dmsc	dmsc	NSB	NSB	NSB	NSB	NSB	NSB	dmsc	dmsc	dmsc	dmsc	dmsc	dmsc	NSB	NSB	NSB	NSB	NSB	NSB
b	dmsc	min	<--	<--	compound 1				<--	<--	max	NSB	dmsc	min	<--	<--	compound 15				<--	<--	max	NSB
c	dmsc	min	<--	<--	compound 2				<--	<--	max	NSB	dmsc	min	<--	<--	compound 16				<--	<--	max	NSB
d	dmsc	min	<--	<--	compound 3				<--	<--	max	NSB	dmsc	min	<--	<--	compound 17				<--	<--	max	NSB
e	dmsc	min	<--	<--	compound 4				<--	<--	max	NSB	dmsc	min	<--	<--	compound 18				<--	<--	max	NSB
f	dmsc	min	<--	<--	compound 5				<--	<--	max	NSB	dmsc	min	<--	<--	compound 19				<--	<--	max	NSB
g	dmsc	min	<--	<--	compound 6				<--	<--	max	NSB	dmsc	min	<--	<--	compound 20				<--	<--	max	NSB
h	dmsc	min	<--	<--	compound 7				<--	<--	max	NSB	dmsc	min	<--	<--	compound 21				<--	<--	max	NSB
i	dmsc	dmsc	dmsc	dmsc	dmsc	dmsc	NSB	NSB	NSB	NSB	NSB	NSB	dmsc	dmsc	dmsc	dmsc	dmsc	dmsc	NSB	NSB	NSB	NSB	NSB	NSB
j	dmsc	min	<--	<--	compound 8				<--	<--	max	NSB	dmsc	min	<--	<--	compound 22				<--	<--	max	NSB
k	dmsc	min	<--	<--	compound 9				<--	<--	max	NSB	dmsc	min	<--	<--	compound 23				<--	<--	max	NSB
l	dmsc	min	<--	<--	compound 10				<--	<--	max	NSB	dmsc	min	<--	<--	compound 24				<--	<--	max	NSB
m	dmsc	min	<--	<--	compound 11				<--	<--	max	NSB	dmsc	min	<--	<--	compound 25				<--	<--	max	NSB
n	dmsc	min	<--	<--	compound 12				<--	<--	max	NSB	dmsc	min	<--	<--	compound 26				<--	<--	max	NSB
o	dmsc	min	<--	<--	compound 13				<--	<--	max	NSB	dmsc	min	<--	<--	compound 27				<--	<--	max	NSB
p	dmsc	min	<--	<--	compound 14				<--	<--	max	NSB	dmsc	min	<--	<--	compound 28				<--	<--	max	NSB

Table 2.3 Example 384 well plate map for 'competition mode' TR-FRET assay. DMSO controls with no compound added (blue) were present in

columns 1 and 13 to assess total binding of a fixed concentration of fluorescent compound. NSB controls in columns 12 and 24 (red) contain a high concentration XAC (10µM FAC) such that non-specific binding of the fixed concentration of fluorescent compound can be determined. DMSO or the high concentration of XAC was also added to rows a and i such that increasing concentration of the fluorescent compound could be added and the kinetics of said tracer could be determined once for every quarter of the plate. In all well expect those in rows a and i, a fixed concentration of fluorescent compound would be added. Compounds were added such that their maximum concentration would be in columns 11 or 23, then they would be diluted 1 in 3 to the well immediately left a total of 9 times. This gives space for 28 compounds to be run at 10 concentrations.

In general, the PheraStar was set to 6 laser flashes, a 5 second cycle time for 240 cycles (15mins). However, this was adjusted depending on the kinetics of the ligands involved. For example, some ligands required

increased resolution (lower cycle time) to get good fitting of the model at the expense of reduced through-put as a lower number of wells could be read per cycle. In general, 36 wells were read per cycle. For BODIPY 630-650 labelled fluorescent ligands (all those except AV050 and AV051), terbium was excited at 337nm, with emissions read at 620 and 665nm. The 620nm emission gives an indication of the signal from terbium in the well, and the 665nm signal measures the ligand emission, giving an indication that FRET has occurred between the terbium and the fluorescent ligand. The resultant FRET signal for binding is calculated as the ratio of 665nm emission to 620nm emission *10,000. For BODIPY FL labelled ligands (AV050 and AV051), terbium was excited at 337nm, but emissions read at 620nm for terbium, and 520nm for ligand emission indicating the occurrence of FRET.

Specific binding (total binding minus non-specific binding) was plotted on the y-axis against time in mins on the x-axis in GraphPad prism v8.2.1 (San Diego, USA).

Data from the 'global fit mode' were fitted using the "nonlinear regression – association kinetics, two or more conc of hot" built in analysis in GraphPad prism. This analysis uses the follow equations:

$$Y=Y_{\max}*(1 - \exp(-1*k_{ob}*X))$$

And

$$k_{ob}=[L]*k_{on}+k_{off}$$

Where Y_{\max} is the maximal binding of a high concentration of ligand, k_{ob} is the observed association rate, and $[L]$ is the concentration of fluorescent ligand (entered into the column headings in nM). The global fitting assumes that the off rate is the same across all ligand concentrations and shares this across each concentration.

Subsequently the on rates can be calculated for each curve from the k_{ob} value.

Data from the 'competition mode' were fitted using the "nonlinear regression – kinetics of competitive binding" built in analysis in

GraphPad prism. This analysis uses equations first described by Motulsky and Mahan when studying enzymatic reactions (Motulsky and Mahan, 1984).

$$KA = K1 * L * 1E-9 + K2$$

$$KB = K3 * I * 1e-9 + K4$$

$$S = \text{SQRT}((KA - KB)^2 + 4 * K1 * K3 * L * I * 1e-18)$$

$$KF = 0.5 * (KA + KB + S)$$

$$KS = 0.5 * (KA + KB - S)$$

$$\text{DIFF} = KF - KS$$

$$Q = B_{\text{max}} * K1 * L * 1e-9 / \text{DIFF}$$

$$Y = Q * (K4 * \text{DIFF} / (KF * KS) + ((K4 - Kf) / KF) * \exp(-KF * X) - ((K4 - KS) / KS) * \exp(-KS * X))$$

Whereby K1 and K2 are constrained to the association and dissociation rates of the tracer compound respectively, and L is constrained to the concentration of tracer used. K3 and K4 are outputted as the association and dissociation rates of the cold compound respectively.

2.2.4 IAM-HPLC

The immobilised artificial membrane-high performance liquid chromatography (IAM-HPLC) assay in this thesis uses a conventional HPLC set up fitted with a 30mm by 4.6mm IAM-PC-DD2 column with 10 μm particle size and 300 Å pore size with a guard kit (Regis Technologies, Illinois, USA). The HPLC set up also has a series 200 autosampler allowing for a degree of automation, a series 1050 degasser, and a UV/VIS photodiode array detector from Perkin Elmer (Massachusetts, USA). Compounds were injected into the system in a volume of 20 μl and the flow rate of the system was 0.5ml/min. Ammonium acetate (Sigma-Aldrich, Gillingham, UK) 50mM dissolved in HPLC grade water (Thermo-Fisher Scientific, Loughborough, UK) at

pH7.4 was used as the aqueous mobile phase, with acetonitrile (Sigma-Aldrich, Gillingham, UK) used as the organic mobile phase.

The system was set to run for 30 mins at the start of each day to equilibrate, and set to run for at least 5 mins if changing the ratio of aqueous to organic mobile phases. 100% organic phase was run through the system at the end of the day for 10 minutes to clean through the column. Propranolol, isoprenaline, nadolol and timolol (all from Sigma-Aldrich, Gillingham, UK) were tested at the start of each day to track for column deterioration or any abnormalities in the system. Citric acid (Sigma-Aldrich, Gillingham, UK) was also run through the system three times at the start of the day to determine the column dead time (t_0) as the compound has essentially zero affinity for the column.

Retention times (t_r) were calculated by determining peak signal in Microsoft Excel. These were normalised to retention factors (k_{IAM}) according to the following equation below:

$$k_{IAM} = \frac{(t_r - t_0)}{t_0}$$

Retention factors correlate with true IAM partition coefficients (K_{IAM}) and can be converted as per the equation below, where V_m is the volume of the mobile phase and V_s is the volume of the stationary phase.

$$K_{IAM} = \left(\frac{V_m}{V_s}\right) k_{IAM} = \phi k_{IAM}$$

More details on the methodology that was optimised in this study can be seen in Chapter 4.

2.2.5 Fluorescence Correlation Spectroscopy (FCS)

As described in more detail in Chapter 5, FCS is a confocal based spectroscopy technique which analyses fluorescent fluctuations from a small, defined Gaussian-Lorentzian shaped confocal detection volume (0.2fL, $\sim 1 \times 0.3 \mu\text{m}$). This allows quantification of the dwell time (diffusion co-efficient) and concentration of fluorescent species (in this case fluorescent ligand molecules). FCS experiments exploit the precise and

accurate positioning of the confocal volume in 3 dimensions (particularly the z-direction where resolution was a single micron).

FCS experiments were conducted at 22°C on a Zeiss LSM510NLO Confocor 3 confocal microscope (Carl Zeiss, Jena, Germany) using a 40 × 1.2NA water-immersion objective lens, with ~2.4 kw/cm² 633 nm excitation and emission measured through an LP650 nm filter and a pinhole of 1 Airy unit diameter. At the start of each experimental day the measurement volume was calibrated by taking 10x10 second fluorescence fluctuations of a 5nM solution of Cy5 NHS ester. Data were analysed in Zen2012 (Zeiss, Oberkochen, Germany).

For FCS experiments, cells were cultured in complete medium in 8-well plates for 48 hours prior to experiment. Cells appeared healthier and more adhered to the coverslip at this time point compared to 24 hours. A seeding density of 5,000 cells per well was found to give the desired confluency where single, isolated groups of cells could be easily identified. Where required, cells were labelled with 0.1 µM SNAP-surface Alexa Fluor 488 diluted in media for 30mins at 37°C. Cells were washed in low fluorescence buffer to remove media (containing high background fluorescence) and fluorescent label. Cells were left to equilibrate to the buffer and temperature for 1 hour. The room containing all equipment was temperature controlled to 22°C. Buffer was then gently removed and replaced with buffer containing fluorescent ligand.

Focus was initially found visually using transmitted light illumination and the field of view adjusted to an area near the centre of well containing a desired confluency of cells. Precise adjustments to the x-y positioning of the volume were then made above a cell, or area of no cells using a live transmitted or confocal image to position the region of interest on the crosshairs marking the central image position. Where fluorescence was used, cells expressing the SNAP-AlexaFluor488 labelled receptor were imaged using the 488nm excitation and a BP505-560 emission filter to identify cells highly expressing labelled receptor (Figure 2.1).

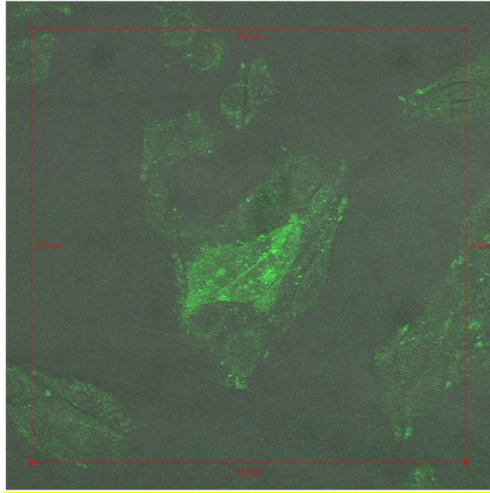


Figure 2.1 field of view of mixed population of cells expressing the A2a adenosine receptor with a SNAP tag labelled with Alexa-fluo 488.

Approximate positioning of the volume in z at the cell membrane (or equivalent height) was made visually by adjusting the fine focus. Subsequently, precise positioning in z was then performed using scans on low laser powers. For cell membranes, a 2% laser power 633nm automated point scan at $8 \times 0.5 \mu\text{m}$ intervals was performed. A single peak was observed for the upper cell membrane. The platform was then programmed to move in defined increments to the desired height above the initial membrane position. It was determined that a minimum distance of $2 \mu\text{m}$ was required above the cell membrane to ensure that no membrane bound ligand was included in the measurements. A similar procedure was used for non-receptor expressing cells. Where FCS measurements were taken above the coverslip, the initial height above the coverslip that was used was the equivalent z-position as that found for those cells measured in the same field of view.

Fluorescence fluctuations were collected for 1x30s at each z position above a receptor-expressing cell, a non-expressing cell and an area with no cell present within the same coverslip. This length of data collection, coupled with the length of time of incubation of ligands, meant that whilst there was a time differential between sets of data in z, this was not substantial compared to the length of ligand incubation overall. Autocorrelation analysis of these fluctuations (Figure 5) was

then used to determine the absolute concentration of ligand at each measured x-y-z position and its diffusion co-efficient.

Autocorrelation analysis was carried out in Zen2012 (Carl Zeiss, Jena, Germany). All curves were fitted to a model using one freely-diffusing 3D component, with a pre-exponential to account for fluorophore photo-physics such as triplet state formation (Gherbi et al., 2018). Initially, the dwell time of Cy5 was determined and used in conjunction with its literature diffusion co-efficient to calculate the dimensions and volume of the detection volume as described in (Briddon et al., 2004). For experimental traces, these were initially examined for large aggregates (such as ligand aggregates or cell debris) For these traces (~ 5%), data were either discarded or, for those <2x the average intensity, these were removed using the Zen “dust filter”. Fitting of these autocorrelation curves gave ligand particle numbers and average dwell times, which were converted to concentrations and diffusion co-efficient using the calibrated volume dimensions (Briddon et al., 2004, Gherbi et al., 2018)

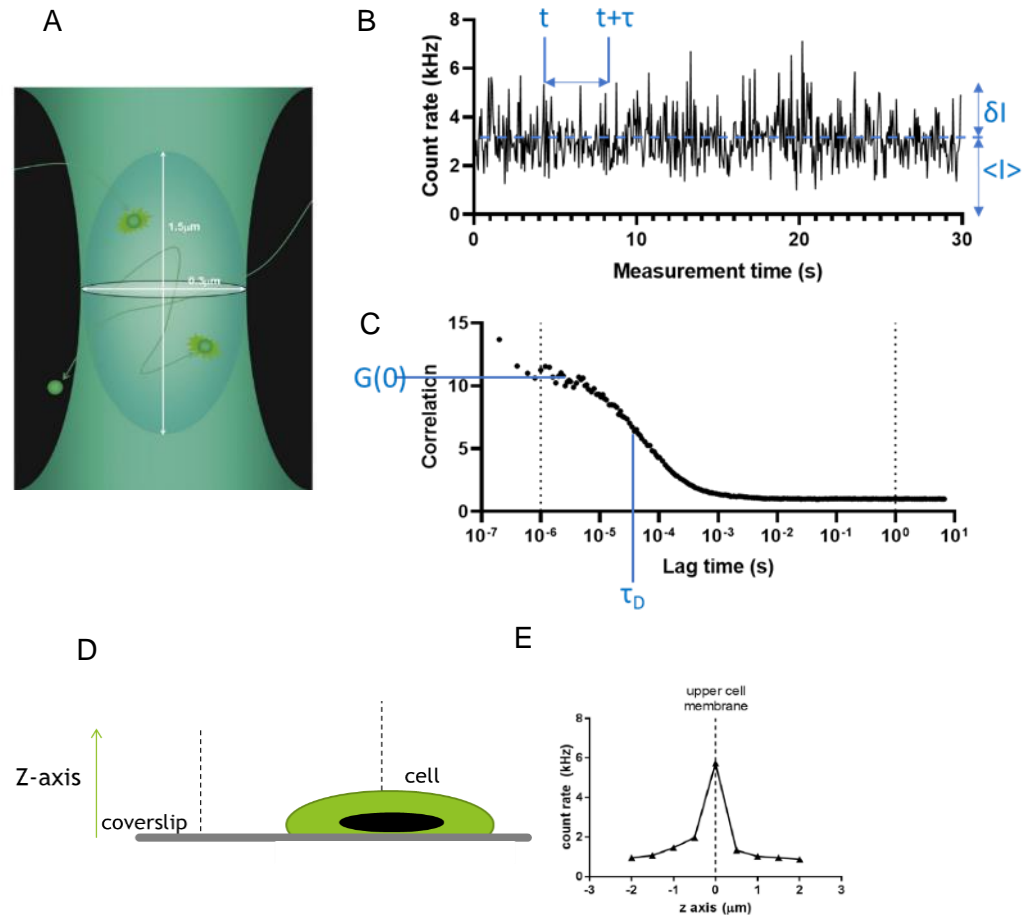


Figure 2.2 Summary of methods of fluorescence correlation spectroscopy (FCS).

A: Fluorescent species travels through confocal volume and is excited. B: example of fluctuations in fluorescence intensity of 15 second period. C: autocorrelation analysis on the trace B. D: schematic showing reads being taken at increasing heights in the z-axis above coverslip and cell. E: Z-scanning on low laser power to find cell membrane.

Autocorrelation analysis of the membranes compares the deviation in intensity, δI , from the average intensity, I , at time t to that of a range of times δt afterwards. This results in an autocorrelation curve which can be fitted to a 3D biophysical model to yield the average dwell time, τ_D , of the fluorescent species and its $G(0)$ value which is inversely proportional to its concentration. Using calibrated volume dimensions, these can be converted to diffusion co-efficient and concentration, respectively.

2.2.5 Statistical analysis

All statistical analysis was performed using GraphPad Prism v8.2.1. Statistic significance was determined when $P < 0.05$, reflecting a less than 5% chance that data were due to random chance.

A two-sample t-test was used when comparing means where the data were from two statistically independent samples. A paired t-test was used when the data were from matched pairs. In all cases t-tests were two-tailed meaning there was no assumption which samples mean was possibly higher than the other.

When computing correlation between two variables either Pearson correlation or Spearman nonparametric correlation calculations were carried out where appropriate. Pearson's correlation takes into account the strength of a linear correlation but requires the assumption that both variables approximately follow a Gaussian distribution. Spearman's correlation considers the rank order of variables, and not the size of the differences, while making no assumption about the Gaussian distributions of the populations. In this thesis a D'Agostino-Pearson normality test was used to test for Gaussian distributions and where possible Pearson's correlation was preferred due to the consideration for the sizes of difference between variables. Typically, the smaller data sets tended to fail the D'Agostino-Pearson normality test in one or more variables and hence the Spearman's correlation test was applied. As Spearman's rank correlation is less susceptible to outliers this is additionally useful in small data sets where a single outlier could make up a significant portion of the data set (although this was not considered when choosing an appropriate test). In all cases correlations were two-tailed meaning there was no assumption as to the direction of potential correlation.

Chapter 3 – Characterising the receptor-ligand kinetic binding properties of a series of adenosine receptor compounds using time-resolved Förster resonance energy transfer (TR-FRET)

3.1 Introduction

Receptor-ligand binding kinetics and the concept residence time are being increasingly viewed as important in addition to conventional equilibrium based pharmacological parameters, such as affinity values, and have been the subject of several reviews (Copeland et al., 2006a; Zhang and Monsma, 2009; Guo et al., 2014; Cusack et al., 2015; Copeland, 2016). Recently, an appreciation of kinetics in the context of the exciting phenomena of signalling bias (drugs have a preference for which signalling cascades they activate through one receptor) has even been proposed (Klein Herenbrink et al., 2016; Lane et al., 2017). The dissociation rate (denoted as k_{off} and in the units min^{-1}) of receptor-ligand complexes divided by the association rate (denoted as k_{on} and in the units $\text{M}^{-1}\text{min}^{-1}$) is equal to the equilibrium dissociation constant (denoted as K_d and in the units M) and represents the concentration at which half the receptors will be occupied at equilibrium (equation 1). The rate at which ligands associate to receptors, but not dissociation rate, is affected by the concentration of ligand in the system and thus the observed association rate (k_{obs}) measured in experimental systems is concentration dependent. k_{obs} can be converted into the concentration independent k_{on} (equation 2 below). The residence time (a measure of how long complexes stay bound, denoted as τ) of a receptor-ligand complex is directly related to k_{off} and can be calculated as the reciprocal of k_{off} (equation 3 below). The receptor-ligand half-life can also be calculated from k_{off} (equation 4 below). Importantly, if the residence time exceeds the pharmacokinetic half-life of a drug, then the drug could in theory still exert its effect once it has been cleared from

the system (Vauquelin and Charlton, 2010). Alternatively, in certain circumstances quick dissociation could be responsible for reduced side effects by allowing endogenous agonists to surmount the blockade (Kapur and Seeman, 2000; Vauquelin et al., 2012). In a relevant example at the A2a adenosine receptor, a study found that efficacy of a series of agonists correlated far better to residence time compared to the more conventional K_d values (Guo et al., 2012a).

1. $K_d = \frac{k_{off}}{k_{on}}$
2. $k_{on} = \frac{k_{obs} - k_{off}}{[\text{radio or fluorescently labelled ligand}]}$
3. $\tau = \frac{1}{k_{off}}$
4. $T_{\frac{1}{2}} = \frac{\ln 2}{k_{off}}$

Historically radiolabelled ligands have been the main tool used to investigate the kinetic properties of receptor-ligand complexes. More recently approaches have been developed using fluorescently labelled ligands with certain advantages and disadvantages compared to radioligand approaches (Emami-Nemini et al., 2013). A key advantage of the later technique is that it has fewer inherent safety and regulatory issues associated with it. A second advantage is that while radioligand experiments generally consist of an endpoint read of several time points to measure the kinetics of binding (with some exceptions in more advanced set ups e.g., Scintillation proximity assay (SPA)), fluorescently labelled ligands can be read in real time with a reading every few seconds or less. This allows a greater resolution of the output, and a less labour-intensive process. Furthermore, fluorescently labelled ligands can be used in various imaging techniques including FCS. A key disadvantage of the FRET based approach is that small molecules are far more extensively modified to add a fluorescent label compared to a radioactive one. For example, a radioligand can be

made by changing one or a few hydrogen atoms for tritium atoms, whereas the addition of a fluorophore and linker region can more than double the molecular weight of the compound, changing the properties and potentially the binding mode.

The first aim of this Chapter is to determine the kinetic binding properties of the series of 8 fluorescent ligands at the A2a and A2b receptors. The ligands share the same core antagonist pharmacophore but different linkers and fluorescent labels thus likely a range of physicochemical properties. Although making the ligands less clinically relevant, the fluorescent labels will allow for later analysis by FCS. The second aim is to develop a robust medium-throughput assay for determining the kinetics of unlabelled compounds at each of the 4 adenosine receptors and to screen a series of 57 commercially available compounds.

3.2 Results

3.2.1 Optimisation of a TR-FRET based assay for determining binding kinetics of fluorescent compounds

Here Chinese Hamster Ovary (CHO) cells transiently transfected with SNAP-tagged adenosine A2a or A2b receptors were labelled with SNAP-Lumi4-Tb substrate for 1 hour at 37°C (Figure 3.1) and subsequently processed into membrane preparations. Experiments were started when membrane was added to wells containing fluorescent ligands +/- 10µM unlabelled antagonist (XAC) to determine non-specific binding. TR-FRET signals were read in a PHERAstar plate reader every 15 seconds following 337nm excitation of the terbium donor. Using lanthanide donors like terbium provides the benefit of having multiple emission peaks allowing for the use of different wavelength acceptors (Figure 3.1). Additionally, the long emission half-life of terbium relative to sources of background fluorescence allows

background noise to be reduced by introducing a delay in the order of milliseconds between excitation and emission reads.

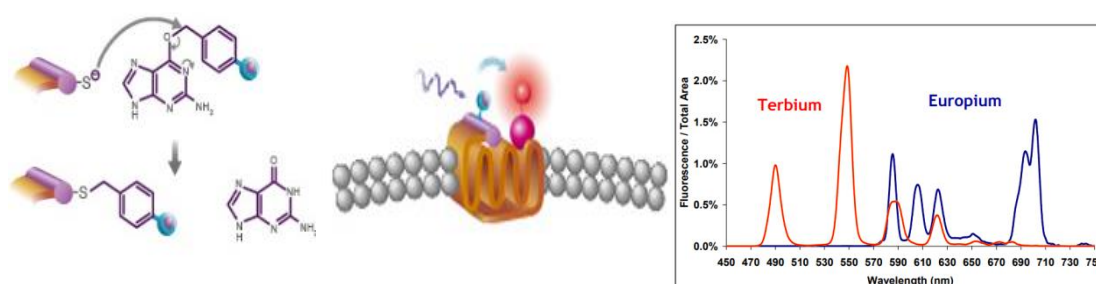


Figure 3.1. Lumi4-Tb labelling of SNAP tagged GPCR. Left: enzymatic reaction covalently attaching substrate to receptor. Middle: TR-FRET occurring as terbium is excited by laser and transfers energy to fluorescent ligand brought into proximity by specific binding to receptor. Right: emission spectrum of lanthanides terbium and europium. Taken from cisbio.com

The assay was initially optimised to remove artefacts and increase its signal-to-noise ratio allowing for greater sensitivity, accuracy and reproducibility. One such artefact observed was that rather than binding plateauing after an initial association phase, it appeared to slowly increase over time (Figure 3.2a). This could be because the membranes are not completely homogenised allowing micelles to form affecting receptor accessibility. This artefact was removed by incubating membranes for 30mins prior to experiment with 100 $\mu\text{g}/\text{ml}$ of the amphipathic glycoside saponin, similar to a study using A1 adenosine receptor membranes (Cohen *et al.*, 1996). A mass of 1 μg of membrane per well was found to be sufficient to achieve a good signal without wasting extra membrane or running the risk of having effects from ligand depletion (Figure 3.2b). Transient transfection was initially optimised using Fugene transfection reagent by varying the reagent:DNA ratio with 3:1 found to be optimal (Figure 3.2c). Transfection was later optimised using the polymer polyethylenimine (PEI) (linear, 25000MW), which is far less expensive than Fugene. Reagent:DNA ratio was again optimised along with the comparisons

between Optimem versus a simple NaCl buffer as the transfection buffer. Furthermore, the addition of the histone deacetylase inhibitor valproic acid was tested as preventing DNA wrapping around histones in this way has previously been shown to improve transiently transfected gene expression for certain genes in CHO cells (Wulhfard *et al.*, 2010). Optimal conditions were found to be 3:1 ratio of PEI:DNA in the salt buffer with valproic acid being found to have little effect (Figure 3.2d). As well as being cheaper than the Fugene control, these conditions were found to be preferential in terms of a signal-noise window.

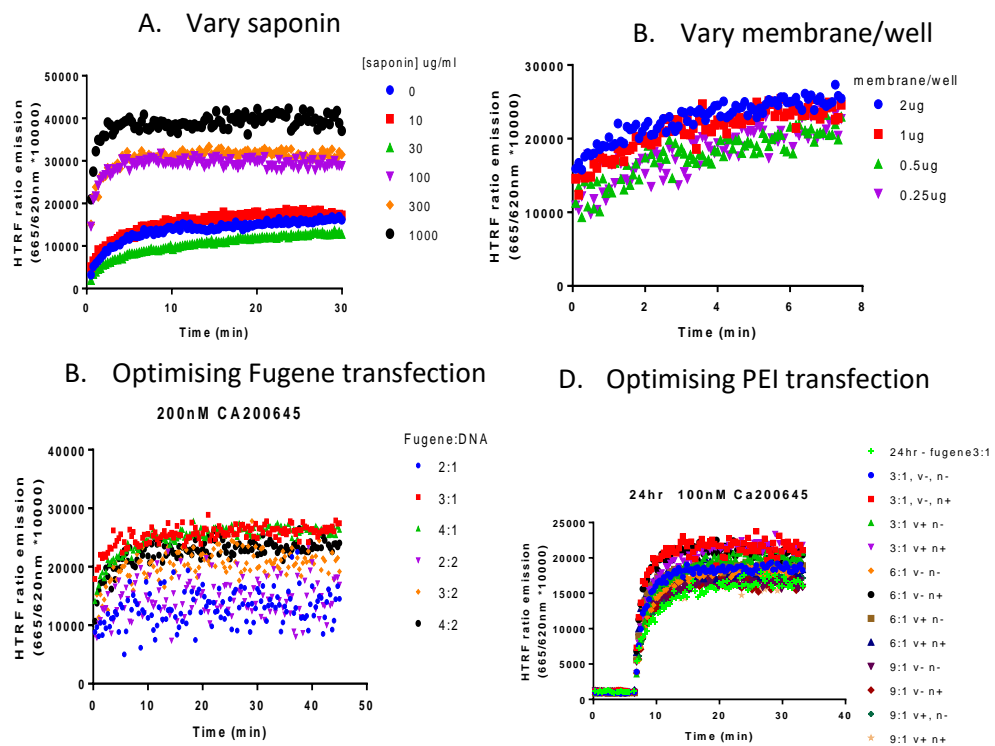


Figure 3.2. Example traces of A2a receptor TR-FRET assay optimisation experiments using single concentrations of CA200645. A: varying saponin concentration in buffer. B: varying mass of membrane per well. C: varying fugene:DNA ratio in transient transfection. D: varying PEI:DNA ratio in transient transfection +/- 10mM valproic acid (denoted as v+/-) and with either optimum as buffer (denoted as n-) or 100mM NaCl buffer (denoted as n+).

3.2.2 Determining the binding kinetics of fluorescent ligands for adenosine A2a and A2b receptors

Once the assay was optimised, a series of fluorescently labelled compounds were screened to determine their kinetic profiles using A2a receptor expressing membranes as well as A2b receptor expressing membranes under the same conditions. The resulting terbium signal and TR-FRET signals from the A2b membranes were comparable to the A2a membranes. There were eight compounds in the series all with the same pharmacophore (XAC), with either BODIPY 630-650 (630nm excitation, 650nm emission) or BODIPY-FL (488nm excitation, 520nm emission) as the fluorophore connected by linkers with varying compositions (Table 2.2). The different fluorophores and linker regions will likely give the molecules different physicochemical properties (see Chapter 4) and may also affect the binding of the molecules to the receptor. k_{on} , k_{off} and K_d values were determined using a global fit to the association kinetic model in GraphPad Prism v8.2.1 with an example trace shown below (Figure 3.3).

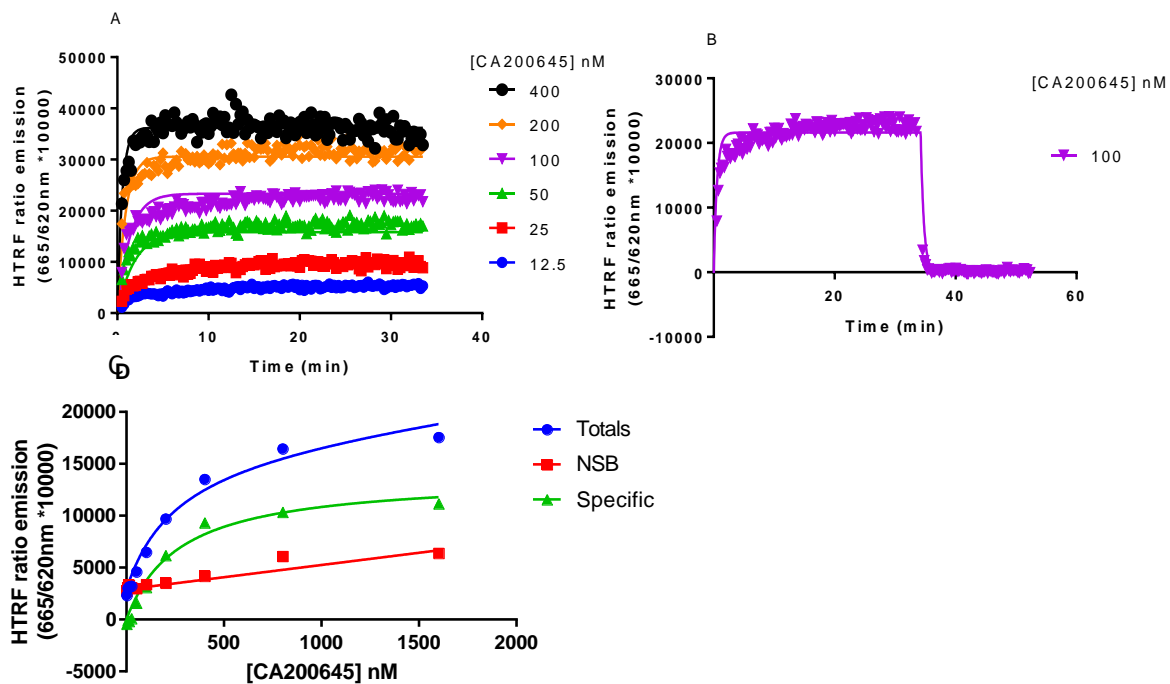


Figure 3.3. Examples of kinetic data for fluorescent compounds. A)

Example of kinetic trace for one ligand (CA200645) at several concentrations with a global fit. B) Example of a single concentration of fluorescent ligand (CA200645, 100 nM) where high concentration of unlabelled antagonist (XAC, 10 μ M) is added to prevent reassociation (this is for illustrative purposes as direct dissociation like this was not measured for the majority of compounds).

C) Example of a saturation plot taken from an average of several points at equilibrium (again this is illustrative of how affinity values could be determined, but was not widely used in this study). Data shown are representative of 3 experiments performed.

A2a receptor-ligand kinetics

Compound	Structure	$k_{\text{off}}(\text{min}^{-1})$	$k_{\text{on}}(\text{min}^{-1}\text{mM}^{-1})$	$K_{\text{d}}(\text{nM})$
XACBY	XAC-X-BY630	0.55±0.23	16700±8030	36.0±6.4
CA200645	XAC-BY630	0.57±0.17	1330±175	461±10.7
AV041	XAC-ser-tyr-X-BY630	0.27±0.09	12900±913	28.7±15.3
AV069	XAC-ala-tyr-X-BY630	0.20±0.02	1220±95.4	430±35.9
AV074	XAC-ala-ser-X-BY630	0.28±0.18	4040±254	70.7±18.3
AV075	XAC-asn-ala-X-BY630	0.17±0.10	791±36.4	346±30.2
AV050	XAC-ser-tyr-BYFL	1.61±0.31	653±33.7	3001±118
AV051	XAC-ser-tyr-X-BYFL	0.51±0.07	4540±1160	121±34.0

A2b receptor-ligand kinetics

Compound	Structure	$k_{\text{off}}(\text{min}^{-1})$	$k_{\text{on}}(\text{min}^{-1}\text{mM}^{-1})$	$K_{\text{d}}(\text{nM})$
XACBY	XAC-X-BY630	0.08±0.02	24100±6860	3.70±1.5
CA200645	XAC-BY630	0.13±0.02	872±144	157±27.5
AV041	XAC-ser-tyr-X-BY630	0.08±0.04	16400±7480	6.50±4.63
AV069	XAC-ala-tyr-X-BY630	0.03±0.02	1150±81.1	69.6±6.9
AV074	XAC-ala-ser-X-BY630	0.09±0.3	5820±201	14.8±4.01
AV075	XAC-asn-ala-X-BY630	0.05±0.01	1040±50.5	43.6±16.8
AV050	XAC-ser-tyr-BYFL	0.52±0.11	491±66.8	1110±339
AV051	XAC-ser-tyr-X-BYFL	0.07±0.03	1820±357	43.8±26.8

Table 3.2. Summary of TR-FRET kinetic data for 8 fluorescent compounds at A2a and A2b receptor expressing cells. In all cases data are shown as mean \pm SEM of 4 independent determinations.

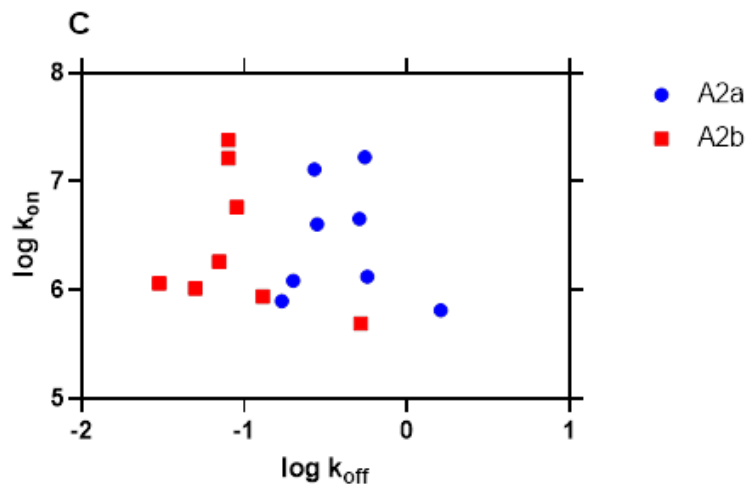
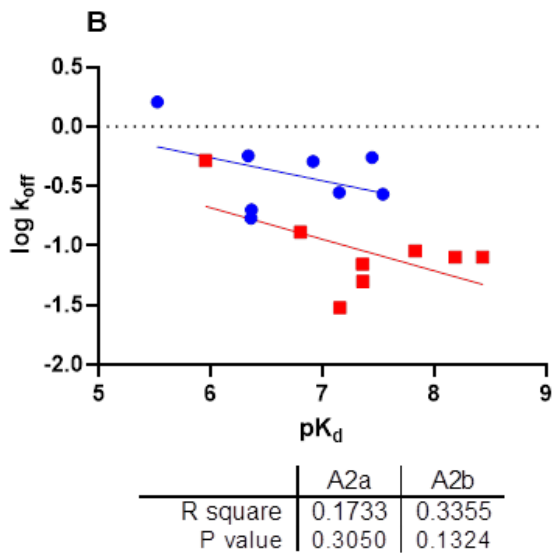
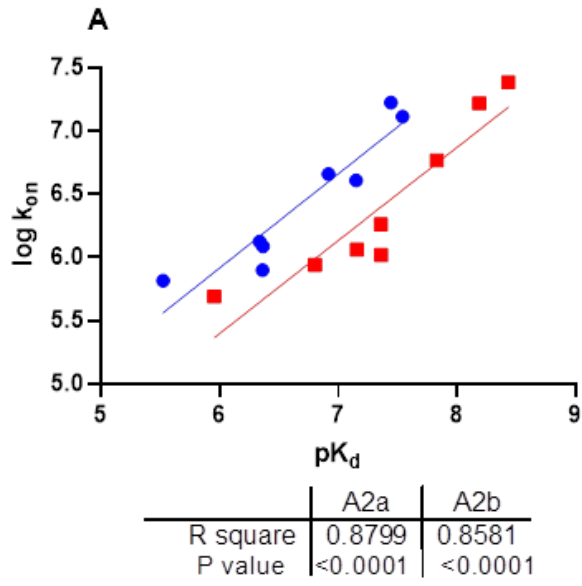


Figure 3.4. TR-FRET kinetic data for 8 fluorescent compounds at A2a and A2b receptor expressing cells. A) log values of the association rate plotted against the affinity values for the 8 compounds at each receptor. B) log values of the disassociation rate plotted against the affinity values for the 8 compounds at each receptor. C) log values of the association rate plotted against log values of the disassociation rate. In all cases blue circles represent A2a receptor data and red circles represent A2b receptor data. R square values determined by Spearman's ranks correlation.

Despite having the same pharmacophore, the series displayed a range of kinetic profiles showing the influence both linker regions and fluorophore can have on measured ligand binding. Noticeably, in A2a membranes association rates varied by 25.6-fold compared to 9.5-fold for dissociation rate compared to 49.1-fold and 17.3-fold in A2b membranes respectively. Correlations that were statistically significant across the 8 compounds were seen between logarithms of k_{on} and K_d for both receptors ($p < 0.0001$, Figure 3.4a), but not between k_{off} and K_d ($p > 0.05$, Figure 3.4b).

The mean K_d of the ligands in the A2a expressing membranes was 573 nM compared to 181 nM for A2b expressing membranes. The mean k_{on} in A2a membranes was $5.27 \times 10^6 \text{ M}^{-1} \text{ min}^{-1}$ compared to $6.46 \times 10^6 \text{ M}^{-1} \text{ min}^{-1}$ in A2b. The mean k_{off} in A2a membranes was 0.52 min^{-1} compared to 0.13 min^{-1} in A2b. Two-tailed paired t-tests found that the differences in K_d and k_{off} , but not k_{on} , were statistically significant ($p < 0.0001$, $p < 0.05$, $p > 0.05$ respectively). Therefore, it appears the ligands tended to have a higher average affinities for A2b membranes, driven by slower dissociation rates. This is best visualised in Figure 3.4c where the cluster of A2a compounds are right-shifted on the X-Y graph, but the spread in the y-axis is more comparable across the receptors.

3.2.3 Determining the binding kinetics of unlabelled compounds at adenosine A1, A2a, A2b and A3 receptors using a competition TR-FRET assay.

Fluorescence-based assays are not limited to only being able to determine the binding properties of fluorescent compounds. Through competition with a well characterised fluorescent ligand, the binding kinetics of unlabelled ligands can be indirectly measured (Sykes et al., 2014). Here a single concentration of CA200645 was used in competition with several concentrations of 59 commercially available unlabelled compounds at all four adenosine receptors. All these compounds are commercially available and believed to have a reasonable affinity for one or more of the adenosine receptors. All compounds were screened to a minimum of 3 replicates at 10 concentrations. The results of the screen can be seen in Tables 3.3-3.6. A limit was applied such that compounds with apparent off rates of more than 3 min^{-1} were disregarded as the associated confidence intervals became too large at this point. However, in many cases where the kinetic properties were unable to be obtained it was still possible to obtain K_d with reasonable confidence.

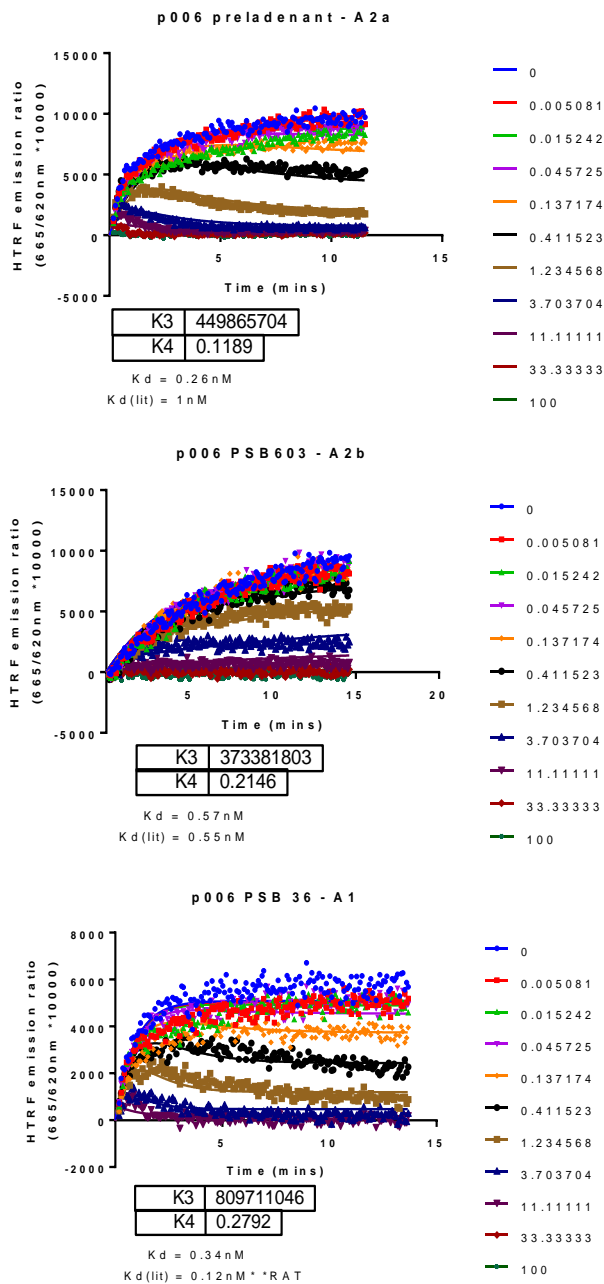


Figure 3.5. Examples of competition kinetic binding experiments from a single test plate (006). A fixed concentration of CA200645 (with the kinetics of the tracer measured at the start of each day) was added to wells along with 10 concentrations of unlabelled ligand (final assay concentration shown in nM on the right of each graph) prior to membrane addition. Membrane expressing one adenosine receptor (A2a-top, A2b-middle, A1-bottom graph) was injected at time 0 to start the reaction. Data were fitted to the “nonlinear regression - kinetics of competitive binding” equation in GraphPad Prism v8.2.1 derived from Motulsky-Mahan equations (see methods) with the k_{on} , k_{off} and

concentration of fluorescent ligand constrained. K_3 is equal to the association rate of the unlabelled compound in units $M^{-1}min^{-1}$ and K_4 is equal to the disassociation rate in units min^{-1} . The K_d of the unlabelled compound derived from this analysis is also listed under each graph. Each graph is a representative trace of an individual experiment. More representative traces can be found in the appendix.

A1	k_{on} ($M^{-1}min^{-1}$)		k_{off} (min^{-1})		pK_d	
	mean	SEM	mean	SEM	mean	SEM
2-CADO	1.03E+05	± 4.64E+04	0.51	± 0.06	5.20	± 0.20
2'-MeCCPA	-	-	-	-	5.56	± 0.03
8-CPT	6.32E+08	± 2.30E+08	1.01	± 0.22	8.70	± 0.14
Adenosine	2.76E+05	± 8.56E+04	3.27	± 0.90	4.89	± 0.05
ANR 94	7.21E+05	± 4.03E+05	1.01	± 0.20	5.73	± 0.15
BAY 60-6583	1.59E+06	± 9.93E+05	0.89	± 0.48	6.21	± 0.06
Caffeine	-	-	-	-	4.17	± 0.06
Capadenoson	-	-	-	-	7.24	± 0.03
CCPA	-	-	-	-	5.68	± 0.05
CGH 2466	7.59E+08	± 6.07E+08	2.48	± 1.79	8.35	± 0.06
CGS 15943	2.03E+09	± 7.46E+08	3.00	± 0.51	8.73	± 0.07
CGS-21680	-	-	-	-	-	-
CI-IB-MECA	-	-	-	-	-	-
Cordycepin	-	-	-	-	4.02	± 0.13
CPA	1.98E+06	± 3.96E+05	3.16	± 0.43	5.74	± 0.04
CSC	-	-	-	-	-	-
CV 1808	-	-	-	-	4.41	± 0.07
DMPX	-	-	-	-	5.01	± 0.09
DPCPX	1.99E+09	± 1.06E+09	1.71	± 0.85	8.95	± 0.12
ENBA	2.76E+07	± 6.05E+06	7.81	± 0.98	6.51	± 0.05
Enprofylline	-	-	-	-	4.60	± 0.05
GR 79236	-	-	-	-	5.32	± 0.03
GS 6201	8.05E+06	± 3.35E+06	0.78	± 0.24	7.11	± 0.10
HEMADO	-	-	-	-	4.54	± 0.12
IB-MECA	3.55E+05	± 2.67E+05	1.02	± 0.28	5.19	± 0.12
Istradefylline	-	-	-	-	-	-
KW-3902	8.31E+08	± 2.69E+08	0.32	± 0.07	9.39	± 0.04
LUF 5834	-	-	-	-	6.85	± 0.16
MRE 3008F20	-	-	-	-	7.16	± 0.11
MRS 1191	-	-	-	-	-	-
MRS 1220	3.49E+07	± 1.92E+07	1.81	± 1.10	7.36	± 0.05
MRS 1334	4.11E+05	± 1.15E+05	1.60	± 0.33	5.40	± 0.11
MRS 1523	-	-	-	-	-	-

MRS 1706	1.21E+07 ± 3.95E+06	2.66 ± 0.35	6.63 ± 0.15
MRS 1754	8.58E+06 ± 5.57E+06	0.38 ± 0.15	7.18 ± 0.13
MRS 3777	- -	- -	5.35 ± 0.18
MRS 5698	- -	- -	- -
NECA	1.96E+05 ± 5.97E+04	1.07 ± 0.34	5.17 ± 0.10
PQ-69	1.18E+09 ± 5.67E+08	0.38 ± 0.15	9.45 ± 0.06
Preladenant	- -	- -	5.95 ± 0.06
PSB 0788	- -	- -	- -
PSB 10	1.75E+06 ± 8.77E+05	0.73 ± 0.25	6.27 ± 0.10
PSB 11	- -	- -	6.55 ± 0.08
PSB 1115	- -	- -	- -
PSB 36	6.44E+08 ± 2.33E+08	0.37 ± 0.15	9.19 ± 0.11
PSB 603	- -	- -	- -
Regadenoson	- -	- -	4.33 ± 0.20
Resveratrol	- -	- -	- -
R-PIA	- -	- -	5.94 ± 0.05
SCH-442,416	2.99E+06 ± 8.75E+05	1.51 ± 0.51	6.31 ± 0.05
SCH-58261	5.55E+06 ± 2.35E+06	0.90 ± 0.39	6.80 ± 0.06
SDZ WAG 994	1.39E+04 ± 5.40E+03	0.53 ± 0.20	4.41 ± 0.04
SLV320	1.22E+09 ± 8.70E+08	0.68 ± 0.29	8.98 ± 0.10
Theophylline	- -	- -	5.30 ± 0.11
Tozadenant	3.27E+05 ± 2.51E+04	0.71 ± 0.12	5.65 ± 0.09
VUF 5574	5.62E+05 ± 2.16E+05	0.71 ± 0.04	5.74 ± 0.13
XAC	1.51E+08 ± 3.00E+07	1.18 ± 0.39	8.08 ± 0.11
ZM-241,385	1.28E+07 ± 7.57E+06	1.38 ± 0.36	6.46 ± 0.22

Table 3.3. Summary of kinetic data for unlabelled adenosine receptor ligand set at the adenosine A1 receptor. Each of the 57 ligands was tested a minimum of 3 times at each of the 4 receptors. A “-” indicates that it was not possible to accurately determine a value. For some compounds it was not possible to accurately determine the kinetics of the ligand, however, pK_d values could still be obtained from the plateaus of the curves. In other cases, even pK_d values could not be accurately determined. In all cases n≥3.

A2a	k_{on} ($M^{-1}min^{-1}$)		k_{off} (min^{-1})		pK_d	
	mean	SEM	mean	SEM	mean	SEM
2-CADO	2.68E+05	± 1.46E+05	0.80	± 0.34	5.48	± 0.08
2'-MeCCPA	-	-	-	-	-	-
8-CPT	6.96E+06	± 2.56E+06	2.60	± 0.54	6.26	± 0.11
Adenosine	2.77E+05	± 1.14E+04	1.11	± 0.08	5.40	± 0.03
ANR 94	7.51E+06	± 1.91E+06	1.17	± 0.32	6.75	± 0.09
BAY 60-6583	-	-	-	-	-	-
Caffeine	2.31E+05	± 1.22E+05	3.08	± 1.03	4.80	± 0.11
Capadenoson	-	-	-	-	-	-
CCPA	-	-	-	-	4.69	± 0.14
CGH 2466	1.56E+06	± 3.46E+05	1.56	± 0.31	5.99	± 0.02
CGS 15943	1.37E+09	± 1.09E+08	0.30	± 0.05	9.64	± 0.10
CGS-21680	1.08E+06	± 1.58E+05	1.46	± 0.18	5.85	± 0.10
CI-IB-MECA	-	-	-	-	-	-
Cordycepin	1.51E+04	± 7.10E+03	0.52	± 0.14	4.32	± 0.12
CPA	-	-	-	-	4.60	± 0.19
CSC	3.96E+06	± 1.50E+06	0.54	± 0.10	6.78	± 0.09
CV 1808	5.13E+05	± 1.39E+05	0.74	± 0.15	5.82	± 0.07
DMPX	9.75E+05	± 3.30E+05	1.70	± 0.40	5.73	± 0.08
DPCPX	1.52E+07	± 3.80E+06	1.72	± 0.43	6.93	± 0.11
ENBA	3.77E+04	± 3.46E+03	1.23	± 0.30	4.49	± 0.08
Enprofylline	3.39E+04	± 1.42E+04	1.43	± 0.39	4.47	± 0.19
GR 79236	-	-	-	-	-	-
GS 6201	6.29E+07	± 3.25E+07	1.23	± 0.26	7.43	± 0.08
HEMADO	-	-	-	-	-	-
IB-MECA	-	-	-	-	-	-
Istradefylline	1.38E+07	± 7.89E+06	2.01	± 0.31	6.53	± 0.25
KW-3902	8.68E+07	± 2.81E+07	3.84	± 0.83	7.38	± 0.11
LUF 5834	-	-	-	-	-	-
MRE 3008F20	-	-	-	-	-	-
MRS 1191	-	-	-	-	-	-
MRS 1220	4.10E+07	± 1.87E+07	0.97	± 0.51	7.73	± 0.10
MRS 1334	9.11E+05	± 2.27E+05	2.90	± 0.46	5.39	± 0.09
MRS 1523	-	-	-	-	-	-

MRS 1706	6.00E+06 ± 1.78E+06	0.80 ± 0.24	6.87 ± 0.03
MRS 1754	2.28E+07 ± 1.68E+07	0.85 ± 0.29	6.85 ± 0.17
MRS 3777	-	-	-
MRS 5698	-	-	-
NECA	1.76E+06 ± 6.64E+05	1.64 ± 0.35	5.95 ± 0.08
PQ-69	2.96E+08 ± 2.32E+08	2.63 ± 0.70	7.59 ± 0.21
Preladenant	4.14E+08 ± 1.26E+08	0.16 ± 0.05	9.38 ± 0.09
PSB 0788	-	-	-
PSB 10	-	-	-
PSB 11	-	-	-
PSB 1115	-	-	-
PSB 36	3.69E+07 ± 1.65E+07	3.48 ± 1.35	6.89 ± 0.14
PSB 603	-	-	-
Regadenoson	2.64E+05 ± 2.94E+04	1.09 ± 0.19	5.40 ± 0.10
Resveratrol	-	-	-
R-PIA	-	-	5.13 ± 0.10
SCH-442,416	5.52E+08 ± 2.10E+08	0.44 ± 0.09	9.00 ± 0.13
SCH-58261	9.61E+08 ± 5.42E+08	1.48 ± 0.36	8.56 ± 0.10
SDZ WAG 994	-	-	-
SLV320	5.40E+06 ± 2.48E+06	2.14 ± 0.63	6.28 ± 0.16
Theophylline	-	-	5.36 ± 0.10
Tozadenant	5.52E+07 ± 2.11E+07	0.50 ± 0.10	7.94 ± 0.09
VUF 5574	-	-	-
XAC	2.80E+08 ± 1.60E+08	1.49 ± 0.35	8.00 ± 0.08
ZM-241,385	1.10E+09 ± 4.07E+08	0.90 ± 0.33	8.89 ± 0.15

Table 3.4. Summary of kinetic data for unlabelled adenosine receptor ligand set at the adenosine A2a receptor. Each of the 57 ligands was tested a minimum of 3 times at each of the 4 receptors. A “-” indicates that it was not possible to accurately determine a value. For some compounds it was not possible to accurately determine the kinetics of the ligand, however, pK_d values could still be obtained from the plateaus of the curves. In other cases, even pK_d values could not be accurately determined. In all cases n≥3.

A2b	k_{on} ($M^{-1}min^{-1}$)		k_{off} (min^{-1})		pK_d	
	mean	SEM	mean	SEM	mean	SEM
2-CADO	-	-	-	-	3.66 ± 0.08	
2'-MeCCPA	-	-	-	-	-	-
8-CPT	-	-	-	-	6.11 ± 0.09	
Adenosine	-	-	-	-	-	-
ANR 94	6.17E+04 ± 2.74E+04		0.88 ± 0.37		4.83 ± 0.03	
BAY 60-6583	-	-	-	-	6.31 ± 0.05	
Caffeine	-	-	-	-	4.10 ± 0.08	
Capadenoson	-	-	-	-	-	-
CCPA	-	-	-	-	-	-
CGH 2466	-	-	-	-	7.42 ± 0.07	
CGS 15943	-	-	-	-	8.13 ± 0.11	
CGS-21680	-	-	-	-	-	-
CI-IB-MECA	-	-	-	-	-	-
Cordycepin	-	-	-	-	-	-
CPA	-	-	-	-	-	-
CSC	-	-	-	-	-	-
CV 1808	-	-	-	-	-	-
DMPX	-	-	-	-	5.12 ± 0.13	
DPCPX	-	-	-	-	7.18 ± 0.12	
ENBA	-	-	-	-	4.06 ± 0.13	
Enprofylline	-	-	-	-	5.11 ± 0.03	
GR 79236	-	-	-	-	-	-
GS 6201	1.81E+08 ± 4.83E+07		0.34 ± 0.06		8.67 ± 0.07	
HEMADO	-	-	-	-	-	-
IB-MECA	-	-	-	-	-	-
Istradefylline	-	-	-	-	-	-
KW-3902	-	-	-	-	7.58 ± 0.09	
LUF 5834	-	-	-	-	-	-
MRE 3008F20	-	-	-	-	-	-
MRS 1191	-	-	-	-	-	-
MRS 1220	4.98E+06 ± 2.40E+06		0.74 ± 0.30		6.42 ± 0.33	
MRS 1334	-	-	-	-	-	-
MRS 1523	-	-	-	-	-	-

MRS 1706	7.71E+06 ± 4.86E+06	0.59 ± 0.30	6.93 ± 0.22
MRS 1754	7.01E+06 ± 2.45E+06	0.20 ± 0.04	7.44 ± 0.12
MRS 3777	-	-	-
MRS 5698	-	-	-
NECA	-	-	4.31 ± 0.12
PQ-69	6.45E+07 ± 1.30E+07	1.61 ± 0.60	7.55 ± 0.17
Preladenant	-	-	-
PSB 0788	3.58E+07 ± 1.16E+07	0.16 ± 0.05	8.31 ± 0.03
PSB 10	-	-	-
PSB 11	-	-	-
PSB 1115	7.79E+06 ± 1.87E+06	0.84 ± 0.32	6.98 ± 0.15
PSB 36	-	-	7.06 ± 0.11
PSB 603	2.08E+08 ± 8.34E+07	0.22 ± 0.03	8.88 ± 0.13
Regadenoson	-	-	-
Resveratrol	-	-	-
R-PIA	-	-	-
SCH-442,416	2.94E+05 ± 2.34E+05	0.74 ± 0.46	5.35 ± 0.17
SCH-58261	-	-	6.42 ± 0.14
SDZ WAG 994	-	-	-
SLV320	-	-	5.30 ± 0.07
Theophylline	-	-	4.74 ± 0.14
Tozadenant	-	-	5.62 ± 0.06
VUF 5574	-	-	-
XAC	7.31E+07 ± 2.25E+07	0.58 ± 0.07	7.88 ± 0.08
ZM-241,385	3.08E+07 ± 8.84E+06	1.92 ± 0.78	7.11 ± 0.29

Table 3.5. Summary of kinetic data for unlabelled adenosine receptor ligand set at the adenosine A2b receptor. Each of the 57 ligands was tested a minimum of 3 times at each of the 4 receptors. A “-” indicates that it was not possible to accurately determine a value. For some compounds it was not possible to accurately determine the kinetics of the ligand, however, pK_d values could still be obtained from the plateaus of the curves. In other cases, even pK_d values could not be accurately determined. In all cases n≥3.

A3	k_{on} ($M^{-1}min^{-1}$)		k_{off} (min^{-1})		pK_d	
	mean	SEM	mean	SEM	mean	SEM
2-CADO	-	-	-	-	5.49 ± 0.24	
2'-MeCCPA	-	-	-	-	4.92 ± 0.08	
8-CPT	-	-	-	-	5.25 ± 0.05	
Adenosine	-	-	-	-	5.07 ± 0.13	
ANR 94	1.21E+04 ± 4.41E+03		1.53 ± 0.73		3.90 ± 0.09	
BAY 60-6583	2.97E+05 ± 7.43E+04		0.26 ± 0.07		6.04 ± 0.09	
Caffeine	-	-	-	-	-	-
Capadenoson	-	-	-	-	-	-
CCPA	-	-	-	-	5.38 ± 0.05	
CGH 2466	-	-	-	-	7.43 ± 0.11	
CGS 15943	-	-	-	-	7.93 ± 0.12	
CGS-21680	-	-	-	-	-	-
CI-IB-MECA	-	-	-	-	7.22 ± 0.17	
Cordycepin	-	-	-	-	-	-
CPA	-	-	-	-	5.16 ± 0.13	
CSC	-	-	-	-	-	-
CV 1808	-	-	-	-	-	-
DMPX	-	-	-	-	4.04 ± 0.16	
DPCPX	-	-	-	-	6.28 ± 0.08	
ENBA	-	-	-	-	5.53 ± 0.04	
Enprofylline	-	-	-	-	3.64 ± 0.05	
GR 79236	-	-	-	-	-	-
GS 6201	-	-	-	-	6.80 ± 0.10	
HEMADO	1.62E+07 ± 2.75E+06		1.98 ± 0.42		6.97 ± 0.12	
IB-MECA	-	-	-	-	6.77 ± 0.21	
Istradefylline	-	-	-	-	-	-
KW-3902	-	-	-	-	6.32 ± 0.12	
LUF 5834	-	-	-	-	-	-
MRE 3008F20	1.44E+08 ± 2.79E+07		0.12 ± 0.02		9.04 ± 0.15	
MRS 1191	3.75E+06 ± 6.34E+05		0.53 ± 0.16		6.87 ± 0.05	
MRS 1220	1.65E+08 ± 3.98E+07		0.19 ± 0.03		8.97 ± 0.12	
MRS 1334	1.12E+07 ± 4.24E+06		0.71 ± 0.27		7.05 ± 0.21	
MRS 1523	7.16E+06 ± 1.67E+06		0.60 ± 0.28		7.20 ± 0.13	

MRS 1706	-	-	-	-	6.20 ± 0.08
MRS 1754	1.63E+06 ± 5.33E+05		0.57 ± 0.21		6.26 ± 0.31
MRS 3777	1.23E+07 ± 4.28E+06		0.76 ± 0.11		7.15 ± 0.10
MRS 5698	1.60E+07 ± 5.61E+06		0.34 ± 0.11		7.51 ± 0.17
NECA	4.09E+04 ± 2.60E+04		1.20 ± 0.61		4.45 ± 0.25
PQ-69	1.49E+08 ± 4.08E+07		0.05 ± 0.02		9.48 ± 0.09
Preladenant	-	-	-	-	4.58 ± 0.09
PSB 0788	-	-	-	-	-
PSB 10	2.16E+08 ± 1.70E+07		0.22 ± 0.02		8.99 ± 0.05
PSB 11	7.03E+07 ± 2.33E+07		0.31 ± 0.12		8.32 ± 0.09
PSB 1115	-	-	-	-	-
PSB 36	-	-	-	-	5.63 ± 0.14
PSB 603	-	-	-	-	-
Regadenoson	-	-	-	-	5.06 ± 0.09
Resveratrol	-	-	-	-	-
R-PIA	-	-	-	-	6.15 ± 0.16
SCH-442,416	-	-	-	-	6.27 ± 0.15
SCH-58261	-	-	-	-	5.90 ± 0.19
SDZ WAG 994	-	-	-	-	3.72 ± 0.08
SLV320	-	-	-	-	6.33 ± 0.06
Theophylline	-	-	-	-	3.99 ± 0.14
Tozadenant	-	-	-	-	5.56 ± 0.06
VUF 5574	2.91E+08 ± 8.81E+07		0.20 ± 0.03		9.10 ± 0.10
XAC	5.01E+07 ± 1.59E+07		1.03 ± 0.24		7.67 ± 0.09
ZM-241,385	-	-	-	-	5.80 ± 0.19

Table 3.6. Summary of kinetic data for unlabelled adenosine receptor ligand set at the adenosine A3 receptor. Each of the 57 ligands was tested a minimum of 3 times at each of the 4 receptors. A “-” indicates that it was not possible to accurately determine a value. For some compounds it was not possible to accurately determine the kinetics of the ligand, however, pK_d values could still be obtained from the plateaus of the curves. In other cases, even pK_d values could not be accurately determined. In all cases $n \geq 3$.

To visualise the relationships between pK_d and k_{on} or k_{off} these values for the whole data were plotted in scatter plots (Figure 3.5).

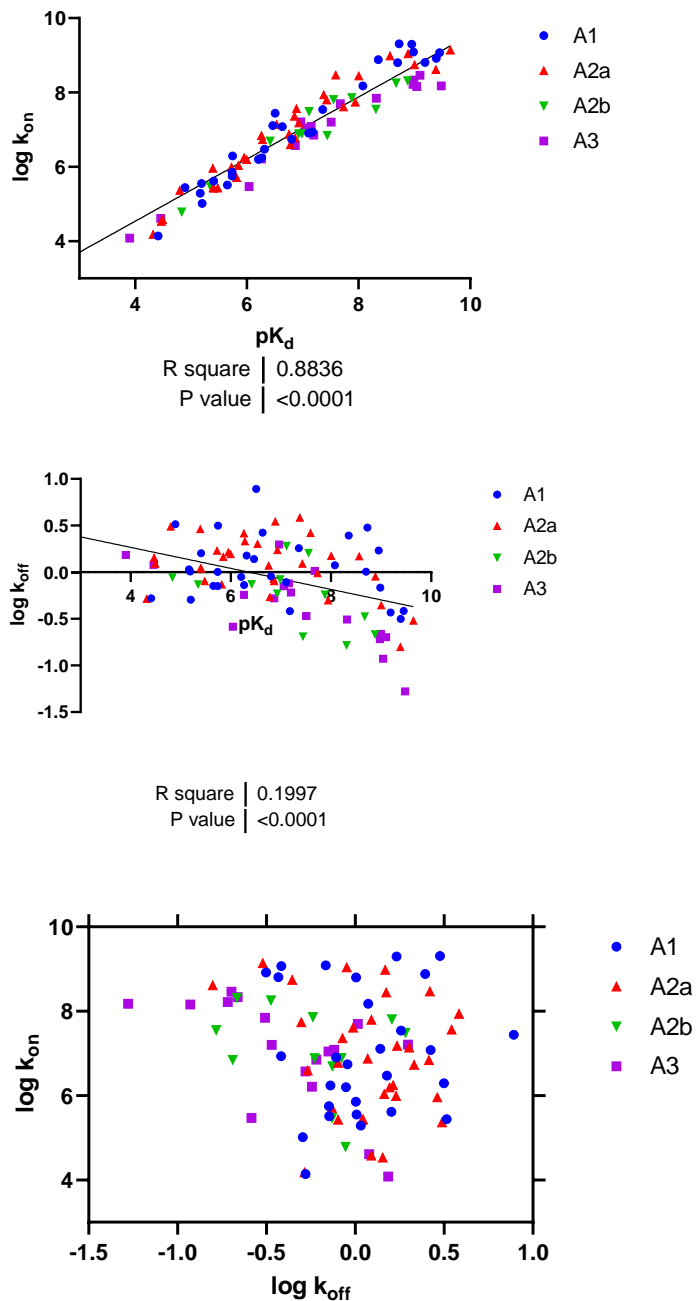


Figure 3.5. Pooled kinetic data from unlabelled compounds. A) \log values of the association rate plotted against the affinity values for the 8 compounds at each receptor. B) \log values of the disassociation rate plotted against the affinity values for the 8 compounds at each receptor. C) \log values of the association rate plotted against \log values of the disassociation rate. In all

cases blue circles represent A1, red triangles pointing up represent A2a, green triangles point down represent A2b, and purple squares represent A3. R squared value determined by Spearman's ranks correlation.

It appears that k_{on} correlates more strongly with pK_d than k_{off} correlates with pK_d . The range of k_{on} values can be seen across approximately 4 orders of magnitude, while the range of k_{off} values spans less than 2 orders of magnitude. These observations appear consistent across all 4 receptors.

3.2.4 Fluorescence interference from unlabelled compounds.

For many compounds the highest possible concentration was not limited by solubility or cost, but by the inability to rule out fluorescence interference between the test compound and the tracer or the terbium labelled receptor. Our group was simultaneously preparing to screen a fragment library using the same experimental set up but using the dopamine D2 receptor. Here we tested 10 known Pan Assay INterfering compounds (PAINs) to help characterise the types of interference that may be seen in a TR-FRET assay.

1. Congo red
2. Indigo
3. Deferoxamine
4. Rottlerin
5. Fluorescein
6. Maleimide
7. 8-Hydroxyquinoline
8. PKF T18-310
9. Acid blue
10. Rhodamide

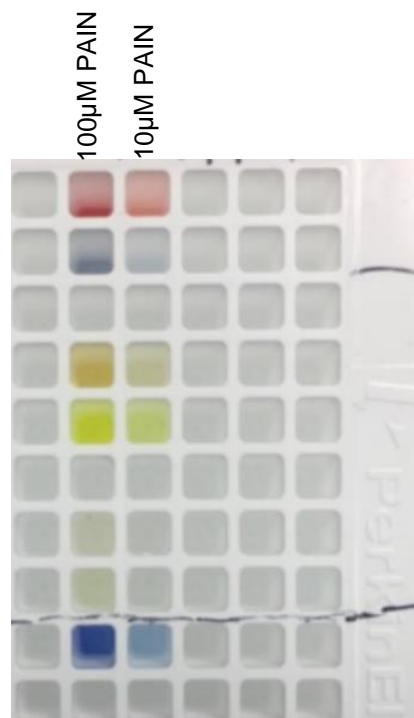
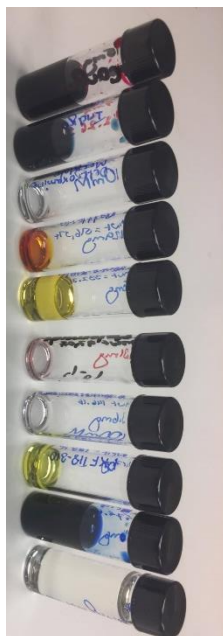


Figure 3.6. Pictures of 10 known Pan Assay INterfering compounds

(PAINs). Left picture shows the PAINs in glass aliquots at stock concentrations of 10^{-1} – 10^{-2} M. Right picture shows the PAINs in a portion of a white 384-well Opti plate at 100 and 10µM. The PAINs display a range of colours or in the case of deferoxamine, 8-hydroxyquinoline and rhodamine little to no visible colour at the concentrations present.

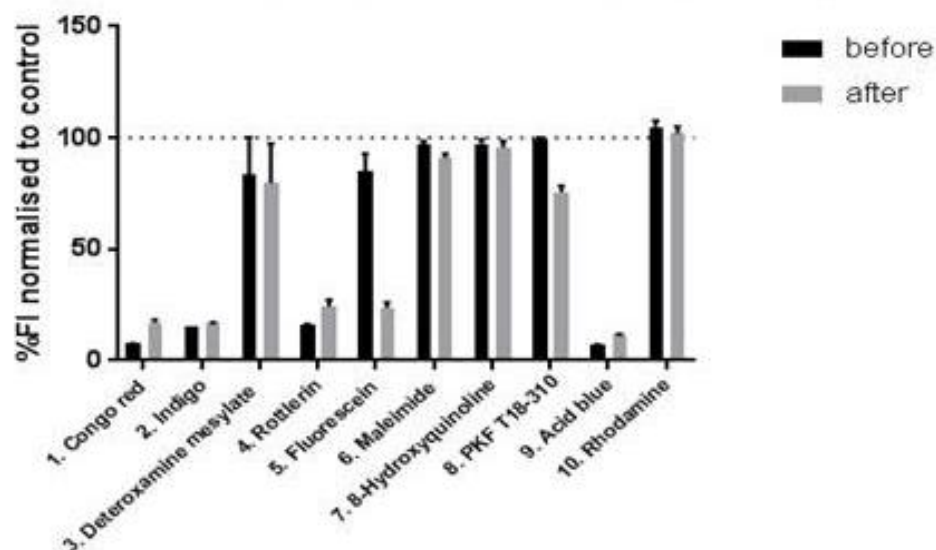


Figure 3.7. Fluorescence intensity (FI) of assay wells containing 100 μ M Pan Assay Interfering compounds (PAINs) and 25nM fluorescently labelled spiperone, before and after addition of 1 μ g of cell membranes expressing the dopamine D2 receptor. FI read on a Pherastar plate reader excitation 650nm, emission 665nm. FI normalised to DMSO control. N=3, mean \pm SEM.

From assessing the PAINs in Figure 3.7 it is clear several compounds quenched the signal of the fluorescent tracer. Interestingly, it appears some PAINs, in particular fluorescein, had a greater quenching effect after membrane had been added to the well. Additionally, several compounds appeared to quench the signal given off by the terbium (emission 620nm) which should remain relatively constant throughout the assay run (data not shown).

With this knowledge derived from looking at known PAINs, extra care was taken to check FI before and after a run, and to check the terbium signal when looking at the unlabelled adenosine compounds. If deviation in FI or terbium signal was observed in a well that data had to be excluded. An example where a compound behaved like a PAIN was resveratrol.

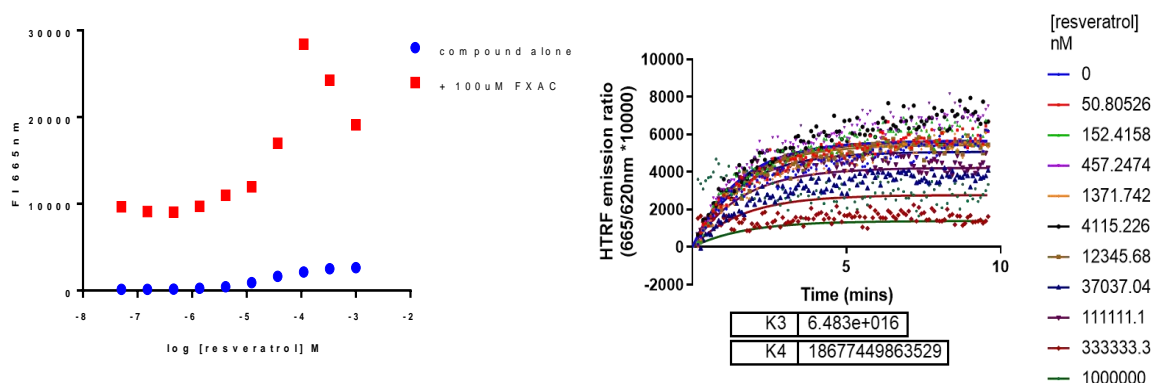


Figure 3.8. Example of a compound where it was impossible to obtain meaningful data due to low affinity and fluorescent interference at high concentration – resveratrol at the A3 receptor. Left – Fluorescence Intensity (FI) (650nm excitation, 665nm emission) of increasing concentrations of resveratrol with (red) or without (blue) 100 μ M a fluorescent-XAC derivative CA200645. Right – observed specific binding of fluorescent-XAC derivative CA200645 100 μ M in the presence of various concentrations of resveratrol over a 10min period. Data is fit to a Motulsky-Mahan competition model in GraphPad Prism to derive an association rate (K3) in M⁻¹min⁻¹ and a disassociation rate (K4) in min⁻¹ for resveratrol at the adenosine A3 receptor.

From Figure 3.8 it can be observed that resveratrol exhibits a detectable fluorescence when excited at 650nm and emission read at 665nm in the given experimental set up, at least above 10 μ M. When fluorescent ligand is added the FI is potentiated significantly. When attempting to measure the kinetics of the ligand at the A3 receptor it is clear model is unable to fit to the data given massive dissociation rate.

3.3 Discussion

Evaluating positives and negatives of the assays

Once the optimised conditions were determined, obtaining the kinetics of the fluorescent ligands was relatively straightforward. Achieving this quantity of data using conventional radioligand binding experiments would have taken many times more laboratory hours and resources. Much of the inter-experimental variation is likely due to difficulties in handling highly lipophilic fluorescent ligands of this nature. From experience, any deviation in the protocol in preparing the ligands (types of test tubes used, sonication times, batch freshness, room temperature etc) can have profound effects in the final assay concentration achieved. While every effort was made to minimise inconsistencies, some variation is still likely to have occurred. Fortunately, when conducting competition binding studies, provided one working stock of the tracer is well characterised on the same plate as test compounds, the measured kinetics of the test compounds should be largely unaffected by variation in the actual concentration of tracer.

The kinetic properties of candidate drugs are often overlooked in the drug discovery process, particularly in the early stages. This is either because of the added effort and resources required when measuring the kinetics of a large number of compounds from a library, or simply because the researcher only deems affinity as an important parameter. However, here it has been demonstrated that a reasonable throughput assay can be developed which measures kinetics of unlabelled compounds. This is particularly useful if the kinetics of the desired drug are well defined and validated, or for detailed SAR studies investigating many compounds. For example, if a drug is desired to have a short residence time (a high k_{off}) but a high affinity (i.e. a high association rate as well), traditionally only lead compounds showing the highest affinities would be screened in a kinetic assay. Compounds showing medium affinities, but desirably short residence times, would be discarded. By screening kinetically early on these types of compounds could be

identified and modified in multiple iterations to arrive at a ligand with the optimal properties.

Clearly it was not possible to detect all compounds kinetically or for some even at steady state. This is of course a feature any drug discovery assay as compounds with too low affinities cannot be measured for multiple reasons (mainly solubility) and in this assay further difficulties were observed. When screening compounds known to be selective at one adenosine receptor it is not surprising that a low affinity is observed at one or more other receptors. Here however two extra complications occur. Firstly, if a compound has too fast a dissociation rate relative to the tracer the Motulsky-Mahan model does not accurately fit the data and the results must be discarded (Sykes et al., 2019). Secondly, certain compounds displayed one or more types of fluorescent interference in the assay in a concentration dependent manner.

As described above, Pan Assay INterfering compounds (PAINs) can disrupt drug screening programs, in particular by creating false positive results. This can lead to an inability to accurately determine the pharmacological properties of candidate drugs, and, if unnoticed, the progression of compounds through the drug discovery process that will ultimately lack *in vitro* to *in vivo* translation.

As evidenced by this study, many “unlabelled compounds” exhibit detectable fluorescence in the plate reader used and can potentiate or quench the signal from labelled ligands or receptors. Even some high affinity compounds were not able to be measured kinetically for these reasons. The prevalence of this is clearly a limitation of the assay, particularly when using low affinity compounds where high concentrations are required to achieve substantial ligand-receptor binding. The rigorous checking of fluorescence intensity of labelled ligand and receptor at each stage of the assay is therefore necessary for robustness and accuracy of data as here many test compounds were found to be PAINs. This is likely underappreciated currently in

many drug discovery programs and, while potentially time consuming in the short term, could save time and money in the longer term.

The measured kinetics of the compounds

When considering fluorescent ligands, one might assume that pharmacophore alone would govern measured affinity and kinetic values. As such, for the 8 fluorescent compounds in this study (all with XAC as the pharmacophore) it might be assumed there would be very little difference in k_{on} , k_{off} and K_d values between ligands. However, a large range of properties were observed across the series at both receptors. This has been found with other series of fluorescent ligands and modelling has alluded to specific interactions between linker regions and receptor (Vernall et al., 2013).

The range of affinity values across the series for a given receptor appeared to be driven association rate and not dissociation rate as shown by the correlation plots (Figure 3.5). This opposes a belief held by many that only dissociation rate/residency time is important for drug action (Copeland et al., 2006b; Copeland, 2016). Other studies have also found association rate to be the key driver of affinity across a set of ligands for a receptor (Sykes et al., 2014). Interestingly however, the ligands showed greater affinity for the A2b receptor with very little difference in association rates. So, association rate appears to be the driver in affinity across the series of ligands for a given receptor, but dissociation rate appears to be the driver in selectivity across receptors. If association rate was being driven by an external factor such as local concentration, then one may expect to see results like this as the effect would be receptor non-specific and dissociation rate would be driving affinity across receptors as observed here.

When contemplating the relative contributions of pharmacophore, linker, and fluorophore to binding kinetics it is tempting to compare fluorescent ligands to their unlabelled counterpart. This should be caveated from the outset by noting the covalent attachment of a linker region could be altering a region of the pharmacophore that is important

for binding. With this caveat in mind, XAC has a similar affinity for both A2a and A2b receptors (9.9nM and 13.3nM), with A2a having a 3.8-fold higher association rate and a 2.6-fold higher dissociation rate compared to A2b. The mean affinities of the fluorescent XAC-based ligands for A2a and A2b were 573nM and 181nM respectively, with A2a having a 1.2-fold lower association rate and a 4.0-fold higher dissociation rate. Clearly the addition of a linker and fluorophore reduced the affinity of XAC to the A2a and A2b receptors (57.7 and 13.7-fold respectively). This corresponds to a decrease in association rate (53.1 and 11.3-fold respectively) and an increase in dissociation rate (2.9 and 4.4-fold respectively).

Here membrane preparations were used instead of intact cells so as to better reflect a one compartment model that is necessary for the fitting of the Motulsky-Mahan equation. A detergent (saponin) was also added to further disrupt micelles that may have formed and may have provided further inaccessible receptor compartments similarly to a whole cell. According to the ternary complex model, agonists have higher affinities for GPCR-G protein complexes compared to receptor alone. This again presents a problem in fitting data to the Motulsky Mahan equation as agonists can exhibit two affinities/kinetics at the same time. As such, GppNHp, an analogue of GTP, was added to the membranes to irreversibly bind G protein, ensuring receptors were maintained in their uncoupled form. In one study the kinetics of NECA at the A2a receptor was found to be unchanged by the presence of GTP (Guo et al., 2012b), however, another study found at the A3 receptor that dissociation rate, but not association rate, was affected by the presence of GTP (Xia et al., 2018).

An alternative explanation for differences in measured kinetic properties is the physicochemical properties of the fluorescent compound linkers and fluorophores and not any specific interactions with the receptors. More lipophilic compounds could be present in higher concentrations in the immediate vicinity of the membrane bound receptors. This hypothesis could explain the apparent association rate-driven

differences in affinity as k_{on} but not k_{off} is dependent on ligand concentration. The true affinities across the series thus may be more similar than the 'apparent' or 'measured' affinities. The differences in k_{off} values between the ligands at each receptor may be real (as the non-specific concentrating effect of physicochemical properties would likely be equal for each membrane preparation) and reflect real differences in strength of interaction between receptor and ligand.

To explore this hypothesis we needed to measure the physicochemical properties of all the ligands in the study.

Chapter 4 – Characterising the physicochemical properties of a series of adenosine receptor compounds using *in silico* approaches and immobilised artificial membrane high performance liquid chromatography (IAM-HPLC)

4.1 Introduction

Physicochemical properties (such as lipophilicity, solubility, molecular weight, polar surface area, hydrogen bond donors and acceptors, and charge) are key determinants in the progression and selection of candidate compounds throughout the drug discovery progress (Hollósy et al., 2006). These properties are used to model pharmacokinetic parameters such as absorption, distribution, metabolism, and excretion (ADME). Seemingly arbitrary cut off points can be applied to drug discovery programs to exclude compounds with undesirable properties. Perhaps the most famous set of guidelines in pharmacology is 'Lipinski's rule of five' (Lipinski et al., 1997). Lipinski *et al.* found that around 90% of orally available small molecules in the World Drug Index at the time could be described as having a molecular weight of less than 500 Daltons, a calculated log P value of less than 5, 5 or fewer hydrogen bond donors, and 10 or fewer hydrogen bond acceptors. This seminal paper has been cited over 6000 times. Subsequently other criteria have been proposed for example compound must have both ≤ 10 rotatable bonds and polar surface area $\leq 140 \text{ \AA}^2$ (or 12 or fewer H-bond donors and acceptors) (Veber et al., 2002).

Of particular interest to us, in addition to classical pharmacokinetic considerations, lipophilicity and other physicochemical properties can drive compounds to concentrate in and around cell membranes (Sargent and Schwyzer, 1986; Sykes et al., 2014). This falls under the remit of 'micro-pharmacokinetics' and could be of high importance to

membrane bound targets (Sykes et al., 2014; Vauquelin, 2015; Gherbi et al., 2018). Lipophilicity/hydrophobicity of a compound is usually quantified in two ways: (1) the log of the partition coefficient (P), defined as the ratio of an unionised form of a molecule between aqueous and lipophilic (typically octanol) phases at equilibrium or (2) the log of the distribution coefficient (D), defined as the ratio of the sum of unionised + ionised forms of a molecule between aqueous and lipophilic phases at equilibrium, at a given pH. For non-ionisable compounds log P will always be equal to log D at any pH. Similarly, if a compound exists at 100% in the unionised state at a given pH then its log P will equal its log D measured at that specific pH. However, if a molecule has one or more positive or negative charges at the measured pH, then its log D will be less than its log P. This is because the charged species have increased affinity for the aqueous over the non-polar environment relative to the uncharged. As such log D values are perhaps more physiologically relevant. However, log P has the advantage over log D in that only one value is needed for a molecule. In practise, most of these values will be estimated *in silico* and not measured.

It is worth noting that, although often used interchangeably, the terms hydrophobic and lipophilic are not quite synonyms as some substances can be described by the former but not the later (e.g. fluorocarbons and silicones). Hydrophobes appear to repel water due to their absence of attraction and the tendency of water to exclude molecules that are non-polar. Non-polar lipophilic compounds are attracted to non-polar organic solvents, like oils and lipids, due to London dispersion forces (aka instantaneous dipole-induced dipole forces), a type of van der Waals force (Adair et al., 2001). The other two van der Waals forces are the Keesom interaction (between two permanent dipoles) and the Debye interaction (between a permanent dipole and a non-permanent dipole). Hydrogen bonding involves two permanent dipoles but is regarded as a distinct force from van der Waal forces. Hydrogen bonding is specifically between an electronegative atom (typically second row elements fluorine, nitrogen or oxygen) and a hydrogen

atom that is covalently linked to another electronegative atom (Arunan et al., 2011; Weinhold and Klein, 2014). The small size of the hydrogen atom allows for a reduced distance between two dipoles or charges, and a greater strength of bond relative to the van der Waal forces (Muller, 1994).

Practically speaking log P and log D can be measured using the 'shake-flask' method (Dearden and Bresnen, 1988; Takács-Novák and Avdeef, 1996). Compound is mixed with unionised water (log P) or ionised water at a given pH (log D) and octanol in a flask and shaken. As the two solvents are immiscible and have different densities the concentration of compound in each phase can be easily measured by various techniques including UV/VIS spectroscopy. Alternatively, log P/log D values can be calculated (clog P/clog D) instantaneously by various computer softwares that break down the structure and assess the contribution every given fragment is likely to have to the overall molecule (Viswanadhan et al., 1989; Klopman et al., 1994; Csizmadia et al., 1997; Bouchard et al., 2001).

High-performance liquid chromatography (HPLC) is a technique whereby a sample dissolved in solvent is pumped through a pressured system containing a column with a solid phase. Different samples, or components of the same sample, will have different affinities for the column, and therefore take differing amounts of time between sample addition and detection/excretion from the system. This is normally used for the identification/quantification or separation/purification of components of a sample. However, reverse-phase HPLC (RP-HPLC) can also be used to measure lipophilicity/hydrophobicity of compounds using columns packed with hydrocarbon chains as the stationary phase. 'Reverse-phase' refers to using columns that are lipophilic in the stationary solid phase, as opposed to the earlier developed 'normal-phase' columns containing hydrophilic stationary phases such as unmodified silica. The retention times of compounds in this system correlates with their octanol-water partition coefficients and thus, with use of standard compounds and a calibration curve, can be used as a

surrogate method to obtain log D/log P values. This approach is more amenable to high throughput drug discovery than the labour-intensive flask method. Additionally, experimental data is likely more accurate than computer-based predictive models.

However, the lipid bilayer of the cell membrane is more complicated than a simple partition between octanol and water. Most notably, phospholipids are amphiphilic, containing a hydrophilic head group and lipophilic tail. The charged head groups lining the outside of the membrane can both attract or repel certain compounds, and therefore log P/log D values alone are unlikely to comprehensively predict membrane affinity. As such, alternative approaches have been introduced including the use of immobilised artificial membranes (IAMs) as the stationary phase of HPLC as developed by Pidgeon and colleagues (Markovich et al., 1989; Pidgeon and Venkataram, 1989; Ong et al., 1994, 1995). These IAM columns consist of a monolayer of phosphatidylcholine, the most abundant phospholipid in cell membranes, covalently bonded to amino-propyl silica phases (Figure 4.1). The retention factors generated using this biomimetic technique (k_{IAM}) have been shown to correlate well with liposome partition coefficients derived from other more labour-intensive methodology (Ong et al., 1995; Cohen and Birdsall, 1996; Caldwell et al., 1998). These k_{IAM} values are related to the retention time of the solute (t_r) and the retention time of a highly hydrophilic control that has essentially zero affinity for the stationary phase, also known as the dead time (t_0).

$$\text{Equation 4.1} \quad k_{IAM} = \frac{(t_r - t_0)}{t_0}$$

Retention time is independent of compound concentration, injection volume and purity (Valkó, 2004) (although all these things can be optimised to provide clearer data). Unless otherwise stated, k_{IAM} values generally refer to when the mobile phase is a 100% aqueous solvent. Hydrophilic compounds can be eluted in 100% aqueous mobile phase in second to minutes so k_{IAM} values are simple to obtain. For more lipophilic compounds (those that can't be eluted in under 10 minutes

under these conditions) it is necessary to add an amount of organic solvent (such as acetonitrile) to the mobile phase to maintain a reasonable throughput. This can be done isocratically (the ratio of aqueous to organic solvent in the mobile phase is constant in a given run) several times to obtain apparent k_{IAM} values at different concentrations of organic solvent. These values can be extrapolated back to give an estimate of what the k_{IAM} value would be if the mobile phase were 100% aqueous (in literature this value is sometimes referred to as $k_{IAM(w)}$, $k_{IAM100\%aq}$ or $k_{IAM(0)}$). Repeating this several times for a single compound can still be quite time consuming, especially if the optimal range of organic solvent is unknown. Therefore, if a large number of compounds need to be screened, it is possible to do this isocratic extrapolation method only for several standard compounds. A gradient protocol can then be devised where the concentration of organic solvent is gradually increased over time. A linear calibration curve can then be made with $k_{IAM(w)}$ values of standard on one axis, and gradient retention times (t_g) on the other. The test compounds can be screened in the gradient protocol and their gradient retention times converted to k_{IAM} values with the calibration curve.

Another potentially useful measurement that can be obtained from this technique is the Chromatographic Hydrophobicity Index (CHI IAM) of compounds. This is the concentration (v/v%) of acetonitrile required for a compound to have an equal affinity for the stationary and mobile phases (i.e. the retention time is double the dead time and $k_{IAM}=1$ or $\log k_{IAM}=0$). In order for consistent interlaboratory comparisons to be made, Valko *et al.* have suggested every laboratory could calibrate their gradient retention times to the CHI IAM values from the Valko lab (Valko *et al.*, 2000).

Retention factors in theory are linearly proportional to IAM partition coefficients (K_{IAM}) as per the equation below where V_m is the volume of the mobile phase and V_s the volume of the stationary phase.

$$\text{Equation 4.2} \quad K_{IAM} = \left(\frac{V_m}{V_s}\right) k_{IAM} = \phi k_{IAM}$$

The constant (V_m/V_s) (also known as the phase ratio, sometimes denoted as ϕ) is dependent on the experimental setup of a given lab. The phase ratio is necessary because the volumes of each phase are unlikely to be equal, thus biasing the apparent affinity for one phase over the other (Taillardat-Bertschinger et al., 2003). In most papers k_{IAM} is never converted to K_{IAM} because due the linear relationship between the two values k_{IAM} is sufficient for rank ordering a series of compounds or for drawing correlations with other variables. While calculating V_m is straight forward (simply the dead time in minutes multiplied by the flow rate in millilitres per minute), calculating V_s is more challenging. A couple of papers have attempted to make this conversion either by approximating V_s (Taillardat-Bertschinger et al., 2002), or by making a calibration curve using compounds where $\log P$ is assumed to equal K_{IAM} (Hollósy et al., 2006).

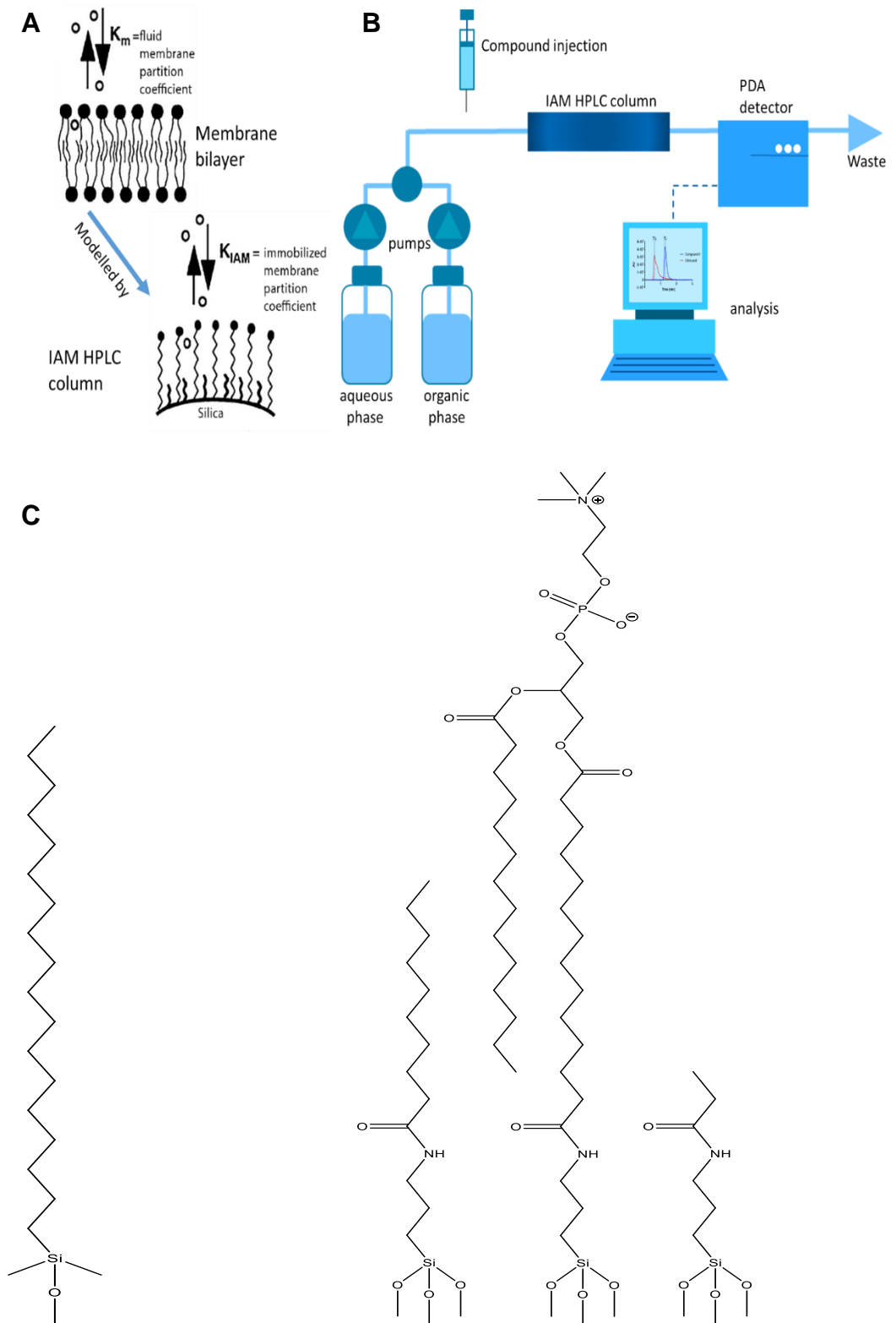


Figure 4.1. Overview of immobilised artificial membrane high-performance liquid chromatography. (A) Schematic showing how the membrane partition coefficient (K_m) for a compound between fluid and a lipid bilayer is modelled by its immobilised artificial membrane coefficient (K_{IAM})

between fluid and a monolayer of lipid on a silica surface. (B) Schematic of the experimental set of IAM-HPLC. In short, aqueous and/or organic solvents are pumped into the system at desired concentrations and mixed. Compound is injected into the system and then passes through the IAM column before being detected by a photodiode-array (PDA) detector and ejected into a waste container. The greater the affinity between a compound and IAM the greater the time taken between injection and detection (for more detail see methods section). (C) Chemical structure of the solid phase of a typical C₁₈ column used to determine traditional lipophilicity measurements (left), and of the solid phase of a IAM.PC.DD2 column (right).

The aim of this Chapter is to characterise the physicochemical properties of a series of 57 commercially available adenosine receptor compounds and a series of 8 fluorescently labelled adenosine compounds. This will include obtaining various *in silico* measurements based on chemical structures, as well as the optimisation of an immobilised artificial membrane high performance liquid chromatography (IAM-HPLC) assay. These values will be accessed in relation to the compounds' receptor-ligand binding kinetics and local concentrating effects in Chapter 5.

4.2 Results

4.2.1 Brief overview of how compounds were stratified into three different screening methods

Obtaining retention factors for each compound in this study was ultimately achieved using one of three methods:

1. The most hydrophilic compounds ($\text{cLog D pH7.4} < \sim -0.25$) would elute in less than 10mins with a 100% aqueous mobile phase.
2. The more lipophilic compounds ($\sim -0.25 < \text{cLog D pH7.4} < \sim 6$) would take longer than 10mins to elute in 100% aqueous mobile phase. These compounds were therefore screened using a gradient protocol with increasing concentration of organic mobile

phase. All unlabelled compounds that were not screened by method 1 were screened using this method.

3. The fluorescent compounds had gradient retention times that were too far out of the range of the standard compounds used and were therefore unsuitable for method 2. These compounds were isocratically screened at multiple concentrations of organic mobile phase and $\text{Log } k_{\text{IAM}100\% \text{aqueous}}$ obtained by extrapolation.

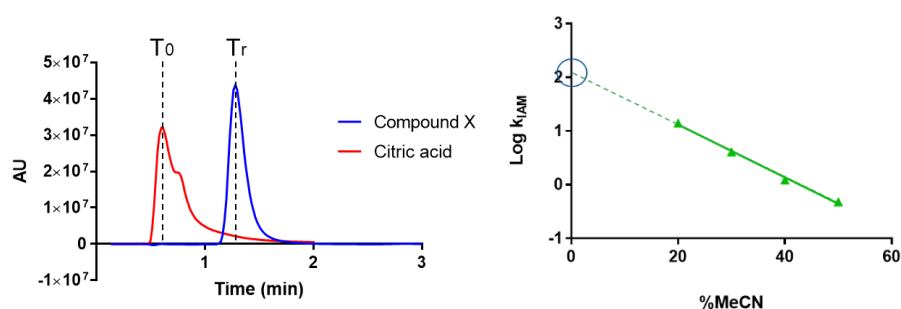


Figure 4.2. Example IAM HPLC data. (Left) Example trace of time taken post-injection for citric acid (red) and compound X (blue) to be detected. As citric acid has essentially no affinity for the IAM, the time take for it to pass through the system represents the dead time (T_0) of the system. The retention time for the compound (T_r) can then be used, along with the T_0 measured that day, to calculate the k_{IAM} of the compound as per equation 4.1. (Right) Example of how k_{IAM} values determined at multiple concentrations of organic solvent can be plotted and extrapolated to give an estimate for k_{IAM} in 100% aqueous conditions.

4.2.2 Optimisation of gradient protocol

A series of seven phenone compounds, with aliphatic tails of varying length, were used as standard compounds (Figure 4.3) as previously described (Valko et al., 2000). These compounds were individually screened isocratically at several concentrations of organic mobile phase to obtain extrapolated $k_{\text{IAM}100\% \text{aqueous}}$ values (Figure 4.4). These values could then be used to make calibration curves to convert gradient retention times (obtained each day of experimenting for the standard compounds) for a given protocol to k_{IAM} values.

The parameters for the gradient protocol used were initially based on protocols in the literature (Valko et al., 2000) then optimised for the specific experimental set up used. Ultimately the objective was to obtain defined peaks in a reasonably short period of time (≤ 10 mins) for applicability to medium throughput drug discovery. A gradient protocol contains an elution phase where the concentration of organic solvent is increase from zero to a high percentage linearly over a define period of time (Figure 4.5). If this period is too short there will be limited definition between peaks and lipophilic compounds will not elute. A wash phase of high concentration organic solvent then cleans the column of residual lipophilic compound or contaminates. Finally, a re-equilibration phase gets the column ready for the next compound to be administered. This stage must be long enough for the trace to have plateaued back to its starting level.

All of the phenone standards could be mixed together and injected without affecting their individual gradient retention times (Figure 4.5). This means one calibration run would need to be completed a day not seven. Gradient protocol 1 appeared to work well as the peaks were somewhat distinct, all compounds were eluted in the correct phase, and the trace had re-equilibration. Gradient protocol 2 was an attempt to increase the speed of the protocol from 10mins (6 compounds/hour) to 6mins (10 compounds/hour). However, with gradient protocol 2 the peaks are not distinct, and the compounds are not all eluted in the correct phase. Gradient protocol 3 elongated the elution phase, relative to protocol 1, at the expense of wash and re-equilibration phase. This gave better definition between peaks, increasing the resolution of the assay, while still having sufficient wash and re-equilibration phases. As such, gradient protocol 3 was chosen for screening the more lipophilic unlabelled compounds.

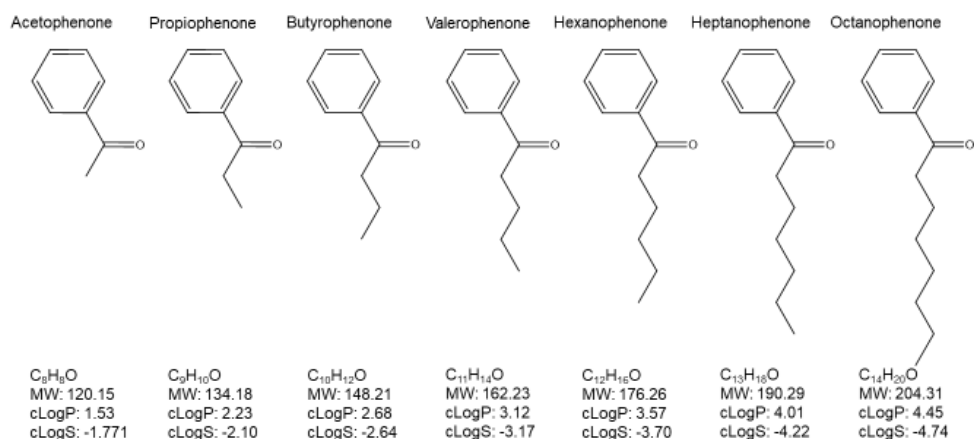


Figure 4.3. Structures of the phenone series used as standards. Each phenone in the series is identical except for increasing length of unbranched aliphatic tail. Also listed for each phenone are the formula, molecular weight, lipophilicity as calculated log partition coefficients (clogP), and calculated intrinsic solubility (clogS). All *in silico* measurements were obtained using Chemicalize software.

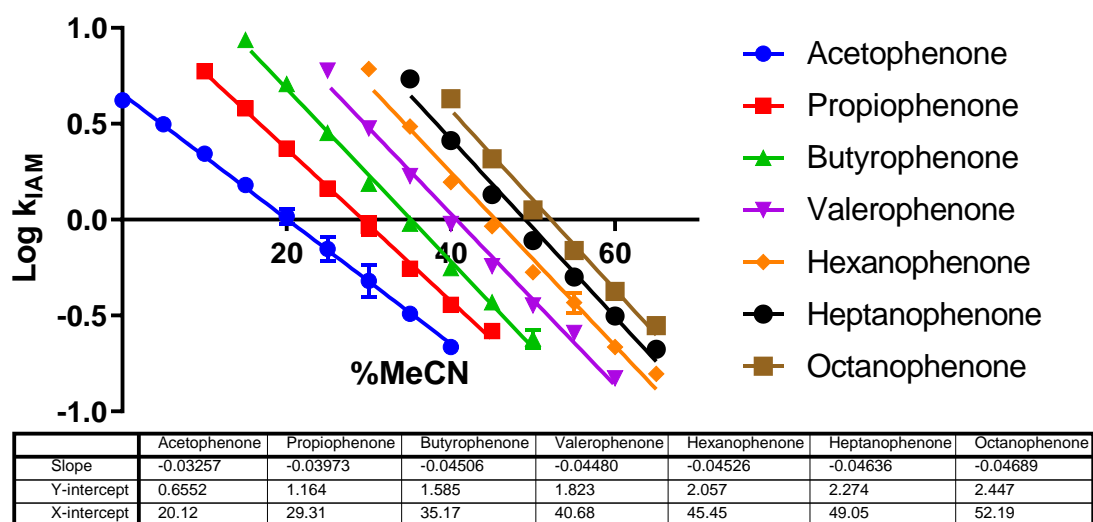


Figure 4.4. Determining the log k_{IAM} values of the phenone standards. For each phenone log k_{IAM} values were determined at several concentrations of acetonitrile (MeCN). Linear regression was plotted to estimate log k_{IAM} in 0% MeCN (y-intercept) and the CHI IAM value (x-intercept) for each compound. $n=3$ in all cases, error plotted \pm SEM.

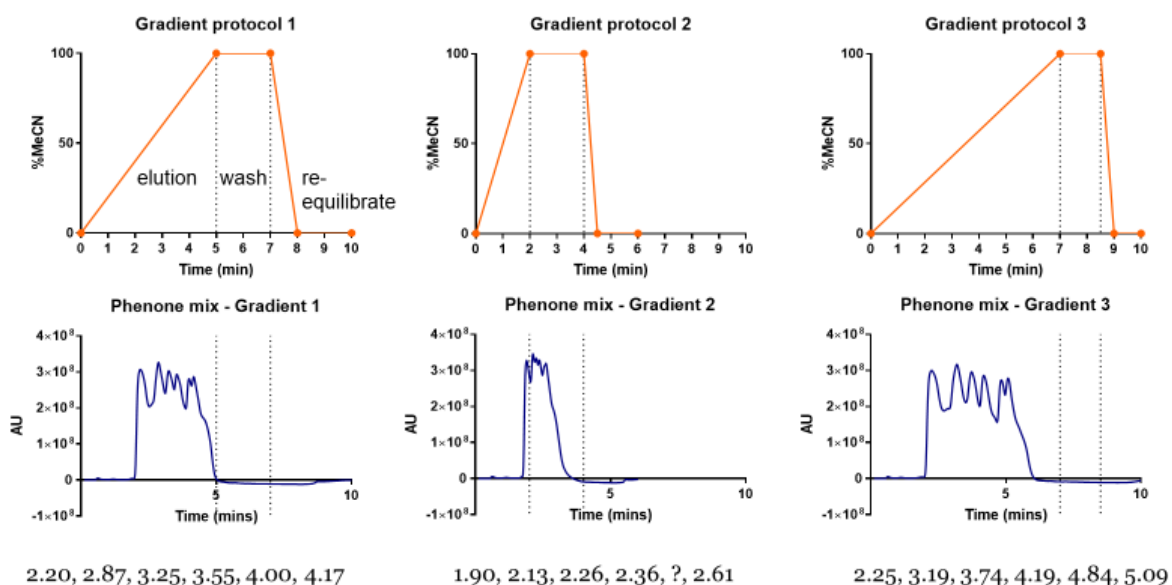


Figure 4.5. Optimisation of gradient protocol. Three gradient protocols were designed with varying elution, wash, and re-equilibration phases. The top row shows the timings of each phase for each protocol. The bottom row shows a representative trace when a mixture of 6 of the phenone standards was run through the given protocol (hexanophenone was on back order during optimisation). The T_r for each phenone (where possible to determine) are shown under the traces.

4.2.3 Determining $\log k_{IAM}$ values of the fluorescent ligands

As previously mentioned, the gradient method was not suitable for the fluorescent compound as their retention times were greater than those of the phenone standards. As such, they were screened isocratically at several concentrations of organic solvent to obtain extrapolated $k_{IAM100\%aqueous}$ values (Figure 4.6), just as the phenone standards were (Figure 4.4).

	AV041	AV050	AV051	AV069	AV074	AV075	CA200645	XACXBY
Slope	-0.06051	-0.05279	-0.05569	-0.06304	-0.05435	-0.05322	-0.05364	-0.05775
Y-intercept	3.427	2.380	2.372	3.498	2.983	2.856	2.806	3.205
X-intercept	56.65	45.09	42.59	55.50	54.88	53.67	52.30	55.51

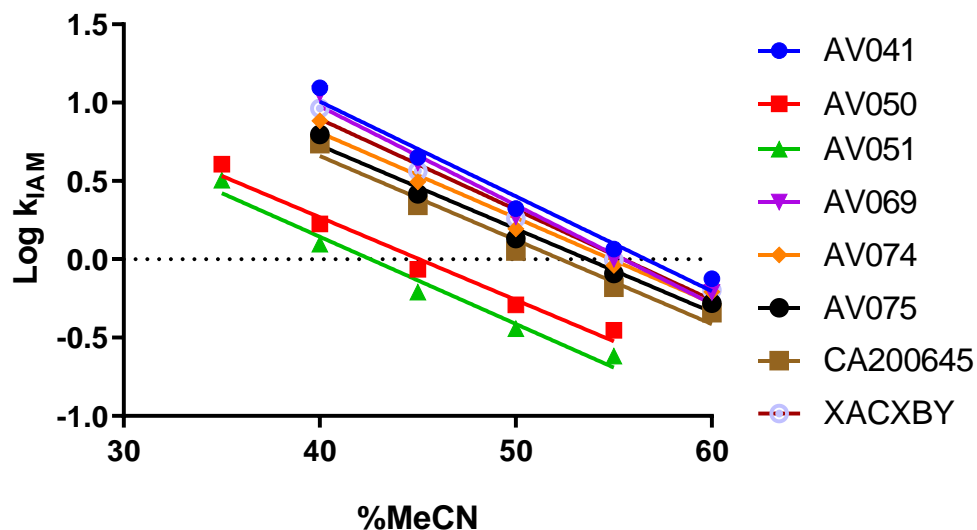


Figure 4.6. Determining the log k_{IAM} values of the fluorescent compounds at multiple concentrations of acetonitrile (MeCN). For each compound log k_{IAM} values were determined at several concentrations of acetonitrile (MeCN). Linear regression was plotted to estimate log k_{IAM} in 0% MeCN (y-intercept) and the CHI IAM value (x-intercept) for each compound. $n=3$ in all cases, error plotted \pm SEM.

It is noticeable from Figure 4.6 that there are two clusters amongst the fluorescent ligands. The two compounds with BODIPY-FL as the fluorophore (AV050 & AV051) display a lower membrane affinity relative to the six compounds with BODIPY-630/650 as the fluorophore. This is true whether the k_{IAM} (y-intercept) or CHI_{IAM} (x-intercept) is used as the value to represent membrane affinity. Due to the particularly large extrapolation required to estimate the y-intercept for these compound, perhaps the x-intercepts could be considered more valid. However, for these compounds the gradients of the slopes have little variation (mean average -0.0564, SEM 0.0013). As such, both measurements correlate well (Pearson's correlation coefficient $r=0.91$, $p(\text{two tailed})=0.002$) and are likely both valid.

4.2.4 Conversion of k_{IAM} to K_{IAM}

As previously discussed, the conversion from an assay specific retention factor (k_{IAM}) to a true immobilised artificial membrane partition coefficient (K_{IAM}) is difficult and rarely considered. One approach from the literature is to calculate the phase ratio (V_m/V_s) (see equation 4.2) based on information from correspondence with the manufacturer of the column (Taillardat-Bertschinger et al., 2003). The column used in this study was different to that of Taillardat-Bertschinger *et al.* so we contacted the manufacturer (Regis technologies) to obtain their estimates for the mass and densities of the constituents of the immobilised artificial membrane in their 3cm IAM.DD2.PC column. Regis estimated there to be 0.48g of packaging material in the column of which 70mg/g is phosphatidylcholine (PhC), 6.7mg/g is ten carbon chain (C_{10}), and 1.2mg/g is three carbon chain (C_3) (see Figure 4.1). The specific weights of these constituents are 1.01779, 0.86, and 0.86 g/ml respectively (Taillardat-Bertschinger et al., 2003). The solid volume of IAM can then be calculated as the sum of the weight of each constituent divided by its specific weight.

$$Vs_{3cm} = \frac{70 \times 10^{-3} \times 0.48g}{1.01779g/ml} + \frac{6.7 \times 10^{-3} \times 0.48g}{0.86g/ml} + \frac{1.2 \times 10^{-3} \times 0.48g}{0.86g/ml}$$
$$= \mathbf{0.0374ml}$$

The mobile volume for the experimental set up was calculated as a dead time of 0.58mins multiplied by a flow rate of 0.5ml/min and equal to 0.29ml.

In theory this should be enough information to convert k_{IAM} to K_{IAM} , however this method has limitations. Firstly, all the numbers used are estimates and understanding the volume a given weight of IAM occupies is difficult. Secondly, although in theory k_{IAM} and K_{IAM} should linearly correlate, there could be experimental reasons why they do not. Therefore, a second method for converting k_{IAM} to K_{IAM} was explored based on work from another group (Hollósy et al., 2006). Here experimentally obtained Log K_{IAM} values of the previously mentioned

phenone series were correlated with their Log P values. The assumption that this method makes is for these neutral, inert compounds the partition between membrane and water would be purely driven by lipophilicity/hydrophobicity, and therefore would be approximately equal to their partition between octanol and water (i.e. for these compounds: $\text{Log } K_{IAM} \approx \text{Log } P$). Given equation 4.2, it would be expected that there be a linear relationship between $\text{Log } K_{IAM}$ and $\text{Log } P$ values. However, Hollósy *et al.* found the relationship seemed exponential not linear in their data. They then instead plotted the exponential of $\text{Log } k_{IAM}$ against $\text{Log } P$, then fit a linear line to get the equation $\text{Log } K_{IAM} = 0.29e^{\text{Log } k_{IAM}} + 0.7$.

The data in this study showed a similar trend to the data from Hollósy *et al.* (Figure 4.7). A potential weakness in fitting the data this way is that even as $\text{Log } k_{IAM}$ tends to $-\infty$, $\text{Log } P/\text{Log } K_{IAM}$ will always remain positive. In reality there is not reason a compound couldn't have a negative K_{IAM} (i.e. have a greater affinity for water over membrane). As such we reasoned that the association fit in GraphPad Prism would be a better method for fitting the data as it could accommodate negative numbers on the Y-axis.

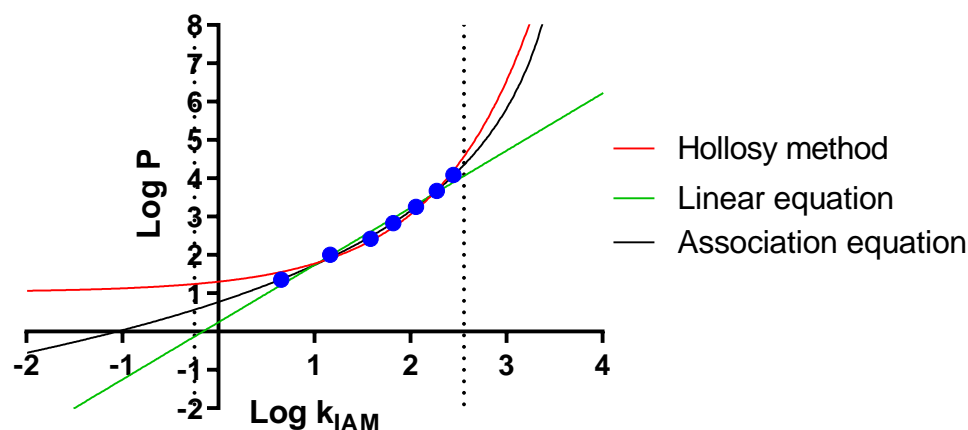


Figure 4.7. Calibration curve relating $\log k_{IAM}$ to $\log P$ for the phenone series. Blue dots represent the $\log k_{IAM}$ for each phenone, obtained from Figure 4.4, plotted against the compounds $\log P$ values with three potential fits to the data. As the compounds are unlikely to have specific interactions with membranes outside of lipophilicity, $\log P$ is assumed to equal $\log K_{IAM}$ (Hollósy et al., 2006). The fit in red represents an equation derived similarly to the Hollósy *et al.* where the exponential of $\log k_{IAM}$ is plotted against $\log P$ and a linear fit applied ($y=0.2743 \cdot e^{x+1.027}$). The green line simply represents a linear fit to the data without transformation ($y=1.4933 \cdot x+0.2404$). The black line represents a fit from GraphPad Prism called the association fit (rearranged to $y=\text{Ln}(1-((x+1.055)/4.785))/-0.3235$). The vertical dotted lines represent the range of $\log k_{IAM}$ values obtained experimentally for the unlabelled compounds.

4.2.5 Summary of all unlabelled compound data

Using the association fit method discussed to generate K_{IAM} values, the membrane affinity experimental data was compiled in Table 4.1 along with *in silico* measurements of $c\text{Log } P$ and $c\text{Log } D$ as well as information on predicted charge states at pH7.4. Additional *in silico* values such as hydrogen bond donors/acceptors, molecular weight, and topological polar surface area (TPSA) can be found in the appendix. In all cases it is clear that the compound list covers a wide range of physicochemical properties.

Compound	cLogP	cLogD	Log k _{IAM}	stdev	n	Log K _{IAM}	acid/base/zwitterion
Regadenoson (Lexiscan; CVT-3146)	-2.25	-2.25	ND	-	-	ND	-
NECA	-2.00	-2.00	0.50	0.01	3	1.22	-
Adenosine	-2.09	-2.09	-0.26	0.06	3	0.56	-
GR 79236	-1.51	-1.51	0.66	0.00	3	1.37	-
Cordycepin (3'-Deoxyadenosine)	-1.40	-1.40	-0.16	0.04	3	0.64	-
2-Chloroadenosine (2-CADO)	-1.18	-1.18	0.32	0.05	3	1.05	-
Theophylline	-0.77	-0.89	-0.01	0.01	3	0.77	acid
caffeine	-0.55	-0.55	0.07	0.00	3	0.83	-
Enprofylline (3-Propylxanthine)	-0.15	-0.39	0.21	0.06	3	0.95	acid
DMPX (3,7-Dimethyl-1-propargylxanthine)	-0.32	-0.32	0.31	0.02	3	1.04	-
CPA (N6-Cyclopentyladenosine)	-0.43	-0.43	0.80	0.01	3	1.52	-
CGS-21680	-0.92	-2.39	1.00	0.01	3	1.73	acid, zwitterion
ZM-241,385	2.93	2.93	1.38	0.02	3	2.20	-
CV 1808 (2-Phenylamino Adenosine) (2-PAA)	0.03	0.03	0.86	0.00	3	1.58	-
CCPA (2-Chloro-N6-cyclopentyladenosine)	0.47	0.47	1.33	0.02	3	2.13	-
SDZ WAG 994	0.65	0.65	1.10	0.03	3	1.85	-
XAC	-0.84	-1.12	2.16	0.01	3	3.45	zwitterion, base
2'-MeCCPA	0.75	0.75	1.40	0.01	3	2.22	-
PSB 1115	0.09	-0.59	0.89	0.01	3	1.62	acid
N6-(2-Phenylisopropyl)adenosine (R-PIA)	0.64	0.64	1.18	0.01	3	1.94	-
8-Cyclopentyl-1,3-dimethylxanthine (8-CPT, CPX)	0.98	0.96	1.76	0.02	3	2.74	acid
(±)-5'-Chloro-5'-deoxy-ENBA	1.11	1.11	1.51	0.01	3	2.38	-
IB-MECA (CF101)	0.60	0.60	1.58	0.01	3	2.48	-
ANR 94	0.93	0.93	0.63	0.02	3	1.35	-
HEMADO	1.07	1.07	1.15	0.01	3	1.91	-
Tozadenant (SYN115)	1.48	1.38	1.21	0.01	3	1.98	acid
CI-IB-MECA (CF102)	1.51	1.51	2.07	0.00	3	3.27	-
PSB 11 hydrochloride	2.26	2.25	1.13	0.01	3	1.88	acid
MRS 1706	3.33	3.00	2.08	0.00	3	3.29	acid
Istradefylline (KW-6002)	2.42	2.42	1.71	0.01	3	2.66	-
PSB 36	2.21	2.09	1.91	0.00	3	2.99	acid
DPCPX (PD-116,948)	2.74	2.72	1.74	0.00	3	2.72	acid
8-(3-Chlorolstyryl)caffeine (CSC)	2.62	2.62	1.86	0.01	3	2.91	-
BAY 60-6583	2.09	2.09	1.75	0.01	3	2.73	-
LUF 5834	2.03	1.99	1.70	0.01	3	2.64	acid, base
PSB 0788	4.05	3.79	2.13	0.01	3	3.38	acid
resveratrol	3.40	3.37	2.06	0.01	3	3.25	acid
MRS 1754	3.62	3.29	2.18	0.00	3	3.49	acid
Preladenant (SCH 420814)	2.72	2.07	1.39	0.01	3	2.22	base
KW-3902	3.23	3.23	2.25	0.00	3	3.62	-
GS 6201 (CVT 6883)	3.52	2.93	1.98	0.01	3	3.10	acid
PSB 603	4.32	3.96	2.20	0.00	3	3.53	acid
CGS 15943	3.37	3.37	2.00	0.01	3	3.15	-
MRS 3777 hemioxalate	3.75	3.75	2.16	0.00	3	3.44	-
SLV320	3.41	3.31	1.76	0.00	3	2.74	base
SCH-58261	3.21	3.21	1.76	0.01	3	2.75	-
PSB 10 hydrochloride	4.07	4.07	1.79	0.01	3	2.79	-
MRS 5698	3.55	3.55	2.21	0.02	3	3.54	-
VUF 5574	4.32	4.32	2.35	0.01	3	3.84	-
SCH-442,416	3.44	3.44	1.86	0.01	3	2.90	-
PQ-69	5.83	5.58	2.56	0.02	3	4.35	base
MRE 3008F20	4.31	4.05	1.93	0.01	3	3.02	acid
CGH 2466	4.15	4.15	2.09	0.01	3	3.32	-
MRS 1220	5.29	5.22	2.16	0.02	3	3.45	acid
MRS 1334	5.74	5.74	2.37	0.01	3	3.89	-
MRS 1191	5.93	5.93	2.38	0.00	3	3.90	-
Capadenoson (BAY 68-4986)	5.04	5.04	2.48	0.00	3	4.14	-
MRS 1523	6.92	6.92	2.56	0.00	3	4.35	-

Table 4.1. Summary of IAM HPLC data and *in silico* lipophilicity data for the unlabelled compounds. cLog P & D data were obtained using Chemicalize software. Log K_{IAM} data was obtained either isocratically with 100% aqueous mobile phase or using a gradient protocol. Log K_{IAM} data was

generated by converting $\log K_{IAM}$ values using the association fit equation described in Figure 4.7. In the final column acid, bases, and zwitterions are noted based on pKa values from Chemicalize software. Only if above 5% of the compound is predicted to exist in either of the three forms at pH7.4 is it noted.

When correlating cLog D to $\log K_{IAM}$ for all compounds there is a statistically significant correlation with a Pearson's correlation coefficient r value of 0.755 (Figure 4.8). When separating out compounds into those that are charged and uncharged at pH7.4 it appears the charge compounds have a weaker correlation ($r^2=0.54$) and the uncharged have a stronger correlation ($r^2=0.87$).

Two of the compounds, XAC and CGS-21680, have a substantial zwitterionic component at pH7.4 and both deviate from the black line of best fit for all compounds. XAC is approximately 60% zwitterionic and 40% with a single protonation. CGS-21680 is approximately 15% zwitterionic and 85% with a single deprotonation (Figure 4.9).

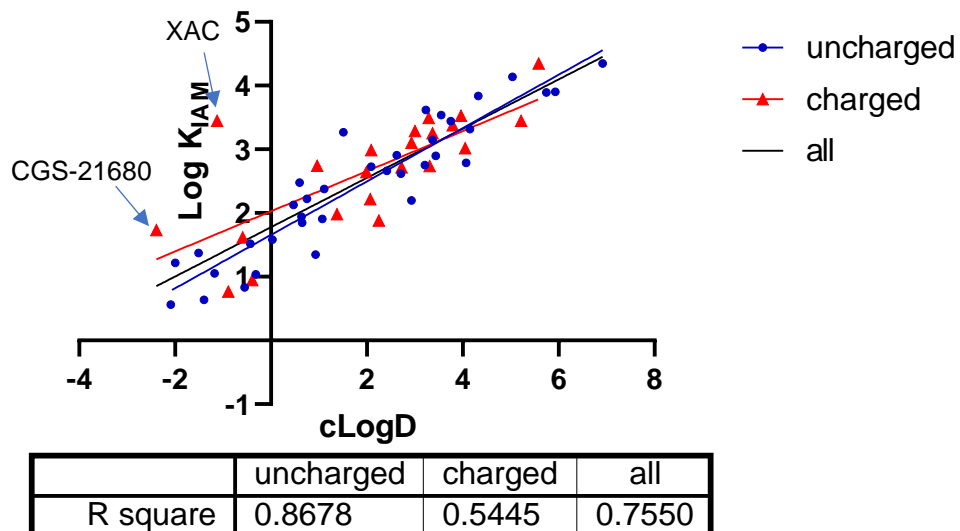


Figure 4.8. Correlation between clog D and log K_{IAM} values for charged and uncharged compounds. XAC and CGS-21680 have been labelled as the two compounds with zwitterionic components at pH7.4. Linear regression plotted, $P < 0.001$ in all cases Pearson's correlation.

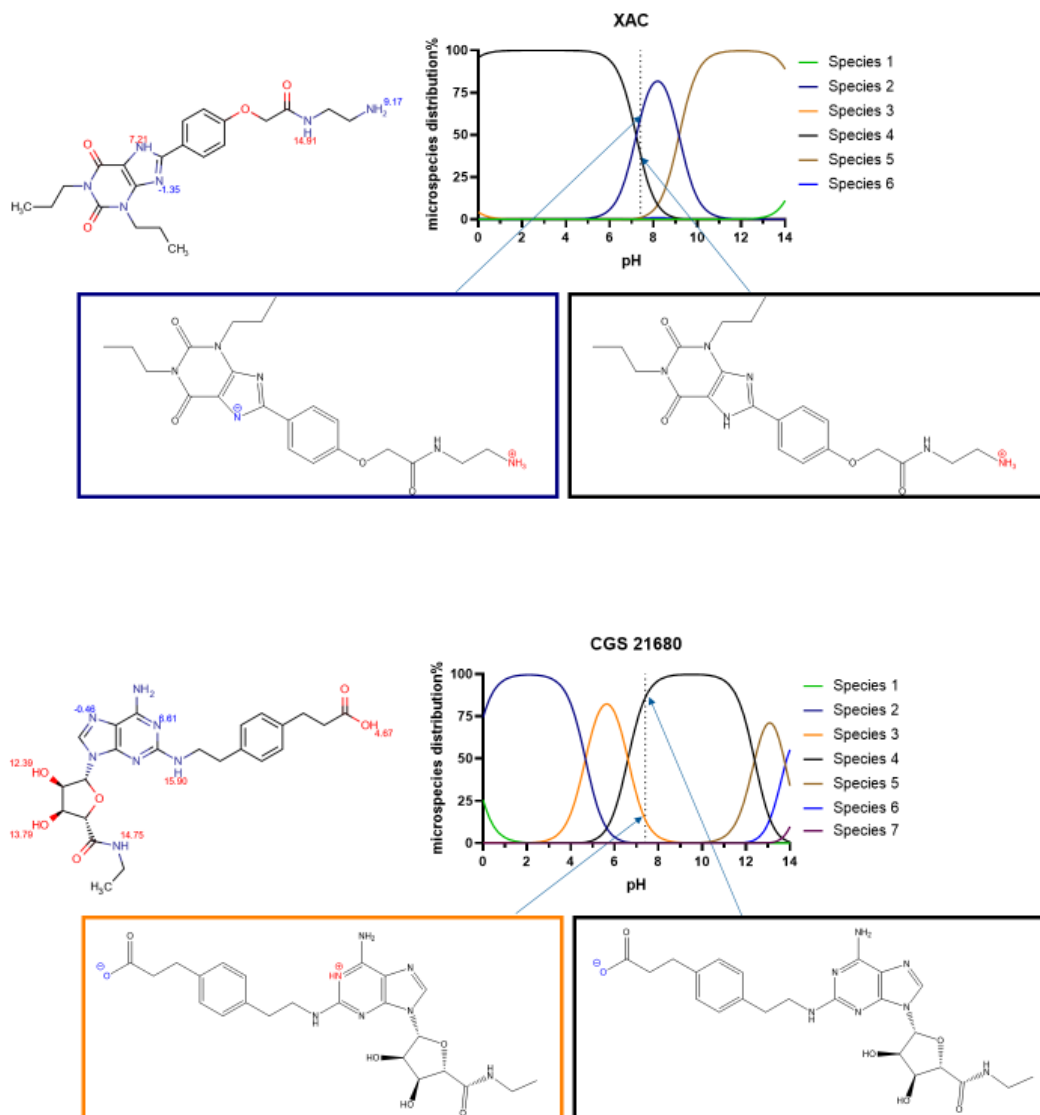


Figure 4.9. Predicted microspecies distribution of XAC and CGS-21680 at pH 0-14. Each compound shows various microspecies across the range of pHs. Predicted pKa for each potential protonation or deprotonation site is also stated. The dotted line represents pH7.4. At pH 7.4 both compounds show zwitterionic components (XAC 60% zwitterion, 39% base; CGS-21680 14% zwitterion, 86% acid). Data generated using Chemicalize software.

4.2.6 Summary of fluorescent compound data

Obtaining *in silico* data for the whole of the fluorescent molecules was not possible with the available software due to its inability to process the fluorinated boron atom in the BODIPY. As such, the *in silico* data refers to a truncated form of the molecule where the same part of each molecule has been removed (Figure 4.10). These data can still be useful for comparisons across the fluorescent series but not to other molecules. It may also not be valid to compare the *in silico* data from the two BODIPY-FL containing molecules (AV050 & AV051) to the other six BODIPY-630/650 containing molecules because, although the same part of the molecule has been removed, the immediately adjoining atoms are different and thus the conjugation may be affected.

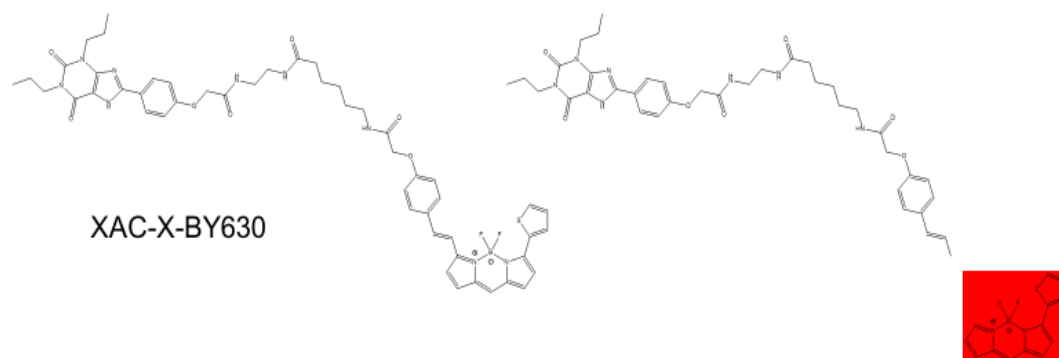


Figure 4.10. The structure of XAC-X-BY630 and the structure of the truncated version used for *in silico* purposes. Due to the inability of computer software packages to process the fluorinated boron atom in the BODIPY fluorescent tag, the part of the molecule highlight in red was omitted from *in silico* measurements.

Another difficulty with obtaining data for the fluorescent compounds is the k_{IAM} values for most of the molecules are larger than that of the phenone series (Figure 4.11). Therefore, the method of converting k_{IAM} to K_{IAM} using a standard curve of the phenone series would likely contain a large margin of error as it is impossible to say if the trend would continue. If it is assumed the trend would be exponential in some

way at $\log k_{IAM}$ values above 2.45, then difference between the $\log K_{IAM}$ values would be larger than the differences between the $\log k_{IAM}$ values.

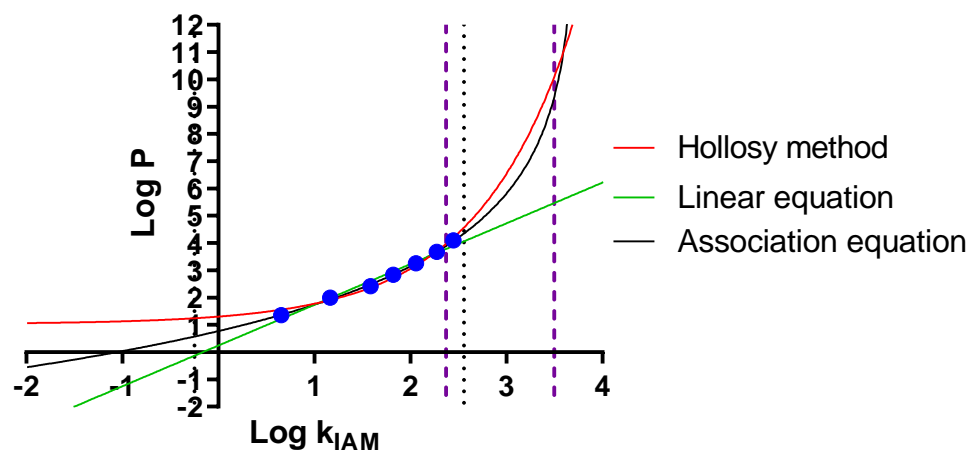


Figure 4.11. Calibration curve relating $\log k_{IAM}$ to $\log P$ for the phenone series with the range of fluorescent compounds illustrated. Here Figure 4.7 has been reproduced with extended axis to illustrate how the range of $\log k_{IAM}$ values for the fluorescent compounds (purple dotted lines) falls outside the range of the standard compounds.

		cLogP	cLogD	Log k_{IAM} (Yin)	CHI (Xin)	Log K_{IAM}
XAC-ser-tyr-X-BY630	AV041	2.96	2.62	3.427	56.65	8.53*
XAC-ser-tyr-BYFL	AV050	1.15	0.82	2.380	45.09	3.91
XAC-ser-tyr-X-BYFL	AV051	1.46	1.13	2.372	42.59	3.89
XAC-ala-tyr-X-BY630	AV069	4.00	3.67	3.498	55.50	9.36*
XAC-ala-ser-X-BY630	AV074	1.60	1.27	2.983	54.88	5.74*
XAC-asn-ala-X-BY630	AV075	1.20	0.87	2.856	53.67	5.26*
XAC---BY630	Ca200645	2.72	2.39	2.806	52.30	5.08*
XAC-X-BY630	XAC-X-BY	3.72	3.39	3.205	55.51	6.83*

Table 4.2. Summary of IAM HPLC data and *in silico* lipophilicity data for the fluorescent compounds. cLog P & D data were obtained using Chemicalize software. Log k_{IAM} data was obtained by isocratically running the compounds at several concentrations of acetonitrile (Figure 4.6). Log K_{IAM} data was generated by converting $\log k_{IAM}$ values using the association fit

equation described in Figure 4.7. *However, only AV050 and AV051 fit into the range of standard compounds used for generating $\log K_{IAM}$ data. The other six compounds required unacceptable extrapolation (see Figure 4.11) thus obtaining accurate $\log K_{IAM}$ data was not possible.

	Log P	Log D	
Alanine (ala) (A)	-2.8	-2.8	Non-polar, aliphatic residues
Serine (ser) (S)	-3.9	-3.9	Polar, non-charged
Tyrosine (tyr) (Y)	-1.5	-1.5	Aromatic
Asparagine (asn) (N)	-4.3	-4.3	Polar, non-charged

Table 4.3. Calculated lipophilicity data for the four amino acids used in the linker regions of some of the fluorescent compounds. Data generated using Chemicalize software.

4.3 Discussion

The IAM assay has many positive attributes that have been highlighted in this study. Firstly, the assay was found to be highly reproducible with the minimal differences between replicates. Indeed, an N of 1 is likely sufficient in drug discovery set up with a high throughput. Perhaps a second replicate could be useful to rule out problems such as injection errors, although these were not seen in this study. This is likely due to having a fixed chemical system, as opposed to biological one where variability is more inherent. Although columns can age over time, if proper controls are in place every day, and columns changed at appropriate time, this should not matter too much. Additionally, impurities were not found to be an issue because as long as the retention time of an impurity is significantly different to the compound being tested the peaks can easily be distinguished. As all the compounds used were bought with relatively high purities, impurity peaks were always small and compound peaks obvious. With more crude solutions it is possible impurity peaks could be similar in size to

compound peaks and separation and analysis would be needed to assign the peaks. If peaks do overlap, the PDA can be set to a specific wavelength provided the compound and the impurity have different absorbance qualities.

56 out of the 57 compounds were able to be detected. The one that could not be detected simply could not be made up to a sufficiently high concentration for solubility reasons even with the use of sonication. Perhaps a more sensitive detector, for example a mass spectrometry detector, could have detected the final three compounds. Although in theory this is a concentration independent technique, in reality trial and error was necessary for many compounds to find a balance between getting a concentration high enough to be detected, but low enough to dissolve the compound and to not risk the compound coming out of solution in the HPLC. As such many compounds predicted to have a low solubility were screened at increasing concentrations until detection was possible. The more lipophilic compounds obviously lacked solubility, although they tended to have greater absorbance.

The throughput for the unlabelled compounds, once the assay was set up, was ≤ 10 mins per compound. A single person with a single machine (with an hour to clean the machine and run standards at the start of the day) could therefore run 50 compounds in a day (or more if automated to run over night). Buffers and compounds can be made up while the machine is running, as multiple compounds can be automated to run in sequence. Although, as mentioned, some compounds were needed to run at multiple concentrations. A more sensitive detector could again possibly negate this problem.

Although the reproducibility was high between replicates, error seems possible more in the form of experimental artifacts. This is evidenced by the non-perfect linearity between $\log k_{IAM}$ values and % concentration of MeCN in compounds screened using the isocratic step method (Figure 4.4 & 4.6) and the non-perfect linearity between $\log P$ and $\log k_{IAM}$ values for the phenone series (Figure 4.11). This is possibly due to

artifacts introduced by the high concentrations of MeCN (Hollósy et al., 2006).

Additionally, further error is likely introduced by imperfect methods of converting $\log k_{IAM}$ to $\log K_{IAM}$ values. The difficulty of doing this, alongside the lack of need to do this if all that is required is to examine relative membrane affinity of a series, is likely why it is rarely attempted.

Log D/P correlated well with $\log K_{IAM}$ values as expected as both are primarily driven by lipophilicity/hydrophobicity. Also as expected, the uncharged compounds correlated better than the charged. This is because introducing a positive or negative charge into a molecule always increases its affinity for water over octanol due to the polar nature of water molecules. However, with membranes there is the added complication that as well as interacting with water molecules, charged compounds can interact with the charged head groups of the lipids. In the case of the IAM used, that lipid is phosphatidylcholine, which contains a positive and a negative charge in the head group (Figure 4.1 & 4.12). As others have noted, there appears to be more variation in K_{IAM} at the hydrophilic end of the compound series (Taillardat-Bertschinger et al., 2002; Barbato et al., 2007). This is possibly because for the highly lipophilic the head group interactions are negligible relative to the attraction to the lipophilic tails of the IAMs.

The two compounds that had large zwitterions components at pH7.4 seem to interact with phosphatidylcholine more than would be predicted from *in silico* lipophilicity data. It is possible they are having a sort of bitopic charge interaction with the head group that increases membrane affinity more than would be expected. Phosphatidylcholine is the main constituent of the membrane and most other lipids in the membrane are zwitterions, but in different spatial arrangements (Figure 4.12).

Phosphatidylserine has the amine and phosphate charges same as phosphatidylcholine, but also an additional negative charge from a carboxylic acid. Phosphatidylinositol only has the negative phosphate

charge. It would be interesting to see if it were possible to make IAM with different lipids.

It is worth noting that while it is the XAC pharmacophore on fluorescent ligands, it is no longer zwitterionic because the linker is attached where the charged amine would be (Figure 4.10).

The effect of charge could be demonstrated further by running at multiple pHs. According to manufacturer guidelines the recommend pH range of the column used is between 2.5 to 7.5. Compounds that remain neutral at the various pHs measured might not change in membrane affinity, however, compounds that are protonated/deprotonated at one pH might have different membrane affinity depending on the pH of the mobile phase.

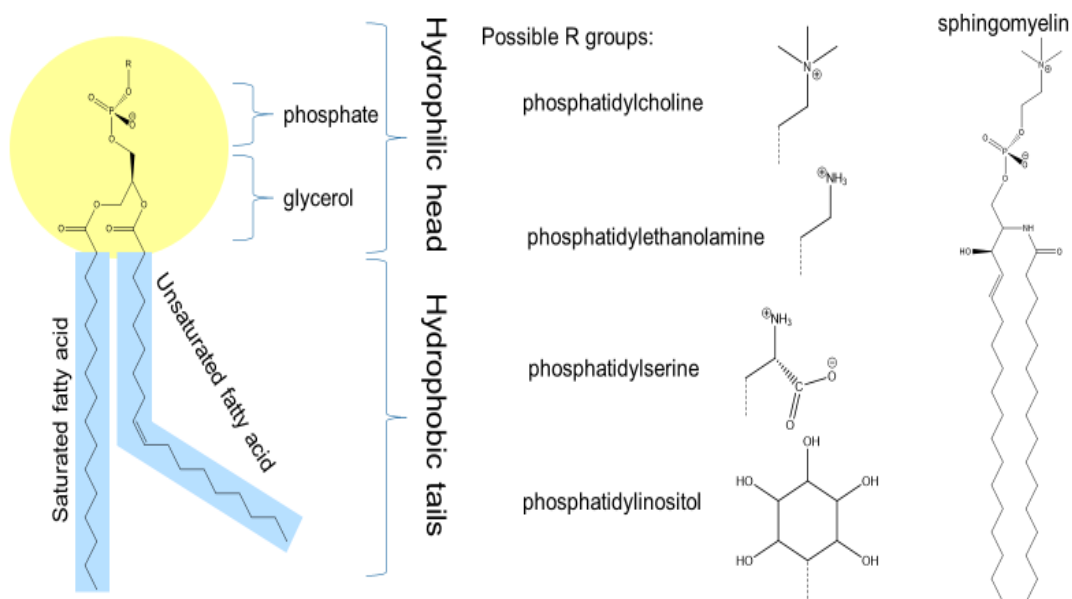


Figure 4.12. Illustration of the main lipid components of cell membranes.

Each lipid contains a hydrophilic head group and a hydrophobic tail. Most lipids contain glycerol, phosphate (negatively charged at pH7.4), and then varying chains coming off the phosphate. Sphingomyelin is similar to phosphatidylcholine in structure but with sphingosine instead of the glycerol.

In conclusion, the IAM HPLC assay was found to be highly reproducible, successful for all but one compound, and amenable to medium throughput drug discovery. Challenges still remain in converting $\log k_{IAM}$ to $\log K_{IAM}$ values, particularly for the extremely lipophilic fluorescent compounds. $\log K_{IAM}$ values correlated well with *in silico* lipophilicity data, but the added value of the technique is shown in the detail of uncharged compounds correlating better than charged compounds, suggesting membrane affinity is not only governed by lipophilicity.

While phosphatidylcholine is the most abundant lipid in mammalian cell membranes, columns designed to incorporate a heterogeneous population of lipids in appropriate ratios could improve the modelling of *in vivo* conditions. In particular, columns could be designed to mimic specific target sites, for example tumours where it has been shown that tumours can alter their lipid composition away from normal physiological ratios (Szlasa et al., 2020).

Chapter 5 – Investigating the local concentration of fluorescent ligands using Fluorescence Correlation Spectroscopy (FCS)

5.1 Introduction

While it is possible to measure the concentration of a substance in a liquid with techniques such as HPLC, in cellular assay it is conventionally assumed that ligands are homogeneously distributed. Local concentrations are seldom considered and are difficult to measure. Fluorescence correlation spectroscopy (FCS) is a powerful quantitative technique that provides useful information such as the concentration and diffusion rate of a fluorescent species in a small defined measurement volume (Briddon and Hill, 2007). Determining concentration in a solution by counting of particles was attempted as early as 1911, where gold particles were visually counted as a function of time (Svedberg and Inouye, 1911). Six decades later, across the 1970s, the theoretical framework for FCS was introduced, with the first definition of FCS published in 1972 (Magde et al., 1972). Here the kinetics of DNA chemically reacting with ethidium bromide was observed. Advancements in laser and optical technologies in the 1990s boosted the practical possibilities of FCS (Elson, 2013; Briddon et al., 2018), with the first FCS measurements on cell membranes published in 1999 (Schwille et al., 1999). The availability of suitable commercial hardware, detectors, and analysis software in the last decade has taken FCS from a highly niche, specialised experimental setup, to one found in many labs around the world today (Briddon et al., 2018). The technique has been applied to investigate oligomerisation of membrane receptors (Briddon et al., 2008; Kwapiszewska et al., 2019), to characterise styrene maleic-acid lipid particles (SMALPs) in solution (Grime et al., 2020), to characterise virus-like particles (Zemanova et al., 2004), to characterise labelled endogenous large protein hormones

(Kilpatrick et al., 2017; Peach et al., 2018), and to study the kinetics of enzymatic reactions (Wenger et al., 2006) to name but a few.

In contrast to most techniques, autocorrelation analysis is more robust the lower the concentration of ligand used, so long as the signal to noise ratio of fluorescence remains above background. A simple metaphor to explain this is that when holding a plastic bag full of tennis balls, a person might not notice when one is removed or added. However, if there are only one or two tennis balls in the bag, the person would feel a significant change in weight when one is added or taken away. In FCS, the more fluorescent species in the confocal volume, the smaller the relative change in intensity when species leave or enter the volume.

In addition to high sensitivity at low concentrations, FCS has many other advantages that have increased its applicability over time. It can determine concentrations with high spatial resolution compared to techniques like HPLC. It is a non-invasive technique and can be used to detect low levels of endogenous receptors (Rose et al., 2012). The process is labour intensive, requires expensive equipment, and the need for specialist training. The technique requires fluorescent or fluorescently labelled species, and these species cannot be stationary.

In the context of micro-pharmacokinetics, FCS has previously been used to quantify the concentration of a single fluorescent compound, BODIPY630/650-PEG8-S-propranolol (BY-propranolol), at varying distances above cell membranes (Gherbi et al., 2018). For the first time it was shown that a ligand could achieve a significantly higher concentration immediately adjacent to a cell membrane compared to the bulk aqueous phase. A concentration of 19.2nM BY-propranolol of was measured 2 μm above adherent CHO cells when the concentration added to the well was 1.8nM ($1 \times K_d$ of the ligand). The concentration steadily decreased with increasing vertical distance to 1.5nM at a distance of 200 μm above cell membrane (considered to be bulk aqueous phase). A similar concentrating effect was seen over the

coverslip to a much lesser extent. Interestingly, the concentration of fluorescent ligand above cells expressing the beta-2 adrenoceptor, was significantly higher than non-receptor expressing cells with a mean concentration of 45.7nM at 2 μ m above cell membrane. The addition of an unlabelled beta-2 receptor antagonist, ICI 118 551, reduced the local concentrating effect in receptor expressing cells, but not non-receptor expressing cells. This further demonstrates a receptor driven component to the observed concentrating effect.

The aim of this Chapter is to investigate if the concentrating effect observed previously for BY-propranolol above cell membranes (Gherbi et al., 2018) is also observed for multiple fluorescent ligands, with identical pharmacophore but differing linker regions, in a different receptor system (A2a receptor). By obtaining local concentration data for multiple ligands whose binding kinetics and physicochemical properties have previously been characterised in Chapters 3 and 4, it will be possible to investigate the relationships between local concentration, and these parameters.

5.2 Results

5.2.1 Determining appropriate time course for reads above cells

Before conducting extensive experiments, it was important to establish an appropriate time course for incubation of cells with fluorescent ligands. In Gherbi et al., 2018 it was shown that the local concentrating effect of the fluorescent ligand above cell membranes was not instantaneous and appeared to increase between 15 and 90 mins before plateauing until the last measured time point of 120 mins. To understand the kinetics of any potential concentrating effect of the three ligands chosen for FCS analysis, reads were taken at four spatial position (4 μ m above cells, 200 μ m above cell, and the equivalent z-axis positions above an area of no cells) (see Figure 5.1, top) at time points ranging from 15-120mins post addition of ligand. Prior to the experiment

cell culture media was removed and cells washed with buffer (see methods) 5 times before being left to equilibrate in buffer for 10 mins. Buffer was gently removed and replaced with buffer containing 1nM fluorescent ligand. The four positions were programmed in the time between ligand addition the first read allowing a degree of automation reducing the time between reads of the same time point. The order the 4 points were read was changed each experiment to remove and possible biases of the 10 second reads being sequentially.

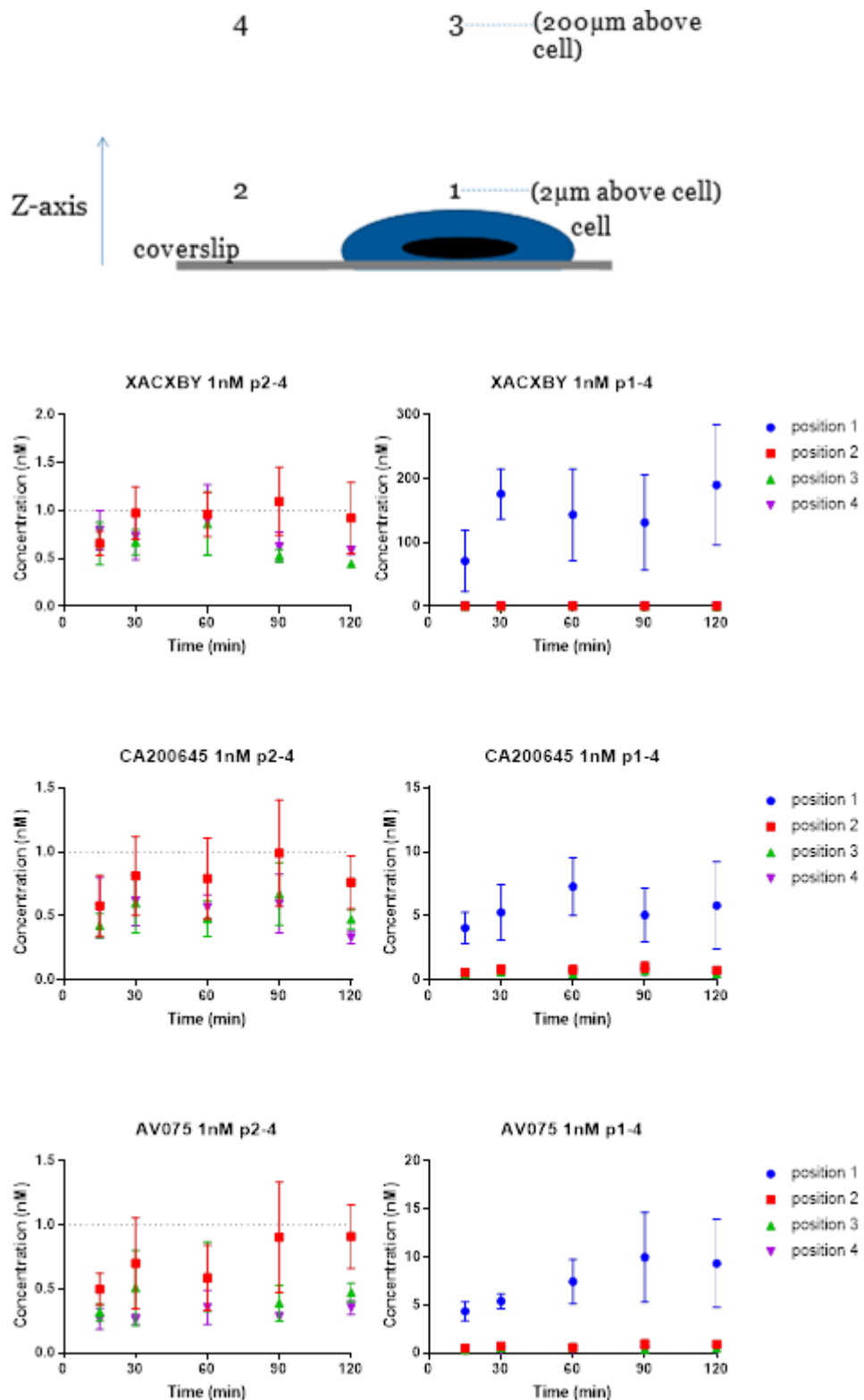


Figure 5.1 Time course of fluorescent ligand concentration determined by FCS at four positions relative to coverslip and native CHO cells. Top: schematic showing four positions from which reads were taken (p1, 2 μm above cell; p2, equivalent height to p1 above nearby area of no cell; p3, 200

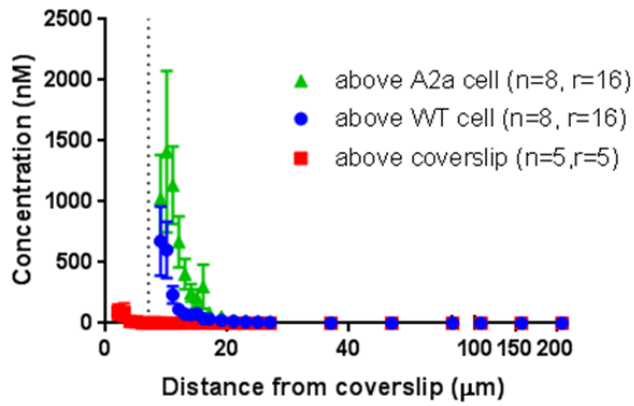
μm above cell; p4, equivalent height to p3 above nearby area of no cell). Left 3 graphs: only positions 2-4 shown. Right 3 graphs: positions 1-4 shown. All graphs: 1nM of fluorescent ligand (XACXBY, CA200645 or AV075) was added to wells containing WT CHO cells at time 0. 10 second reads were taken sequentially in each of the 4 positions at 15-, 30-, 60-, 90- and 120-mins post ligand addition. Data are shown as mean \pm S.E.M from single reads taken in 6 independent experiments.

The ligands appeared to reach equilibrium after 60 mins, although the error bars are reasonably large. Based on these data, an incubation time of 90mins was chosen for further experiments. Based on the kinetic data already obtained, this incubation time would also allow receptor-ligand binding to reach equilibrium for all ligands if receptors were present

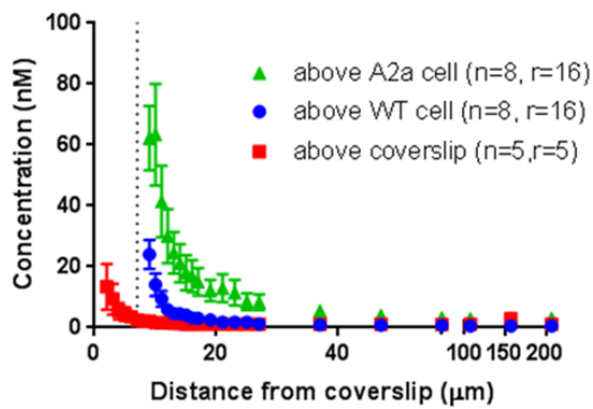
5.2.2 Determining ligand concentrations above CHO cells expressing the adenosine A2a receptor.

Having established an appropriate time period of incubation, the extent of the gradient was examined in more detail by quantifying ligand concentrations at increasing distances above the cell membrane. FCS reads (1x30s) were conducted at distances of 2-200 μm above the surface of individual WT or A2a-expressing CHO cells which were labelled with SNAP Surface Alexa-fluor 488 and imaged accordingly. From this, highly expressing cells could be selected (Figure 2.1). Ligands were incubated with cells at 0.1 μM concentrations for 90mins to achieve similar levels of receptor occupancy. Intensity reads were then taken from 2-207 μm above the coverslip or 2-200 μm above cells for 30 seconds per position (Figure 5.1). The average height of a cell was determined to be 7 μm .

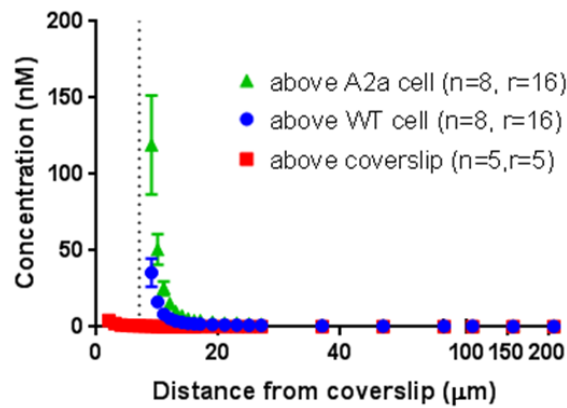
XAC-X-BY630 3.6nM added



CA200645 46nM added



AV075 35nM added



compound	K_d (nM)	K_{on} ($\text{M}^{-1}\text{min}^{-1}$)
XACXBY	36	1.67E+07
Ca200645	460	1.33E+06
AV075	346	7.91E+05



Figure 5.3. Concentration of fluorescent ligands at varying distances above CHO cells expressing the A2a receptor (green), WT CHO cells (blue), or coverslip (red) determined by FCS. Dotted line represents the level of the cell membrane at 7 μm above coverslip. In all cases the added concentration of ligand was equal to 0.1 times the K_d determined in Table 2. n represents individual experiments where r represents total number of replicates carried out. In all cases error bars are equal to \pm S.E.M. Bottom right) schematic showing reads being taken at increasing heights in the z-axis above coverslip and cell.

All ligands clearly display a gradient of increasing concentration as distance from cell membranes is reduced. This is also apparent above the coverslip to a smaller degree. There also appears to be a receptor-driven local concentrating effect. XAC-X-BY630 has a higher concentration at 2 μm above the membrane of A2a expressing cells (1024 ± 347.4 nM) compared to CA200645 (62.3 ± 9.5 nM) and AV075 (111.3 ± 30.1 nM) despite being added at a lower concentration. The concentration of ligand measured in the bulk aqueous phase (207 μm from coverslip) was in all cases lower than the nominal concentration thought to be added. This occurs with or without cells (data not shown) suggesting the ligands are sticking to either the well and/or or sticking to plastics during the process of dilutions from stocks.

5.2.3 Confirming spatial accuracy of FCS measurements

In many types of imaging, it is possible to observe a scattering effect where light, particularly of a high intensity, from a lower z-position is detected when attempting to image a higher z-position. As such, one might assert the results here could simply be caused by the ligands aggregating in the membrane in high concentrations and scattering light which appears when taking reads in the immediate vicinity of the cells. To test this potential artefact experiments were completed using TetraSpeck silicon beads. These spherical beads have a defined

diameter of 0.1 or 4 μm (height of cells used were approximately 7 μm for comparison) and are highly fluorescent (coated with blue, green, orange, and red fluorophores). A drop of beads dissolved in ethanol can be placed on a coverslip and left overnight to dry to weakly fix the beads on the surface. Buffer can gently be added to the wells without dislodging the beads. The 0.1 μm diameter beads were chosen as the 4 μm beads were far brighter than cells in buffer containing fluorescent ligand and as such the laser power had to be reduced to get a comparable count rate. Additionally, the 0.1 μm beads could be considered the same height as the coverslip. The well was gently filled with 100nM CA200645 solution and reads were taken 5 μm above beads or at a comparable height above coverslip with no beads present (Figure 5.4).

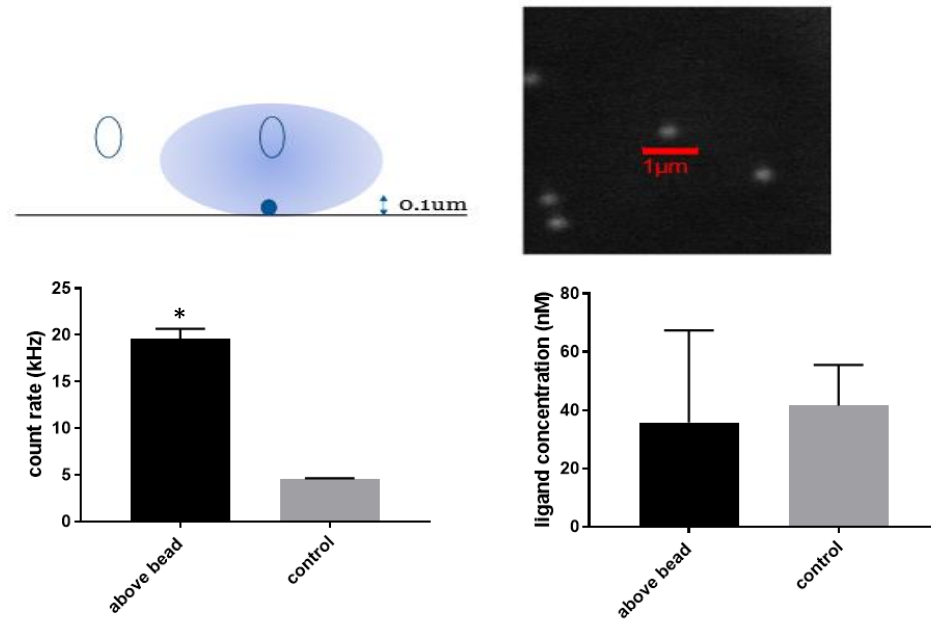


Figure 5.4. Above TetraSpek bead reads. Top left, schematic showing position of reads above and to the side of tetraSpek bead. Top right, image of bead adhered to coverslip. Bottom left, count rate of representative experiment ($n=1$, $r=10$) above bead and above area of no bead in well with $100 \mu\text{M}$ CA200645. The two are significantly different (t-test, $p<0.001$). Bottom right, ligand concentration of representative experiment ($n=1$, $r=10$) above bead and above area of no bead in well with $100 \mu\text{M}$ CA200645. The two are not significantly different across the 10 reads for each condition (t-test, $p>0.05$).

From the representative data (Figure 5.4) it can be seen that the count rate is significantly higher above the bead compared to above an area of coverslip with no bead present (control). However, this does not alter the ligand concentration as calculated by autocorrelation analysis. Referring back to Figure 2.2, this is manifested by an increase in average intensity (I), but no changes in the fluctuation patterns from which the concentration is determined. These fluctuations are subjected to more noise (non-correlating background from beads) and predictably lead to larger error bars in the concentration above bead relative to control. FCS measurements require movement and correlation.

5.3 Discussion

All the ligands tested displayed the same concentrating effect that has previously been shown by this group with BY-propranolol (Gherbi et al., 2018). This demonstrates that the results of the previous study were not unique to single ligand. Indeed, the results of the present study, in particular the ligand XACXBY, displayed even greater concentrating effect relative to BY-propranolol (with estimated comparable expression). Furthermore, an increased concentrating effect in the presence of a cognate receptor was observed using cells expressing a different receptor showing the effect is not unique to a single receptor. These data suggest that the local concentrating effects could be a generalised phenomenon seen with many ligands.

If this is a generalised phenomenon affecting all ligands, or all ligands above a certain threshold of attraction to cell membranes, the implications to drug discovery and pharmacological assays could be large. All equations used to analyse pharmacological assays rely on the assumption that the concentration of ligand being added to the assay is the concentration being directly exposed to the target. Taking the key pharmacological value of affinity as an example, if the concentration of a ligand is 10 times higher at the target than expected, the true affinity of the ligand will be 10 times lower than the apparent/measured affinity. One might argue that this is not of particular relevance – ‘if the end result is the same, it does not matter if an increase in affinity is driven by a true ligand-protein interaction or a concentrating effect’. However, in reality an increase in local concentration will likely increase the apparent affinity for off-target receptors, particularly in the same local environment e.g., synapse. In primary drug screens often only the target receptor is considered, with assays focusing on screening compounds against a cell over expressing said receptor. The addition of lipophilic or charged groups may appear to increase affinity and lead the researcher down the wrong path, chasing a compound that will later prove to be non-selective. This information can also mislead molecular

docking and structure activity relationship studies, where only true affinities should be considered.

Although local concentration may be thought of as an artefact that is distorting drug discovery programs and needs to be accounted for, there could be some instances where one might design a ligand specifically to exploit this phenomenon. For example, topical treatments like drugs delivered to the lungs by inhalers may benefit from a high concentrating effect, with less inherent concern about off-target effects relative to a systemically administered drug.

When speculating as to the mechanism behind these local concentrating effects, perhaps the most likely explanation is the 'membrane sink' hypothesis. This idea has long been proposed as a possible explanation for the extended duration of action of long acting beta agonists (LABAs) (Anderson et al., 1994b). As the name suggests, the membrane could act as a sink/reservoir, accumulating lipophilic/uncharged ligands at high concentrations, which in turn slowly leak out of the membrane, and possibly re-enter many times. While normally thought of in the context of long duration of action, it could explain the observed data in the present Chapter.

For some receptors, ligands are believed to enter the binding pocket of the receptor via lateral diffusion through the membrane for example at the Sphingosine 1-phosphate (S1P) receptor (Hanson et al., 2012). Thus for these receptors accumulation in the membrane would directly drive measured affinities. More typically, as with the case of the adenosine A2a receptor, it is believed ligands enter membrane bound receptors via the extracellular space (Doré et al., 2011). Thus, the local concentration formed as ligand leaks from the membrane would be the key determinate in differences between measured and true affinities.

The receptor driven component of local concentration could be a direct observation of rebinding. Similarly, to the membrane sink hypothesis, ligands bind receptor, subsequently dissociate, but then rather than form part of the homogenous bulk aqueous, there is a chance the

ligand rebinds to the same or a nearby receptor before it leaves the local vicinity. It is worth noting that the experiments in this Chapter involve recombinant cells over-expressing the A2a receptor. Thus, the receptor driven component may be of less significance *in vivo*. However, there may still be areas *in vivo* where expression levels of receptor could be high enough for significant rebinding to occur. For examples in synapses where the shape and size of the extracellular space may further drive rebinding or where expression levels within a single cell are high in localised microdomains (Sykes et al., 2017). Further experiments using primary cells could begin to explore this, although applying FCS to such cells may prove technically challenging.

The data of the present Chapter not only suggests potential difficulties for drug discovery assays in terms of concentrating effects at cell membranes, but also the considerably lower than expected concentrations in the bulk aqueous could indicate an overlooked hazard. The ligands may have been depleted by sticking to cells, the coverslips (as evidenced by the concentrating effect above the coverslips), and/or the pipette tips and tubes used to store and dilute the ligands. This adds further ambiguity to the concentrations used in pharmacological assay questions. Similar results have been seen measuring the concentration of a labelled protein, VEGF, in solution (Kilpatrick et al., 2017). The authors found that the addition of 0.1% bovine serum albumin (BSA) to the assay buffer significantly increased the measured concentration of protein, suggesting that the BSA was blocking interaction with non-specific binding sites like glass and plastic.

Ideally, we would have successfully achieved more data incorporating multiple X and Y points above and around cells with multiple Z positions, instead of fixed X and Y positions with multiple Z positions. This could allow for 3D reconstructions of local concentration around a cell. Attempts were made to achieve this using count rate scans and simple photocounting approaches (up to 512x512 pixels). However, both were susceptible to bleed through as demonstrated using beads (Figure 5.4). This shows the necessity of using auto correlation analysis

where the background noise is accounted for. Attempts were also made to manually position 25 points in a 5x5 grid in the X and Y axis above cells for FCS reads. These needed to be read in a reasonable time frame such that there were not large discrepancies in incubation times between data points. The process was attempted to be automated by pre-programming the 25 positions. However, more often than not the software crashed under the amount of data being processed. This is potentially an option moving forward using better software or computing power.

FCS gives detailed quantitative information with a high degree of spatial resolution that cannot be replicated with other techniques currently available. However, the throughput has limited the data set to three fluorescent compounds a single concentration. With more time, more ligands would be assessed to better draw correlations with physicochemical properties. In particular recently published fluorescent adenosine ligands that are significantly less lipophilic would be interesting to measure (Comeo et al., 2019). Additionally, with more time multiple nominal concentration would be measured as well as measuring the same ligands using different adenosine receptors.

However, by obtaining high quality data for three ligands, we can draw comparisons with the already obtained kinetic and physicochemical data.

Chapter 6 – General discussion: Understanding the relationships between kinetics, physicochemical properties, and local concentration of drugs

6.1 Introduction

In the previous Chapters we have characterised three distinct groups of properties of multiple adenosine receptor ligands. Using TR-FRET, the association, dissociation, and affinity values of a series of 8 fluorescently labelled were obtained at the A2a and A2b receptors. Also using TR-FRET, in this case with a labelled competitor ligand, the same values were attempted to be measured for 57 unlabelled ligands at all four adenosine receptors. The same ligands were screened in an immobilised artificial membrane-high performance liquid chromatography (IAM-HPLC) assay to obtain experimentally derived physicochemical values relating to membrane affinities (K_{IAM} values), as well as values for several other physicochemical properties derived *in silico* (Log P, Log D, tPSA etc). Finally, three of the fluorescently labelled ligands were selected (due to varying properties) for experiments using FCS to measure local concentration accumulation at precise varying heights above adherent cells compared to measurements in the bulk aqueous. In this discussion the data collected from each Chapter will be analysed in the context of the other Chapters along with an extended discussion on the relationships between kinetics, physicochemical properties, and local concentration of drugs.

Our group has previously studied the kinetic binding properties and K_{IAM} values of a smaller series of commercially available β_2 adrenoceptor ligands (Sykes et al., 2014). Retention factors (K_{IAM}) were assumed to be a surrogate for local concentration, although no corrections to

partition coefficients (K_{IAM}) were made. Additionally, no measurements were made in the immediate vicinity of the receptor on the extracellular site. As with the A2a adenosine receptor, the β 2 adrenoceptor is thought to be accessed via the extracellular space and not through the membrane. Therefore K_{IAM} values were used to calculate “real” concentrations at the receptor level.

Our group has also used FCS before to measure local concentration, however this was only with a single ligand and with no physicochemical measurements (Gherbi et al., 2018). Therefore no attempts were made to draw trends across a data set of multiple ligands.

The main aim of this Chapter is to combine and analyse the data of the previous Chapters to explore the relationships between kinetics, physicochemical properties, and local concentration of drugs. In particular, discussion will focus on the wider implications to drug discovery.

6.2 Combining results of previous chapters, with discussion

6.2.1 Relationship between kinetics and physicochemical properties of 8 fluorescent compounds

Firstly in this chapter the fluorescent ligands will be considered. Before a subset of ligands were chosen to be used in FCS experiments, kinetic data for all 8 fluorescent compounds were obtained at the A2a and A2b receptors (see Chapter 3, Table 3.2), as well as physicochemical data (see Chapter 4, Table 4.2). As noted in these previous Chapter, simply changing the linker regions and/or fluorophores, while maintaining the same pharmacophore, led to a range of kinetic and physicochemical values. We correlated these differences to explore the relationship between kinetics and physicochemical properties.

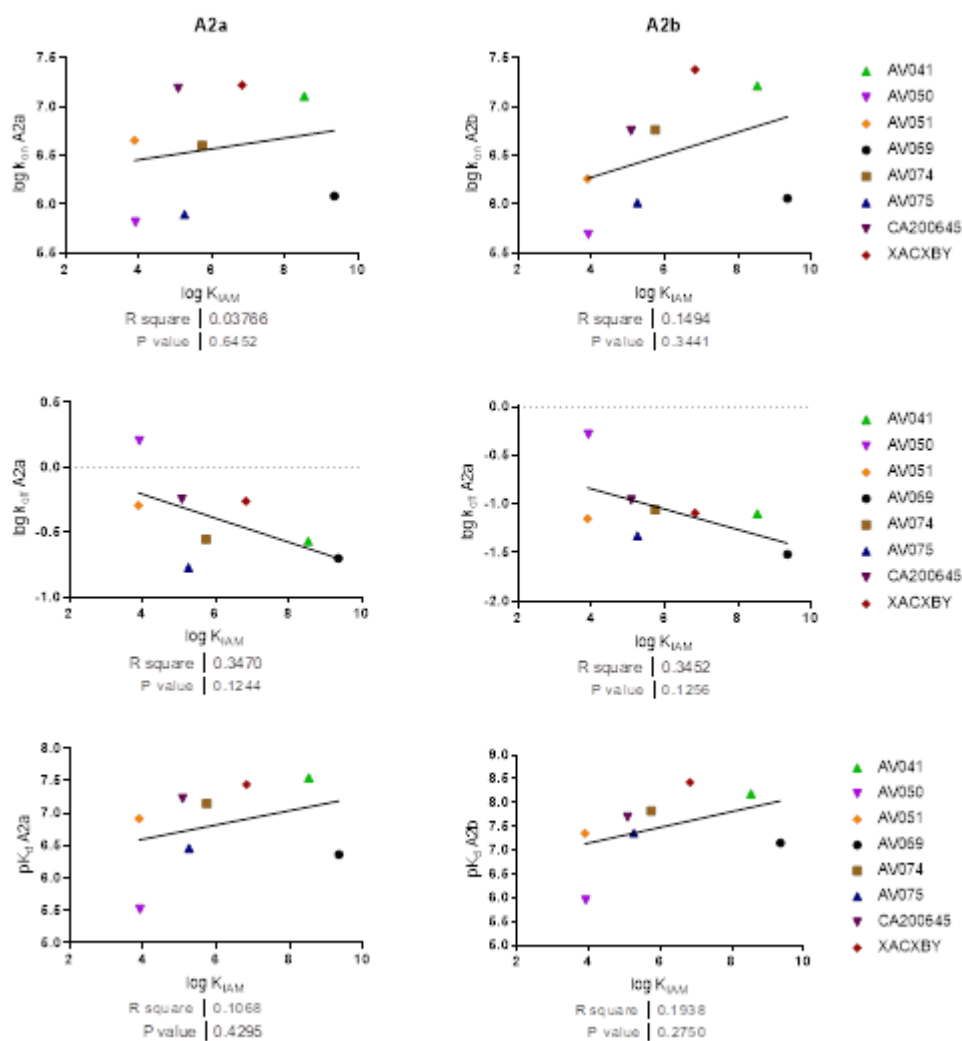


Figure 6.1. Lack of correlations between kinetic binding value and membrane affinities for fluorescent ligands. A2a (left column), A2b (right column), log k_{on} (top row), log k_{off} (middle row), and pK_d (bottom row). P values determined by Pearson correlation coefficient.

Similar patterns were seen across both receptors where there appears to be a weak positive correlation between log k_{on} and log K_{IAM} values, also a weak positive correlation between pK_d and log K_{IAM} values, and a weak negative correlation between log k_{off} and log K_{IAM} values. In all cases these correlations were not statistically significant ($p > 0.05$). Therefore limited conclusions can be drawn from this data alone. The next step was to see how this data related to measured local concentrations.

6.2.2 Relationship between kinetics, physicochemical properties, and local concentration of CA200645, AV075 and XACXBY

Due to labour intensive methodology of FCS only three out of the eight fluorescent ligands were chosen for experiments (AV075, CA200645, and XACXBY). These were selected due to their range of physicochemical and kinetic properties (AV050 and AV051 were also excluded due to the complications of using ligands with different fluorophores). Despite only being a small data set, these three ligands were well characterised in a way no other set of ligands has been before.

Compound	Local concentration 2 μ m above membrane (nM)	k_{on} (min ⁻¹ mM ⁻¹)	k_{off} (min ⁻¹)	K_d (nM)	cLogD	Log K_{IAM}	Log K_{IAM}
XACXBY	1024.6 \pm 347.4	0.55 \pm 0.23	16700 \pm 8030	36.0 \pm 6.4	3.39	3.21	6.83*
CA200645	62.3 \pm 9.5	0.57 \pm 0.17	1330 \pm 175	461 \pm 10.7	2.39	2.81	5.08*
AV075	111.3 \pm 30.1	0.17 \pm 0.10	791 \pm 36.4	346 \pm 30.2	0.87	2.86	5.26*

Table 6.1. Summary key data from Chapters 3-6 relating to AV075, CA200645, and XACXBY.

As noted in Chapter 5, AV075 and CA200645 had similar (within 2-fold) measured local (2 μ m) concentrations, when added at similar (within 2-fold) concentrations due to having similar K_d values (ligands were added at 0.1x their apparent K_d concentrations). XACXBY however was added at a lower concentration, but measured at approximately a 9-16-fold higher concentration 2 μ m from the cell membrane than the other two ligands. It may have been expected that XACXBY would have the highest propensity for concentrating around the cell membrane as it appears to be the most lipophilic (highest LogD). However, by the same logic the cLogP/D values also indicate that CA200645 would have a much higher propensity for concentrating around the cell membrane compared to AV075 as CA200645 has 1.52 log units higher calculated

lipophilicity values. In fact, the opposite is true as CA200645 was measured at a slightly lower concentration than AV075. Of course it should be noted that only 3 compounds have been tested here and more data are needed to draw correlations.

In contrast, when considering the experimentally derived K_{IAM} or K_{IAM} values instead of Log P/D, local concentration data is perhaps better understood. CA200645 and AV075 are only 0.16 log units different in K_{IAM} values with CA200645 being the lower of the two. Whereas XACXBY is over 1.5 log units higher than the other two compounds. As explained in Chapter 4, the K_{IAM} values for the fluorescent compounds require extrapolation due to the standard compounds having too low affinity for the membrane column, and this caveat should be considered when thinking about precise value, however it gives a good indication of the relative membrane affinities.

According to the pK_a values generated by the chemicalize software used for the in silico physicochemical analysis, at pH7.4 neither AV075 nor CA200645 should have a unique charged moiety. Therefore, the discrepancy between relative logP/D values and K_{IAM} values is most likely explained by some form of steric interaction between the fluorescent compounds and the immobilised phosphatidylcholine i.e., the shape AV075 is driving an increased affinity for membrane relative to CA200645 in a way that isn't related to the overall charge or lipophilicity of the entire molecule.

The seemingly better correlation between K_{IAM} and local concentration, although only a small data set, suggests a benefit to using an IAM-HPLC approach instead of experimentally or computationally derived lipophilicity values when considering true membrane interactions.

Importantly, XACXBY has a significantly faster on-rate, higher K_d , a much larger local concentration despite lower nominal concentration, and higher cLogD/P and K_{IAM} values compared to the other two ligands. This fits with the hypothesis that the physicochemical properties of

ligands could be driving local concentrations of drugs, which distorts observed affinity and kinetic binding parameters of drugs.

6.2.3 Relationship between kinetics and physicochemical properties for unlabelled compounds

It is an important next step to explore the hypothesis in context of more drug-like, unlabelled molecules. While it is not possible to perform FCS on these compounds to directly measure local concentration, there are the benefits that a much larger data set can be practically screened as fluorescent compounds can be expensive and few in number, and the results could arguably be more relevant to clinically relevant compounds, particularly as the fluorescent compounds are so large and lipophilic.

In addition to have a compound list of 57 unlabelled compounds compared to 8 fluorescently labelled compounds, due to cost and availability, it was possible to screen all the unlabelled compounds at all four adenosine receptors. This was also made feasible with a degree of automation. Having data for the same ligands at multiple receptors is potentially interesting as any effect driven by an affinity for membrane would likely be non-specific i.e., if a compound was 10 times as concentrated in the immediate vicinity of the membrane compared to the nominal concentration thought to be added, the apparent affinity would be artificially 10 times greater (10x smaller K_d) for the ligand at all receptors.

As noted in Chapter 3, it was possible to obtain more K_d data than kinetic data due to limitations in data fitting. Therefore, we first considered just affinity values in relation to physicochemical data.

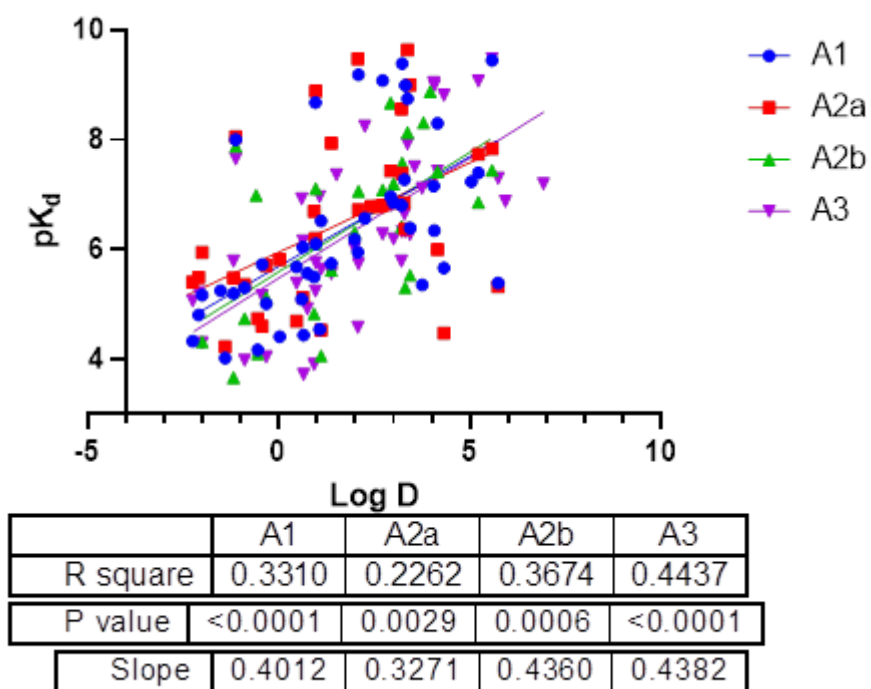
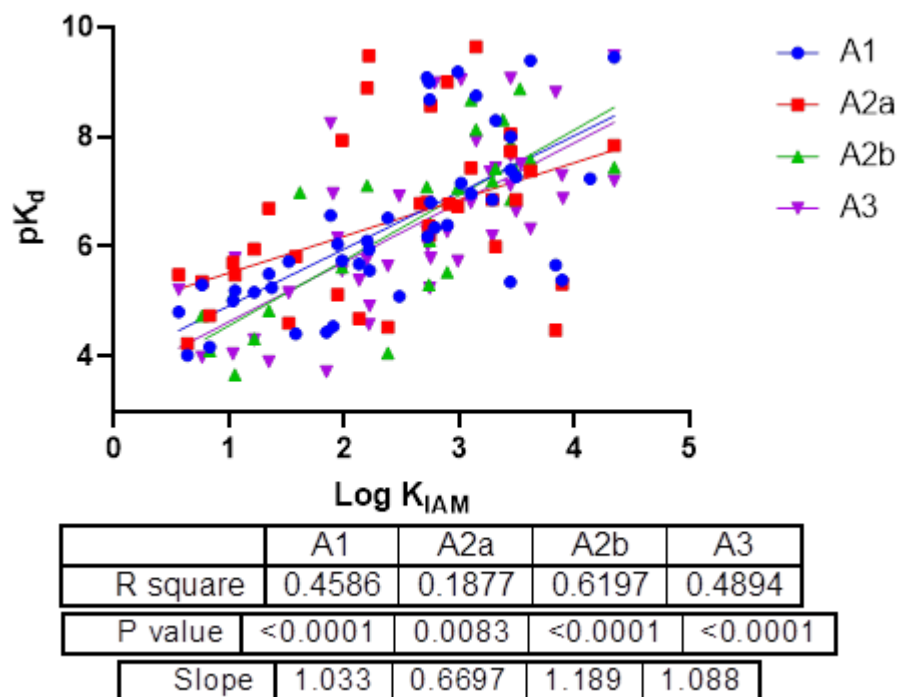
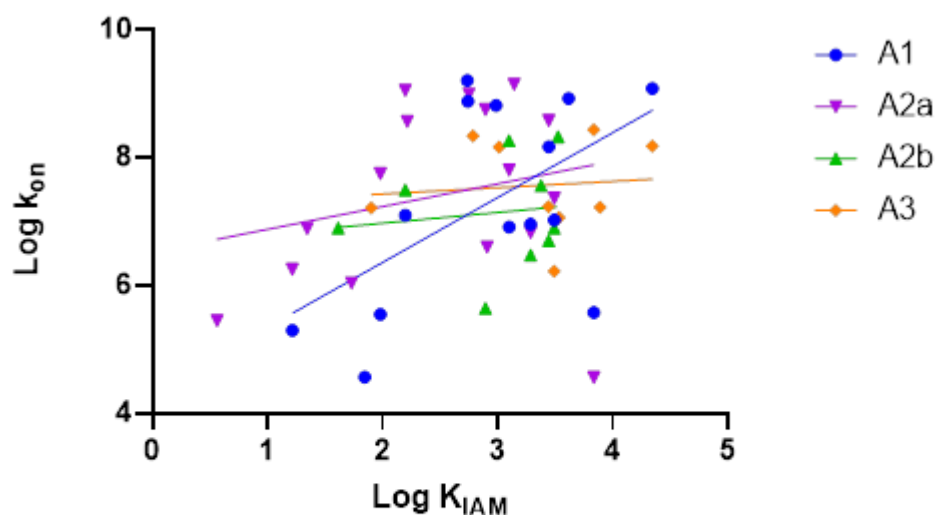


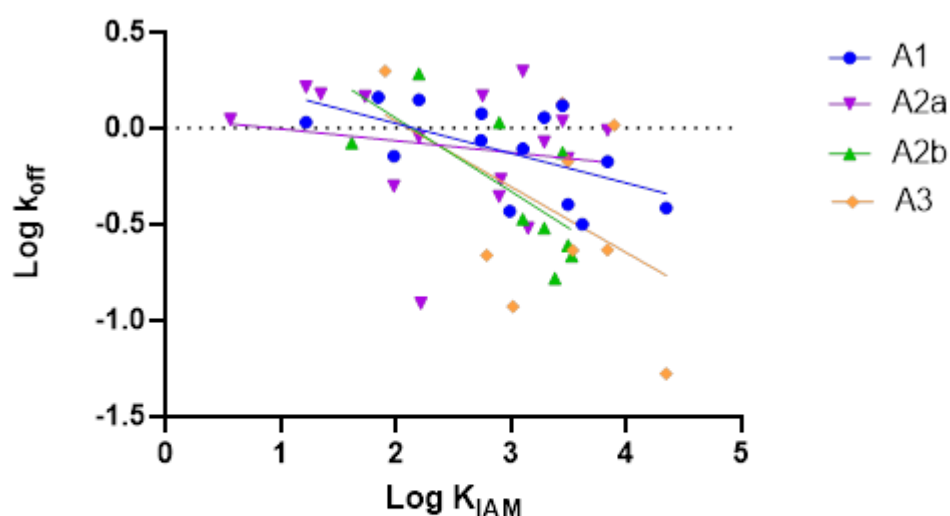
Figure 6.2. Correlations between receptor-ligand affinity values (pK_d) and membrane affinity values ($\text{Log } K_{IAM}$) or calculated lipophilicity values ($\text{Log } D$) for unlabelled adenosine ligands. Data shown for adenosine A1 (blue), A2a (red), A2b (green), and A3 (purple) receptors. In all cases $n \geq 3$ (excluding in silico data). P value determined by Pearson correlation coefficient.

Statistically significant correlation was observed between pK_d and both Log K_{IAM} and Log D for all receptors. The overall correlation between pK_d and Log K_{IAM} for all receptors was R squared of 0.4039, (p<0.0001). The overall correlation between pK_d and Log D for all receptors was R squared of 0.3321, (p<0.0001) (Pearson's correlation in both cases). Interestingly, the slopes of the curves are all quite similar, particularly A1, A2b and A3. This potentially suggest a receptor non-specific effect.

To investigate further, kinetic data (where it was possible to obtain) for the compounds at given receptors was correlated with Log K_{IAM} values.



	A1	A2a	A2b	A3
R square	0.3021	0.05683	0.01678	0.008850
P value	0.0418	0.3739	0.7398	0.8098
Slope	1.014	0.3554	0.1683	0.09839



	A1	A2a	A2b	A3
R square	0.3261	0.03305	0.4823	0.2173
P value	0.0329	0.5004	0.0379	0.2060
Slope	-0.1553	-0.06125	-0.3814	-0.3425

Figure 6.3. Correlations between association rates ($\text{Log } k_{\text{on}}$; top) or dissociation rates ($\text{Log } k_{\text{off}}$; bottom) and membrane affinity values ($\text{Log } K_{\text{IAM}}$) for unlabelled adenosine ligands. In all cases $n \geq 3$ P value determined by Pearson correlation coefficient.

When analysing by receptor, statistically significant correlation ($p < 0.05$) between $\text{Log } k_{\text{on}}$ and $\text{Log } K_{\text{IAM}}$ was only seen for the A1 receptor, and between $\text{Log } k_{\text{off}}$ and $\text{Log } K_{\text{IAM}}$ for A1 and A2b. This is perhaps surprising, however the data set is quite small due to limitations in measuring many of the compounds kinetically. When combining the data for all receptors statistically significant correlation was observed between $\text{Log } k_{\text{on}}$ and K_{IAM} values ($p = 0.03$), and between $\text{Log } k_{\text{off}}$ and K_{IAM} values ($p = 0.0012$). Again, this is perhaps surprising as observed association but not dissociation rates should be affected by concentration, therefore if $\text{Log } K_{\text{IAM}}$ values are correlating to increased local concentration then the stronger correlation should be with $\text{Log } k_{\text{on}}$ values. $\text{Log } k_{\text{on}}$ values ranged over 5 orders of magnitude, whereas $\text{Log } k_{\text{off}}$ values ranged less than 2 orders of magnitude.

6.2.4 Relationship between other *in silico* derived physicochemical properties and receptor kinetics for unlabelled compounds

While the virtues of IAM-HPLC have been discussed throughout the thesis so far, often in comparison with $\text{Log } P$ or $\text{Log } D$ measurements, it is useful also to consider other physicochemical properties. These other parameters could help in understanding the importance of K_{IAM} values, or provide alternative explanations for the trends shown. The Chemicalize software used to calculate cLogP/D values also provides several other useful values such as molecular weight (MW), hydrogen bond donor/acceptor numbers, and calculates a topological polar surface area (tPSA) value for each compound. As the MW of the compounds in the series increases, so does $\text{Log } K_{\text{IAM}}$ ($r^2 = 0.3390$, $p < 0.0001$), cLogD ($r^2 = 0.1428$, $p = 0.0032$), hydrogen bond donors + acceptors ($r^2 = 0.1012$, $p = 0.0141$), and tpsa ($r^2 = 0.1832$, $p = 0.0007$). These are all understandable, because as the molecules become larger they are more likely to have additional lipophilic groups, polar groups and hydrogen bond forming atoms. cLogD and tpsa negatively correlate

($r^2=0.2556$, $p<0.0001$) across the series, however Log K_{IAM} and t_{spa} do not significantly correlate ($r^2=0.05842$, $p=0.0676$).

It is difficult to discount the possibility that any correlations between Log K_{IAM} and affinity is not the result of causation, but is instead the result of correlation to a third factor. For example, as described above bigger molecules in the data set have higher K_{IAM} values, but also by virtue to their size may form more contact points with the receptor, thus increasing affinity. However, this is unlikely to explain correlations with association rate as Log k_{off} negatively correlates with MW ($r^2=0.1266$, $p=0.0121$), but Log k_{on} does not ($r^2=0.001215$, $p=0.8121$).

6.3 General concluding discussion

This thesis has for the first time measured the local concentrations of multiple ligands using FCS whilst also exploring the kinetic binding and physicochemical properties of these ligands and a large set of unlabelled ligands. The hypothesis that our group has been exploring is that the physicochemical properties of potential drug candidates drive local accumulation of drug at the cell membrane, thus distorting true pharmacological parameters such as affinity values obtained from *in vitro* drug discovery assays for membrane bound receptors. The most compelling evidence to support this hypothesis resides in data for the three compounds which were used in FCS experiments (XACXBY, CA200645 and AV075). XACXBY was the most lipophilic, has the highest affinity for membrane, highest association rate and highest affinity. The difference between CA200645 and AV075 were better explained by Log K_{IAM} values rather than the cLogD values, thus providing support for the benefits of using IAM-HPLC over more conventional lipophilicity measurements.

Strong correlations between affinity or association rate values and Log K_{IAM} values were not always seen, thus weakening the argument for the

significance of local concentrations of drugs. These could be related to limitations in the study, or be due to many compound factors, such as true structure activity relationships. The fluorescent compounds used are all on or above the high end of the spectrum of Log K_{IAM} values of the unlabelled compounds containing many clinically relevant drugs. The need for exceptionally well-fitting data for the Motulsky-Mahan competition kinetic approach meant that the range of kinetic data was limited, particularly by dissociation rate.

If this is a generalised phenomenon affecting all ligands, or all ligands above a certain threshold of attraction to cell membranes, the implications to drug discovery and pharmacological assays could be large. All equations used to analyse pharmacological assays rely on the assumption that the concentration of ligand being added to the assay is the concentration being directly exposed to the target. Taking the key pharmacological value of affinity as an example, if the concentration of a ligand is 10 times higher at the target than expected, the true affinity of the ligand will be 10 times lower than the apparent/measured affinity. One might argue that this is not of particular relevance – ‘if the end result is the same, it does not matter if an increase in affinity is driven by a true ligand-protein interaction or a concentrating effect’. However, in reality an increase in local concentration will increase the apparent affinity for off-target receptors by the same fold shift as on-target. In primary drug screens often only the target receptor is considered, with assays focusing on screening compounds against a cell over expressing said receptor. The addition of lipophilic or charged groups may appear to increase affinity and lead the researcher down the wrong path, chasing a compound that will later prove to be non-selective. This information can also mislead molecular docking and structure activity relationship studies, where only true affinities should be considered.

Although local concentration may be thought of as an artefact that is distorting drug discovery programs and needs to be accounted for, there could be some instances where one might design a ligand

specifically to exploit this phenomenon. For example, topical treatments like drugs delivered to the lungs by inhalers may benefit from a high concentrating effect, with less inherent concern about off-target effects relative to a systemically administered drug (Anderson et al., 1994a).

6.4 Future Directions

If this study were repeated, using adenosine receptor or another receptor or group of receptors, it would be useful to use a range of fluorescent compounds with lower, more clinically relevant, membrane affinities. This could be achieved using different fluorophores (as BODIPY is extremely lipophilic) and less lipophilic linker regions.

Additionally, while using a largely clinically relevant unlabelled data set had advantages (for example, higher affinity compounds proved easier to capture their kinetic properties and measuring the properties of clinically relevant compounds may be of use to other research groups), it potentially provided a bias that could have undermined the impact of local concentration and micro-PK/PD. This is because most of the compounds used were the product of extensive design through structure-activity relationship studies, and thus this could overshadow any changes in affinity from local concentrating effects.

If the FCS experimental set up could be adapted to be higher throughput (e.g., only measuring 1 height or greater automation), a greater number of compounds could be screened leading to more powerful and convincing correlations. Similarly, by using multiple competitor ligands, kinetic experiments could capture a wider range of kinetic values in the unlabelled data set (Sykes et al., 2019). Finally, computation modelling of binding in combination with estimates for local concentrations could be implemented to better understand kinetic data sets, and in particular to try to understand why some compounds translate from *in vitro* studies to successful *in vivo* studies and some do not (Dickson et al., 2016). Improving the quality and quantity of these data sets could help further probe the significance of micro-PK/PD.

Chapter 7 – References

Adair, J., Suvaci, E., and Sindel, J. (2001). Surface and Colloid Chemistry. *Encycl. Mater. Sci. Technol.* (Second Ed. 1–10.

Allard, B., Beavis, P.A., Darcy, P.K., and Stagg, J. (2016). Immunosuppressive activities of adenosine in cancer. *Curr. Opin. Pharmacol.* 29: 7–16.

Allard, D., Turcotte, M., and Stagg, J. (2017). Targeting A2 adenosine receptors in cancer. *Immunol. Cell Biol.* 95: 333–339.

Anderson, G., Lindén, A., and Rabe, K. (1994a). Why are long-acting beta-adrenoceptor agonists long-acting? *Eur. Respir. J.* 7: 569–578.

Anderson, G.P. (1993). Formoterol: pharmacology, molecular basis of agonism, and mechanism of long duration of a highly potent and selective beta 2-adrenoceptor agonist bronchodilator. *Life Sci.* 52: 2145–60.

Anderson, G.P., Lindén, A., and Rabe, K.F. (1994b). Why are long-acting beta-adrenoceptor agonists long-acting? *Eur. Respir. J.* 7: 569–78.

Andrews, S.S. (2005). Serial rebinding of ligands to clustered receptors as exemplified by bacterial chemotaxis. *Phys. Biol.* 2: 111–22.

Arunan, E., Desiraju, G.R., Klein, R.A., Sadlej, J., Scheiner, S., Alkorta, I., et al. (2011). Definition of the hydrogen bond (IUPAC Recommendations 2011)*. *Pure Appl. Chem* 83:

1637–1641.

Avdeef, A., Box, K.J., Comer, J.E.A., Hibbert, C., and Tam, K.Y. (1998). pH-Metric logP 10. Determination of Liposomal Membrane-Water Partition Coefficients of Ionizable Drugs. *Pharm. Res.* 15: 209–215.

Barbato, F., Cirocco, V., Grumetto, L., and Immacolata La Rotonda, M. (2007). Comparison between immobilized artificial membrane (IAM) HPLC data and lipophilicity in n-octanol for quinolone antibacterial agents. *Eur. J. Pharm. Sci.* 31: 288–297.

Beavis, P.A., Divisekera, U., Paget, C., Chow, M.T., John, L.B., Devaud, C., et al. (2013). Blockade of A_{2A} receptors potently suppresses the metastasis of CD73⁺ tumors. *Proc. Natl. Acad. Sci.* 110: 14711–14716.

Borea, P.A., Gessi, S., Merighi, S., Vincenzi, F., and Varani, K. (2018). Pharmacology of Adenosine Receptors: The State of the Art. *Physiol. Rev.* 98: 1591–1625.

Bouchard, G., Carrupt, P.A., Testa, B., Gobry, V., and Girault, H.H. (2001). The apparent lipophilicity of quaternary ammonium ions is influenced by galvanic potential difference, not ion-pairing: A cyclic voltammetry study. *Pharm. Res.* 18: 702–708.

Bridson, S., Gandía, J., Amaral, O., Ferré, S., Lluís, C., Franco, R., et al. (2008). Plasma membrane diffusion of G protein-coupled receptor oligomers. *Biochim. Biophys. Acta* 1783: 2262–2268.

Briddon, S., Kilpatrick, L., and Hill, S. (2018). Studying GPCR Pharmacology in Membrane Microdomains: Fluorescence Correlation Spectroscopy Comes of Age. *Trends Pharmacol. Sci.* 39: 158–174.

Briddon, S.J., Middleton, R.J., Cordeaux, Y., Flavin, F.M., Weinstein, J.A., George, M.W., et al. (2004). Quantitative analysis of the formation and diffusion of A1-adenosine receptor-antagonist complexes in single living cells. *Proc. Natl. Acad. Sci.* 101: 4673–4678.

Caldwell, G.W., Masucci, J.A., Evangelisto, M., and White, R. (1998). Evaluation of the immobilized artificial membrane phosphatidylcholine: Drug discovery column for high-performance liquid chromatographic screening of drug-membrane interactions. *J. Chromatogr. A* 800: 161–169.

Cekic, C., Sag, D., Li, Y., Theodorescu, D., Strieter, R.M., and Linden, J. (2012). Adenosine A2B Receptor Blockade Slows Growth of Bladder and Breast Tumors. *J. Immunol.* 188: 198–205.

Chen, J.-F., Eltzschig, H.K., and Fredholm, B.B. (2013). Adenosine receptors as drug targets — what are the challenges? *Nat. Rev. Drug Discov.* 12: 265–286.

Cheng, X., Ji, Z., Tsalkova, T., and Mei, F. (2008). Epac and PKA: a tale of two intracellular cAMP receptors. *Acta Biochim. Biophys. Sin. (Shanghai)*. 40: 651–62.

Choudhury, H., Chellappan, D.K., Sengupta, P., Pandey, M., and Gorain, B. (2019). Adenosine Receptors in Modulation of Central Nervous System Disorders. *Curr. Pharm. Des.* 25:

2808–2827.

Cieślak, M., Komoszyński, M., and Wojtczak, A. (2008). Adenosine A2A receptors in Parkinson's disease treatment. *Purinergic Signal.* 4: 305.

Cohen, F.R., and Birdsall, N.J.M. (1996). The effects of saponin on the binding and functional properties of the human adenosine A1 receptor. 1521–1529.

Coleman, R.A., Johnson, M., Nials, A.T., and Vardey, C.J. (1996). Exosites: their current status, and their relevance to the duration of action of long-acting beta 2-adrenoceptor agonists. *Trends Pharmacol. Sci.* 17: 324–30.

Comeo, E., Kindon, N.D., Soave, M., Stoddart, L.A., Kilpatrick, L.E., Scammells, P.J., et al. (2019). Subtype-Selective Fluorescent Ligands as Pharmacological Research Tools for the Human Adenosine A2A Receptor. *J. Med. Chem.* 63: 2656–2672.

Coombs, D., and Goldstein, B. (2004). Effects of the geometry of the immunological synapse on the delivery of effector molecules. *Biophys. J.* 87: 2215–20.

Copeland, R. (2016). The drug–target residence time model: a 10-year retrospective. *Nat. Rev. Drug Discov.* 15: 87–95.

Copeland, R.A., Pompliano, D.L., and Meek, T.D. (2006a). Drug–target residence time and its implications for lead optimization. *Nat. Rev. Drug Discov.* 5: 730–739.

Copeland, R.A., Pompliano, D.L., and Meek, T.D. (2006b). Drug–target residence time and its implications for lead

optimization. *Nat. Rev. Drug Discov.* 5: 730–739.

Csizmadia, F., Tsantili-Kakoulidou, A., Panderi, I., and Darvas, F. (1997). Prediction of distribution coefficient from structure. 1. Estimation method. *J. Pharm. Sci.* 86: 865–871.

Cusack, K.P., Wang, Y., Hoemann, M.Z., Marjanovic, J., Heym, R.G., and Vasudevan, A. (2015). Design strategies to address kinetics of drug binding and residence time. *Bioorg. Med. Chem. Lett.* 25: 2019–2027.

Dearden, J.C., and Bresnen, G.M. (1988). The Measurement of Partition Coefficients. *Quant. Struct. Relationships* 7: 133–144.

Desai, A., Victor-Vega, C., Gadangi, S., Montesinos, M.C., Chu, C.C., and Cronstein, B.N. (2005). Adenosine A2A Receptor Stimulation Increases Angiogenesis by Down-Regulating Production of the Antiangiogenic Matrix Protein Thrombospondin 1. *Mol. Pharmacol.* 67: 1406–1413.

Desai, A.J., and Miller, L.J. (2018). Changes in the plasma membrane in metabolic disease: impact of the membrane environment on G protein-coupled receptor structure and function. *Br. J. Pharmacol.* 175: 4009–4025.

Dickson, C.J., Hornak, V., Velez-Vega, C., McKay, D.J.J., Reilly, J., Sandham, D.A., et al. (2016). Uncoupling the Structure–Activity Relationships of β 2 Adrenergic Receptor Ligands from Membrane Binding. *J. Med. Chem.* 59: 5780–5789.

Dityatev, A., Frischknecht, R., and Seidenbecher, C.I. (2006).

Extracellular matrix and synaptic functions. *Results Probl. Cell Differ.* 43: 69–97.

Doré, A.S., Robertson, N., Errey, J.C., Ng, I., Hollenstein, K., Tehan, B., et al. (2011). Structure of the adenosine A(2A) receptor in complex with ZM241385 and the xanthines XAC and caffeine. *Structure* 19: 1283–93.

Dror, R.O., Pan, A.C., Arlow, D.H., Borhani, D.W., Maragakis, P., Shan, Y., et al. (2011). Pathway and mechanism of drug binding to G-protein-coupled receptors. *Proc. Natl. Acad. Sci. U. S. A.* 108: 13118–23.

Elson, E.L. (2013). 40 Years of FCS: How it all began. *Methods Enzymol.* 518: 1–10.

Emami-Nemini, A., Roux, T., Leblay, M., Bourrier, E., Lamarque, L., Trinquet, E., et al. (2013). Time-resolved fluorescence ligand binding for G protein-coupled receptors. *Nat. Protoc.* 8: 1307–1320.

Erdmann, A.A., Gao, Z.-G., Jung, U., Foley, J., Borenstein, T., Jacobson, K.A., et al. (2005). Activation of Th1 and Tc1 cell adenosine A2A receptors directly inhibits IL-2 secretion in vitro and IL-2-driven expansion in vivo. *Blood* 105: 4707–4714.

Ernens, I., Bousquenaud, M., Lenoir, B., Devaux, Y., and Wagner, D.R. (2015). Adenosine stimulates angiogenesis by up-regulating production of thrombospondin-1 by macrophages. *J. Leukoc. Biol.* 97: 9–18.

Feoktistov, I., Goldstein, A.E., Ryzhov, S., Zeng, D.,

Belardinelli, L., Voyno-Yasenetskaya, T., et al. (2002). Differential expression of adenosine receptors in human endothelial cells: role of A2B receptors in angiogenic factor regulation. *Circ. Res.* 90: 531–8.

Feoktistov, I., Ryzhov, S., Goldstein, A.E., and Biaggioni, I. (2003). Mast Cell-Mediated Stimulation of Angiogenesis: Cooperative Interaction Between A2B and A3 Adenosine Receptors. *Circ. Res.* 92: 485–492.

Franco, R., Cordoní, A., Llinas del Torrent, C., Lillo, A., Serrano-Marín, J., Navarro, G., et al. (2021). Structure and function of adenosine receptor heteromers. *Cell. Mol. Life Sci.* 2021 788 78: 3957–3968.

Gherbi, K., Briddon, S.J., and Charlton, S.J. (2015). Micro-Pharmacokinetics: The Quantification Of Ligand Concentration At The Membrane Of Single Living Cells Using Fluorescence Correlation Spectroscopy. *Pa2 Online*.

Gherbi, K., Briddon, S.J., and Charlton, S.J. (2018). Micro-pharmacokinetics: Quantifying local drug concentration at live cell membranes. *Sci. Rep.* 8: 1–8.

Goldstein, B., and Dembo, M. (1995). Approximating the effects of diffusion on reversible reactions at the cell surface: ligand-receptor kinetics. *Biophys. J.* 68: 1222–1230.

Grime, R.L., Goulding, J., Uddin, R., Stoddart, L.A., Hill, S.J., Poyner, D.R., et al. (2020). Single molecule binding of a ligand to a G-protein-coupled receptor in real time using fluorescence correlation spectroscopy, rendered possible by nano-encapsulation in styrene maleic acid lipid particles.

Nanoscale 12: 11518–11525.

Guo, D., Hillger, J.M., IJzerman, A.P., and Heitman, L.H. (2014). Drug-Target Residence Time-A Case for G Protein-Coupled Receptors. *Med. Res. Rev.* 34: 856–892.

Guo, D., Mulder-Krieger, T., IJzerman, A.P., and Heitman, L.H. (2012a). Functional efficacy of adenosine A_{2A} receptor agonists is positively correlated to their receptor residence time. *Br. J. Pharmacol.*

Guo, D., Mulder-Krieger, T., IJzerman, A.P., and Heitman, L.H. (2012b). Functional efficacy of adenosine A_{2A} receptor agonists is positively correlated to their receptor residence time. *Br. J. Pharmacol.* 166: 1846–59.

Gupta, A., and Bajaj, N.S. (2017). Regadenoson use for stress myocardial perfusion imaging in advance chronic kidney disease and dialysis: Safe, effective, and efficient. *J. Nucl. Cardiol.*

Hanahan, D., Weinberg, R.A., Pan, K.H., Shay, J.W., Cohen, S.N., Taylor, M.B., et al. (2011). Hallmarks of Cancer: The Next Generation. *Cell* 144: 646–674.

Hanson, M.A., Roth, C.B., Jo, E., Griffith, M.T., Scott, F.L., Reinhart, G., et al. (2012). Crystal Structure of a Lipid G Protein-Coupled Receptor. *Science* (80-.). 335: 851–855.

Hollósy, F., Valkó, K., Hersey, A., Nunhuck, S., Kéri, G., and Bevan, C. (2006). Estimation of volume of distribution in humans from high throughput HPLC-based measurements of human serum albumin binding and immobilized artificial

membrane partitioning. *J. Med. Chem.* 49: 6958–6971.

Jaakola, V.-P., Griffith, M.T., Hanson, M.A., Cherezov, V., Chien, E.Y.T., Lane, J.R., et al. (2008). The 2.6 angstrom crystal structure of a human A2A adenosine receptor bound to an antagonist. *Science* 322: 1211–7.

Jenner, P., Mori, A., Aradi, S.D., and Hauser, R.A. (2021). Istradefylline - a first generation adenosine A 2A antagonist for the treatment of Parkinson's disease. *Expert Rev. Neurother.* 21: 317–333.

Jimenez, J.L., Punzón, C., Navarro, J., Muñoz-Fernández, M.A., and Fresno, M. (2001). Phosphodiesterase 4 inhibitors prevent cytokine secretion by T lymphocytes by inhibiting nuclear factor-kappaB and nuclear factor of activated T cells activation. *J. Pharmacol. Exp. Ther.* 299: 753–9.

Johnson, M. (2001). Beta2-adrenoceptors: mechanisms of action of beta2-agonists. *Paediatr. Respir. Rev.* 2: 57–62.

Kapur, S., and Seeman, P. (2000). Antipsychotic agents differ in how fast they come off the dopamine D2 receptors. Implications for atypical antipsychotic action. *J. Psychiatry Neurosci.* 25: 161–6.

Kilpatrick, L.E., Friedman-Ohana, R., Alcobia, D.C., Riching, K., Peach, C.J., Wheal, A.J., et al. (2017). Real-time analysis of the binding of fluorescent VEGF165a to VEGFR2 in living cells: Effect of receptor tyrosine kinase inhibitors and fate of internalized agonist-receptor complexes. *Biochem. Pharmacol.* 136: 62–75.

Klein Herenbrink, C., Sykes, D.A., Donthamsetti, P., Canals, M., Coudrat, T., Shonberg, J., et al. (2016). The role of kinetic context in apparent biased agonism at GPCRs. *Nat. Commun.* 7: 10842.

Klopman, G., Li, J.Y., Wang, S., Dimayuga, M., Wang, S., and Dimayuga, M. (1994). Computer Automated log P Calculations Based on an Extended Group Contribution Approach. *J. Chem. Inf. Comput. Sci.* 34: 752–781.

Kwapiszewska, K., Kalwarczyk, T., Michalska, B., Szczepański, K., Szymański, J., Patalas-Krawczyk, P., et al. (2019). Determination of oligomerization state of Drp1 protein in living cells at nanomolar concentrations. *Sci. Rep.* 9:

Lane, J.R., May, L.T., Parton, R.G., Sexton, P.M., and Christopoulos, A. (2017). A kinetic view of GPCR allostery and biased agonism. *Nat. Chem. Biol.* 13: 929–937.

Leibovich, S.J., Chen, J.-F., Pinhal-Enfield, G., Belem, P.C., Elson, G., Rosania, A., et al. (2002). Synergistic Up-Regulation of Vascular Endothelial Growth Factor Expression in Murine Macrophages by Adenosine A2A Receptor Agonists and Endotoxin. *Am. J. Pathol.* 160: 2231–2244.

Li, H., Zhao, T., and Sun, Z. (2018). Analytical techniques and methods for study of drug-lipid membrane interactions. *Rev. Anal. Chem.* 37:.

Lipinski, C.A., Lombardo, F., Dominy, B.W., and Feeney, P.J. (1997). Experimental and computational approaches to estimate solubility and permeability in drug discovery and development settings. *Adv. Drug Deliv. Rev.* 23: 3–25.

- Liu, W., Chun, E., Thompson, A.A., Chubukov, P., Xu, F., Katritch, V., et al. (2012). Structural Basis for Allosteric Regulation of GPCRs by Sodium Ions. *Science* 337: 232.
- Liu, Y.J., Chen, J., Li, X., Zhou, X., Hu, Y.M., Chu, S.F., et al. (2019). Research progress on adenosine in central nervous system diseases. *CNS Neurosci. Ther.* 25: 899–910.
- Long, J.S., Crighton, D., O'Prey, J., MacKay, G., Zheng, L., Palmer, T.M., et al. (2013). Extracellular Adenosine Sensing—A Metabolic Cell Death Priming Mechanism Downstream of p53. *Mol. Cell* 50: 394–406.
- Ma, S.-R., Deng, W.-W., Liu, J.-F., Mao, L., Yu, G.-T., Bu, L.-L., et al. (2017). Blockade of adenosine A2A receptor enhances CD8+ T cells response and decreases regulatory T cells in head and neck squamous cell carcinoma. *Mol. Cancer* 16: 99.
- Magde, D., Elson, E., and Webb, W.W. (1972). Thermodynamic Fluctuations in a Reacting System—Measurement by Fluorescence Correlation Spectroscopy. *Phys. Rev. Lett.* 29: 705.
- Markovich, R.J., Stevens, J.M., and Pidgeon, C. (1989). Fourier transform infrared assay of membrane lipids immobilized to silica: Leaching and stability of immobilized artificial membrane-bonded phases. *Anal. Biochem.* 182: 237–244.
- McCloskey, M.A., and Poo, M.M. (1986). Rates of membrane-associated reactions: reduction of dimensionality revisited. *J. Cell Biol.* 102: 88–96.

Mosenden, R., and Taskén, K. (2011). Cyclic AMP-mediated immune regulation — Overview of mechanisms of action in T cells. *Cell. Signal.* 23: 1009–1016.

Motulsky, H.J., and Mahan, L.C. (1984). The kinetics of competitive radioligand binding predicted by the law of mass action. *Mol. Pharmacol.* 25.

Muller, P. (1994). Glossary of terms used in physical organic chemistry (IUPAC Recommendations 1994). *Pure Appl. Chem.* 66: 1077–1184.

Nishida, N., Yano, H., Nishida, T., Kamura, T., and Kojiro, M. (2006). Angiogenesis in cancer. *Vasc. Health Risk Manag.* 2: 213–9.

Ohta, A., and Sitkovsky, M. (2001). Role of G-protein-coupled adenosine receptors in downregulation of inflammation and protection from tissue damage. *Nature* 414: 916–920.

Ong, S., Cal, S.J., Bernal, C., Rhee, D., Qiu, X., and Pidgeon, C. (1994). Phospholipid Immobilization on Solid Surfaces. *Anal. Chem.* 66: 782–792.

Ong, S., Liu, H., Qiu, X., Pidgeon, C., and Bhat, G. (1995). Membrane Partition Coefficients Chromatographically Measured Using Immobilized Artificial Membrane Surfaces. *Anal. Chem.* 67: 755–762.

Peach, C., Kilpatrick, L., Friedman-Ohana, R., Zimmerman, K., Robers, M., Wood, K., et al. (2018). Real-Time Ligand Binding of Fluorescent VEGF-A Isoforms that Discriminate between VEGFR2 and NRP1 in Living Cells. *Cell Chem. Biol.*

25: 1208-1218.e5.

Pidgeon, C., and Venkataram, U. V. (1989). Immobilized artificial membrane chromatography: Supports composed of membrane lipids. *Anal. Biochem.* 176: 36–47.

Rose, R., Briddon, S., and Hill, S. (2012). A novel fluorescent histamine H(1) receptor antagonist demonstrates the advantage of using fluorescence correlation spectroscopy to study the binding of lipophilic ligands. *Br. J. Pharmacol.* 165: 1789–1800.

Sadée, W., Perry, D.C., Rosenbaum, J.S., and Herz, A. (1982). [3H]diprenorphine receptor binding in vivo and in vitro. *Eur. J. Pharmacol.* 81: 431–40.

Sands, W.A., and Palmer, T.M. (2008). Regulating gene transcription in response to cyclic AMP elevation. *Cell. Signal.* 20: 460–466.

Santos, R., Ursu, O., Gaulton, A., Bento, A.P., Donadi, R.S., Bologa, C.G., et al. (2016). A comprehensive map of molecular drug targets. *Nat. Publ. Gr.* 16: 19–34.

Sargent, D.F., and Schwyzer, R. (1986). Membrane lipid phase as catalyst for peptide-receptor interactions. *Proc. Natl. Acad. Sci. U. S. A.* 83: 5774–8.

Schwille, P., Haupts, U., Maiti, S., and Webb, W.W. (1999). Molecular dynamics in living cells observed by fluorescence correlation spectroscopy with one- and two-photon excitation. *Biophys. J.* 77: 2251.

Seddon, A.M., Casey, D., Law, R. V., Gee, A., Templer, R.H.,

and Ces, O. (2009). Drug interactions with lipid membranes. *Chem. Soc. Rev.* 38: 2509–2519.

Sepúlveda, C., Palomo, I., and Fuentes, E. (2016). Role of adenosine A2b receptor overexpression in tumor progression. *Life Sci.* 166: 92–99.

Sheth, S., Brito, R., Mukherjea, D., Rybak, L.P., and Ramkumar, V. (2014). Adenosine receptors: expression, function and regulation. *Int. J. Mol. Sci.* 15: 2024–52.

Svedberg, T., and Inouye, K. (1911). Eine neue Methode zur Prüfung der Gültigkeit des Boyle-Gay-Lussacschen Gesetzes für kolloide Lösungen. *Zeitschrift Für Phys. Chemie* 77U: 145–191.

Sykes, D., Jain, P., and Charlton, S. (2019). Investigating the Influence of Tracer Kinetics on Competition-Kinetic Association Binding Assays: Identifying the Optimal Conditions for Assessing the Kinetics of Low-Affinity Compounds. *Mol. Pharmacol.* 96:.

Sykes, D.A., Moore, H., Stott, L., Holliday, N., Javitch, J.A., Lane, J.R., et al. (2017). Extrapiramidal side effects of antipsychotics are linked to their association kinetics at dopamine D2 receptors. *Nat. Commun.* 8: 763.

Sykes, D.A., Parry, C., Reilly, J., Wright, P., Fairhurst, R.A., and Charlton, S.J. (2014). Observed Drug-Receptor Association Rates Are Governed by Membrane Affinity: The Importance of Establishing " Micro-Pharmacokinetic/Pharmacodynamic Relationships " at the b2 -Adrenoceptor s. *Mol. Pharmacol.* Mol Pharmacol 85: 608–

617.

Szlasa, W., Zendran, I., Zalesińska, A., Tarek, M., and Kulbacka, J. (2020). Lipid composition of the cancer cell membrane. *J. Bioenerg. Biomembr.* 2020 525 52: 321–342.

Szlenk, C.T., Gc, J.B., and Natesan, S. (2019). Does the Lipid Bilayer Orchestrate Access and Binding of Ligands to Transmembrane Orthosteric/Allosteric Sites of G Protein-Coupled Receptors? *Mol. Pharmacol.* 96: 527.

Taillardat-Bertschinger, A., Carrupt, P.A., Barbato, F., and Testa, B. (2003). Immobilized artificial membrane HPLC in drug research. *J. Med. Chem.* 46: 655–665.

Taillardat-Bertschinger, A., Martinet, C.A.M., Carrupt, P.A., Reist, M., Caron, G., Fruttero, R., et al. (2002). Molecular factors influencing retention on immobilized artificial membranes (IAM) compared to partitioning in liposomes and n-octanol. *Pharm. Res.* 19: 729–737.

Takács-Novák, K., and Avdeef, A. (1996). Interlaboratory study of log P determination by shake-flask and potentiometric methods. *J. Pharm. Biomed. Anal.* 14: 1405–1413.

Theocharis, A.D., Skandalis, S.S., Gialeli, C., and Karamanos, N.K. (2016). Extracellular matrix structure. *Adv. Drug Deliv. Rev.* 97: 4–27.

Valkó, K. (2004). Application of high-performance liquid chromatography based measurements of lipophilicity to model biological distribution. *J. Chromatogr. A* 1037: 299–

310.

Valko, K., Du, C.M., Bevan, C.D., Reynolds, D., and Abraham, M.H. (2000). Rapid-gradient HPLC Method for Measuring Drug Interactions With Immobilized Artificial Membrane: Comparison With Other Lipophilicity Measures. *J. Pharm. Sci.* 89:.

Vang, A.G., Housley, W., Dong, H., Basole, C., Ben-Sasson, S.Z., Kream, B.E., et al. (2013). Regulatory T-cells and cAMP suppress effector T-cells independently of PKA–CREM/ICER: a potential role for Epac. *Biochem. J.* 456: 463–473.

Vauquelin, G. (2013). Simplified models for heterobivalent ligand binding: when are they applicable and which are the factors that affect their target residence time. *Naunyn. Schmiedebergs. Arch. Pharmacol.* 386: 949–962.

Vauquelin, G. (2015). On the ‘micro’-pharmacodynamic and pharmacokinetic mechanisms that contribute to long-lasting drug action. *Expert Opin. Drug Discov.* 10: 1085–1098.

Vauquelin, G., Bostoen, S., Vanderheyden, P., and Seeman, P. (2012). Clozapine, atypical antipsychotics, and the benefits of fast-off D2 dopamine receptor antagonism. *Naunyn. Schmiedebergs. Arch. Pharmacol.* 385: 337–372.

Vauquelin, G., Bricca, G., and Liefde, I. Van (2014). Avidity and positive allosteric modulation/cooperativity act hand in hand to increase the residence time of bivalent receptor ligands. *Fundam. Clin. Pharmacol.* 28: 530–543.

Vauquelin, G., and Charlton, S.J. (2010). Long-lasting target

binding and rebinding as mechanisms to prolong in vivo drug action. *Br. J. Pharmacol.* *161*: 488–508.

Veber, D.F., Johnson, S.R., Cheng, H.Y., Smith, B.R., Ward, K.W., and Kopple, K.D. (2002). Molecular properties that influence the oral bioavailability of drug candidates. *J. Med. Chem.* *45*: 2615–2623.

Vernall, A.J., Stoddart, L.A., Briddon, S.J., Ng, H.W., Laughton, C.A., Doughty, S.W., et al. (2013). Conversion of a non-selective adenosine receptor antagonist into A3-selective high affinity fluorescent probes using peptide-based linkers. *Org. Biomol. Chem.* *11*: 5673–5682.

Viswanadhan, V.N., Ghose, A.K., Revankar, G.R., and Robins, R.K. (1989). Atomic Physicochemical Parameters for Three Dimensional Structure Directed Quantitative Structure-Activity Relationships. 4. Additional Parameters for Hydrophobic and Dispersive Interactions and Their Application for an Automated Superposition of Certain Naturally Occurring Nucleoside Antibiotics. *J. Chem. Inf. Comput. Sci.* *29*: 163–172.

Weinhold, F., and Klein, R.A. (2014). What is a hydrogen bond? Resonance covalency in the supramolecular domain. *Chem. Educ. Res. Pract.* *15*: 276–285.

Wenger, J., Boned, A., Gérard, D., Conchonaud, F., Rigneault, H., Dintinger, J., et al. (2006). Dual-color fluorescence cross-correlation spectroscopy in a single nanoaperture: towards rapid multicomponent screening at high concentrations. *Opt. Express*, Vol. 14, Issue 25, Pp.

12206-12216 14: 12206–12216.

Wilson, J.M., Kurtz, C.C., Black, S.G., Ross, W.G., Alam, M.S., Linden, J., et al. (2011). The A2B Adenosine Receptor Promotes Th17 Differentiation via Stimulation of Dendritic Cell IL-6. *J. Immunol.* 186: 6746–6752.

Xia, L., Kyrizaki, A., Tosh, D.K., Duijl, T.T. van, Roorda, J.C., Jacobson, K.A., et al. (2018). A binding kinetics study of human adenosine A₃ receptor agonists. *Biochem. Pharmacol.* 153: 248–259.

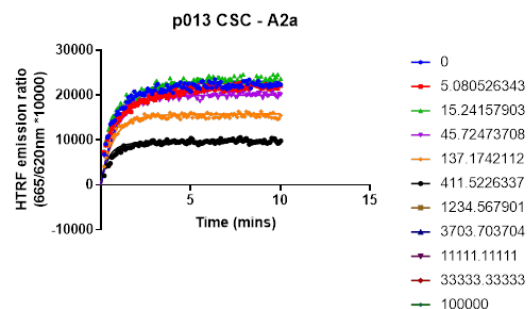
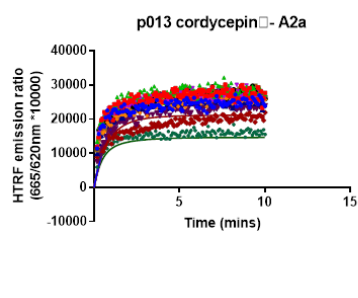
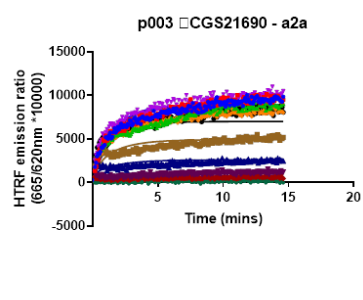
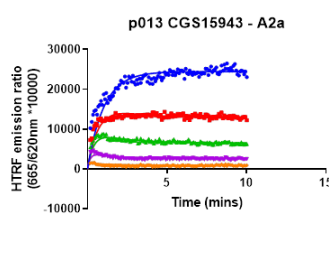
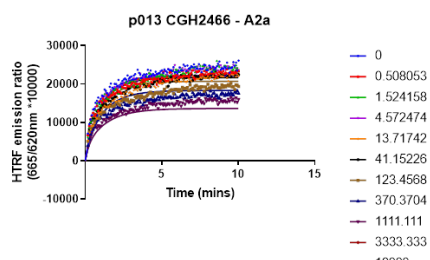
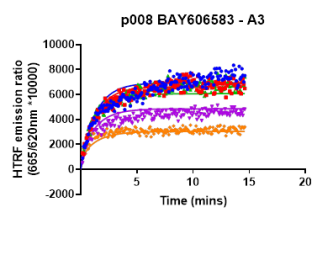
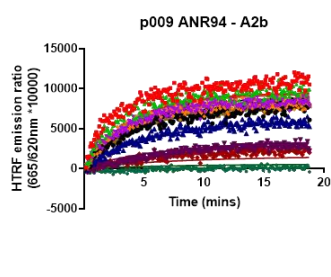
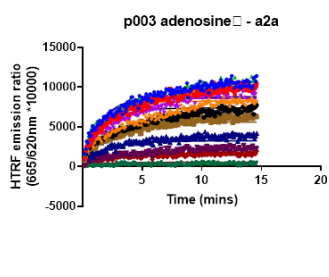
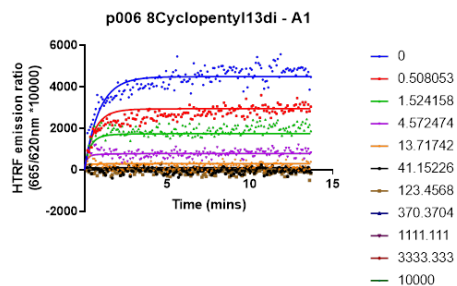
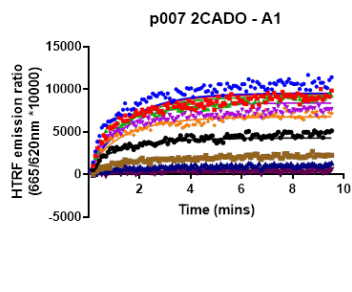
Zarek, P.E., Huang, C.-T., Lutz, E.R., Kowalski, J., Horton, M.R., Linden, J., et al. (2008). A2A receptor signaling promotes peripheral tolerance by inducing T-cell anergy and the generation of adaptive regulatory T cells. *Blood* 111: 251–259.

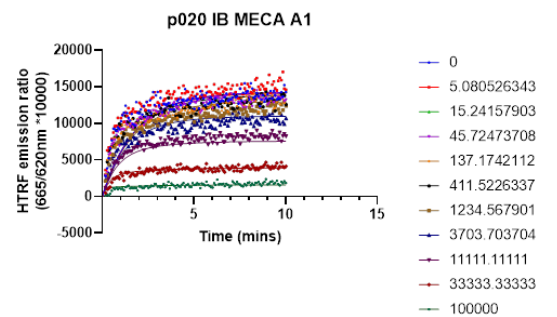
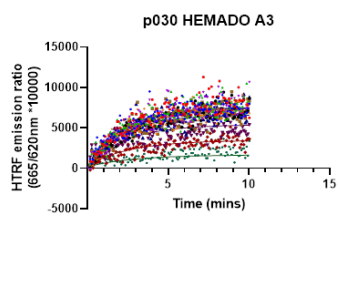
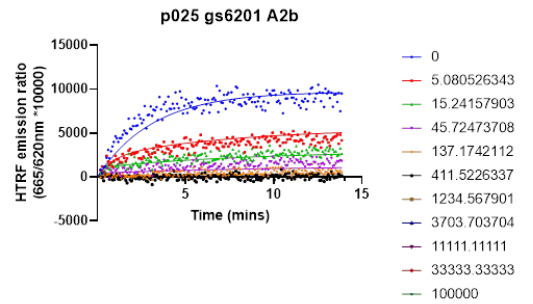
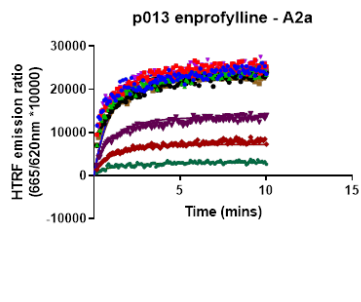
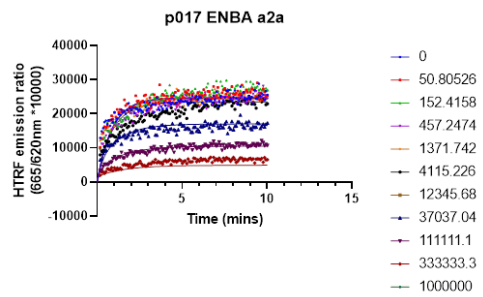
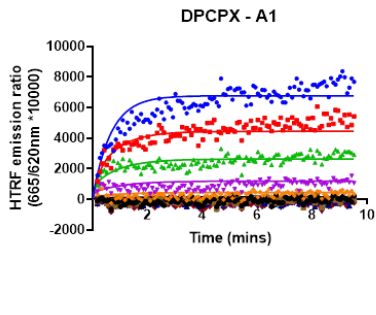
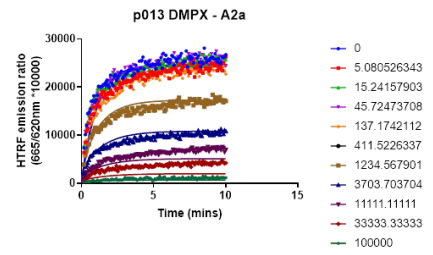
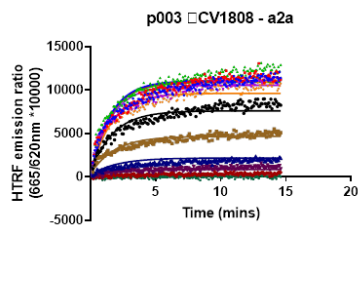
Zemanova, L., Schenk, A., Hunt, N., Nienhaus, U., and Heilker, R. (2004). Endothelin receptor in virus-like particles: ligand binding observed by fluorescence fluctuation spectroscopy. *Biochemistry* 20: 9021–8.

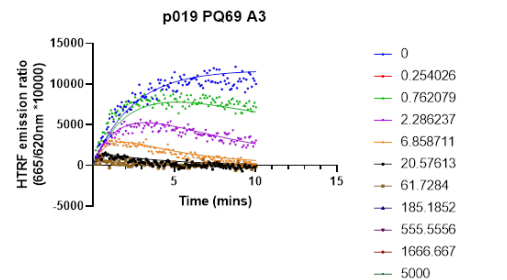
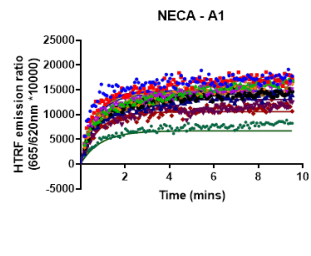
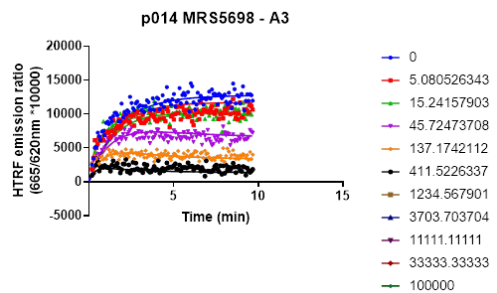
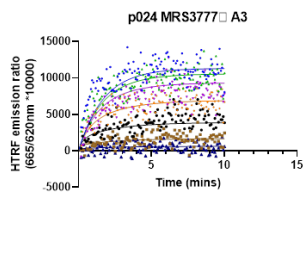
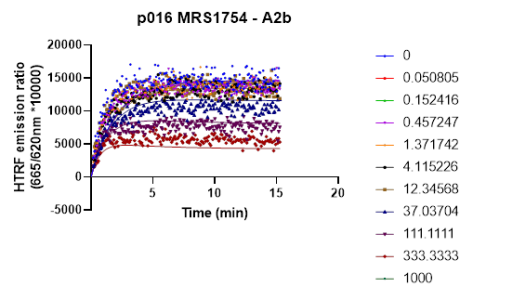
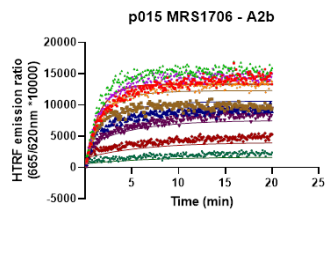
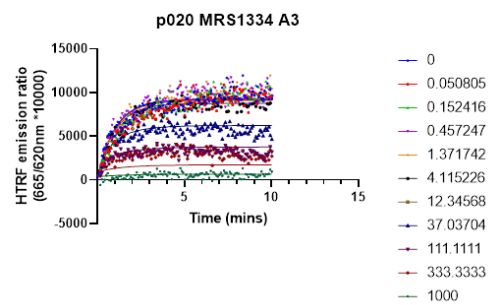
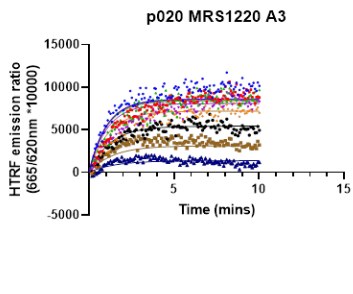
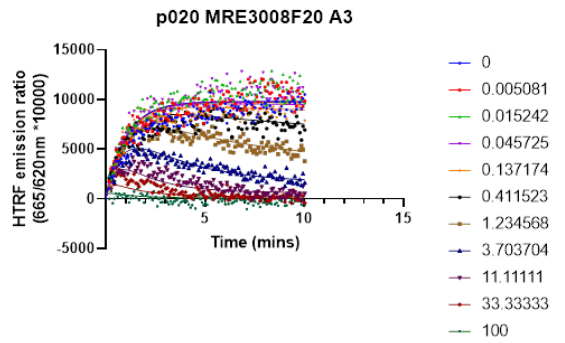
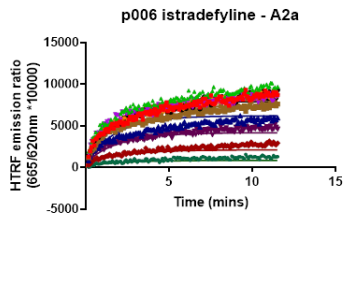
Zhang, R., and Monsma, F. (2009). The importance of drug-target residence time. *Curr. Opin. Drug Discov. Devel.* 12: 488–96.

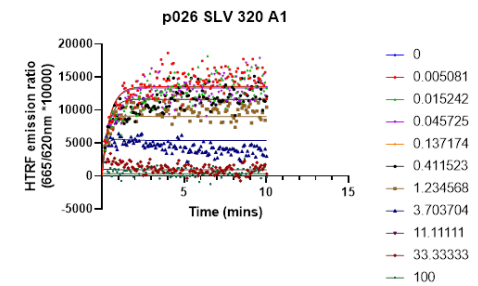
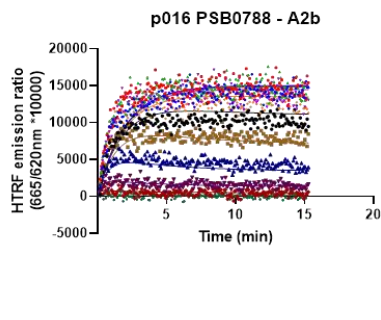
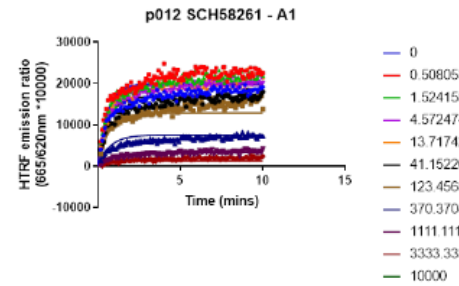
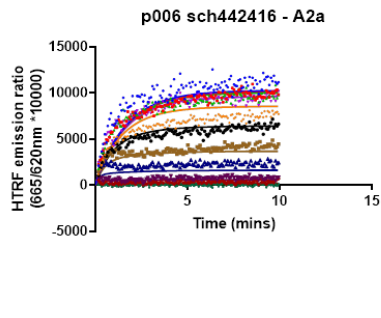
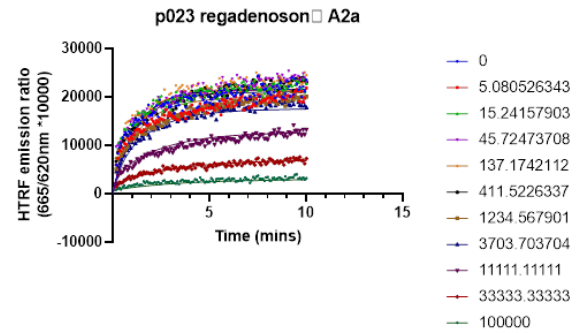
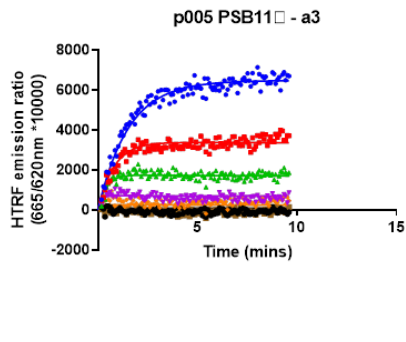
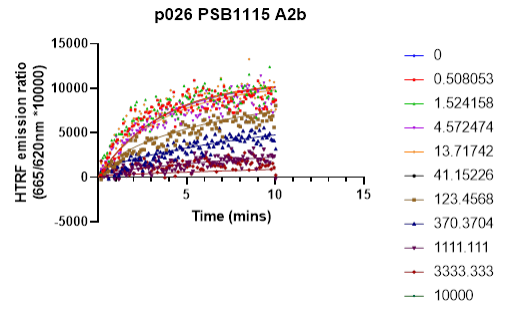
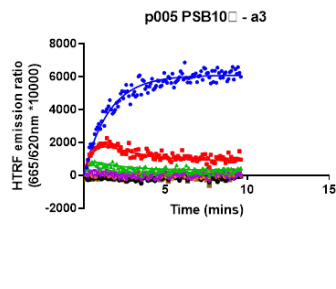
Zhou, Y., Chu, X., Deng, F., Tong, L., Tong, G., Yi, Y., et al. (2017). The adenosine A_{2b} receptor promotes tumor progression of bladder urothelial carcinoma by enhancing MAPK signaling pathway. *Oncotarget* 8: 48755–48768.

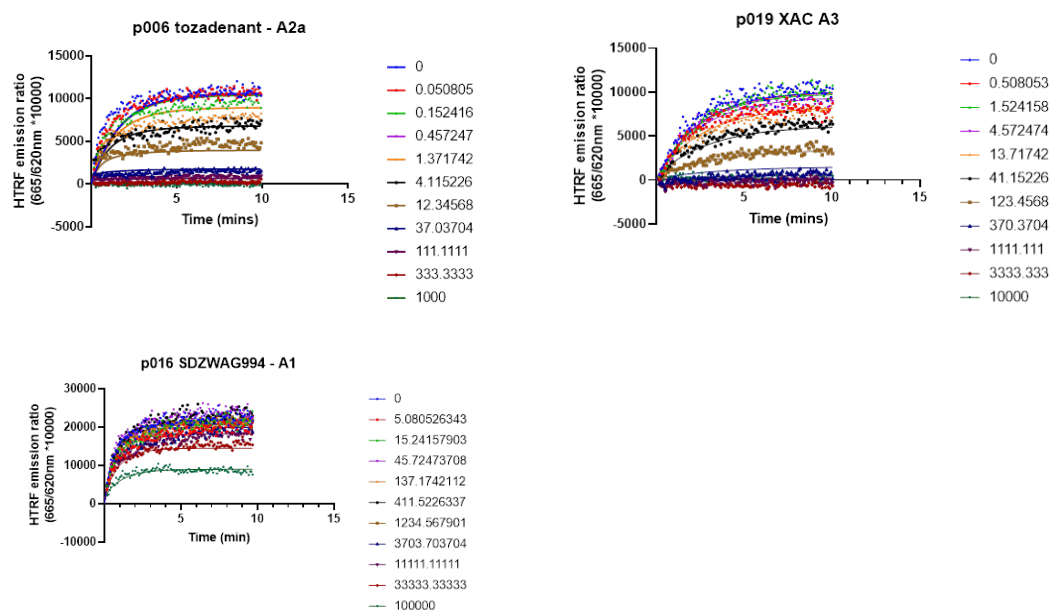
Chapter 8 – appendix



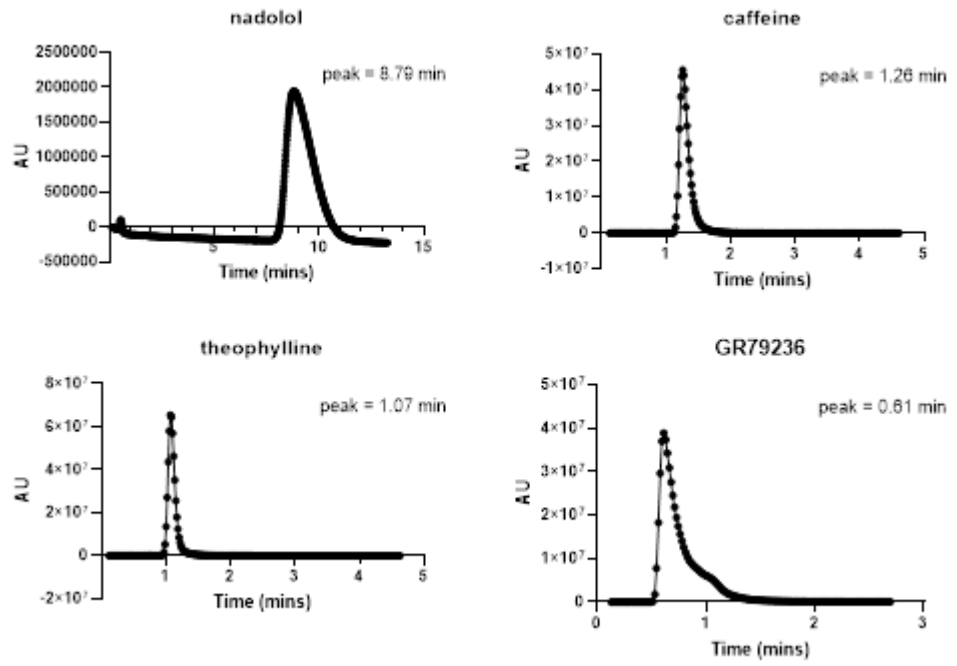




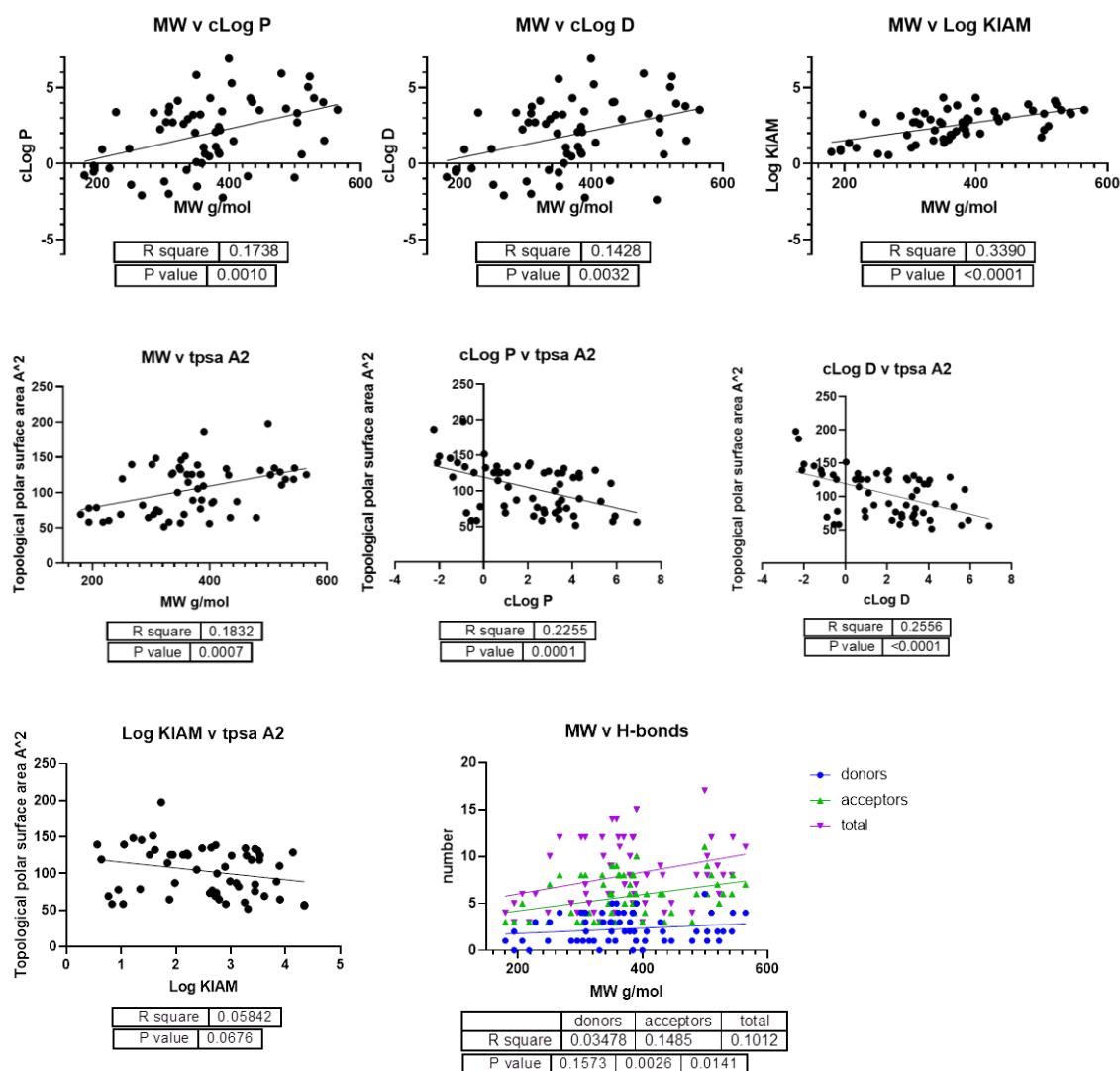




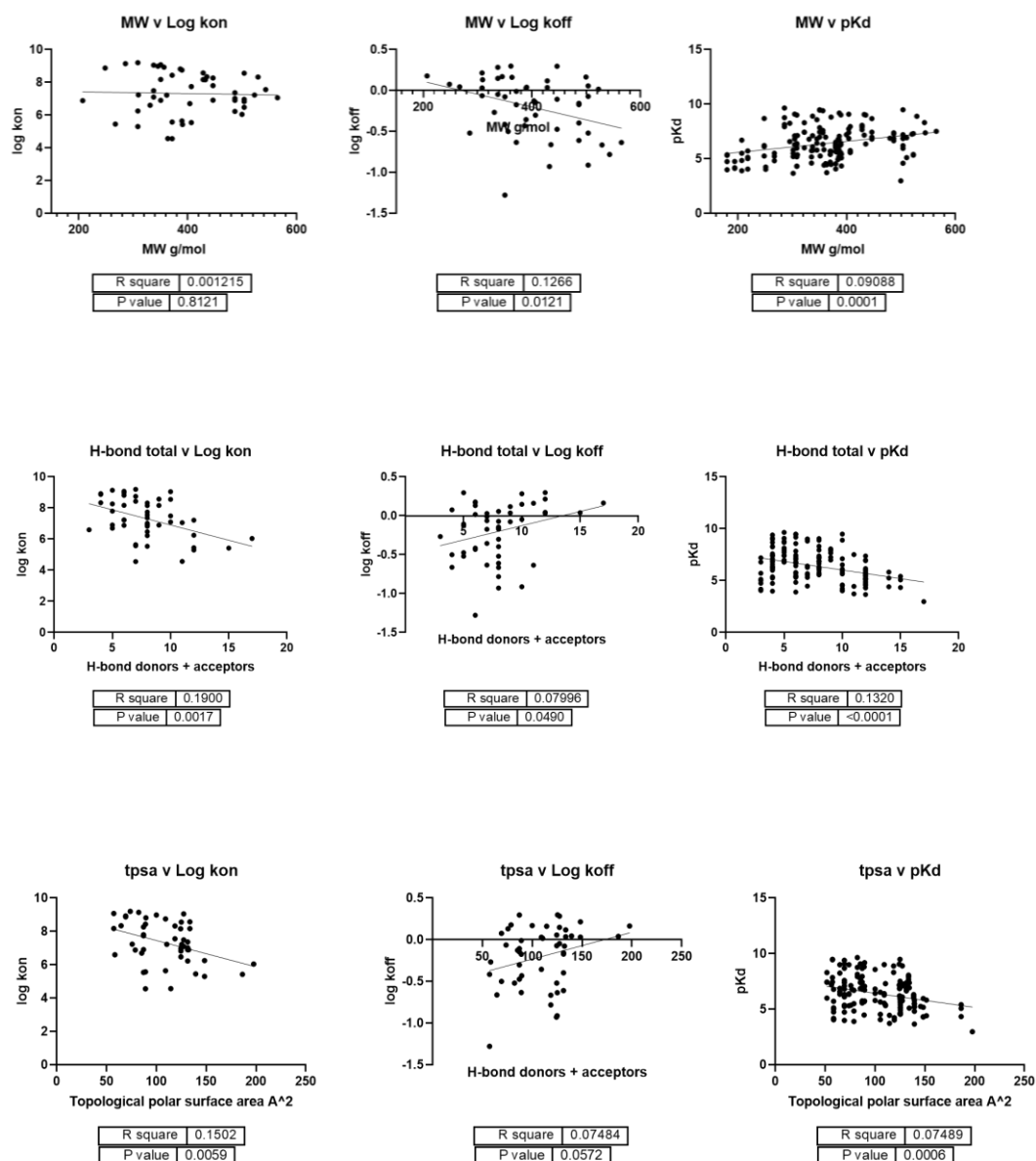
Appendix Figure 1. Examples of competition kinetic binding experiments from a single test plate (006). A fixed concentration of CA200645 (with the kinetics of the tracer measured at the start of each day) was added to wells along with 10 concentrations of unlabelled ligand (final assay concentration shown in nM on the right of each graph) prior to membrane addition. Membrane expressing one adenosine receptor (displayed at the top of each graph) was injected at time 0 to start the reaction. Data were fitted to the “nonlinear regression - kinetics of competitive binding” equation in GraphPad Prism v8.2.1 derived from Motulsky-Mahan equations (see methods) with the k_{on} , k_{off} and concentration of fluorescent ligand constrained. Each graph is a representative trace of an individual experiment.



Appendix Figure 2. Example traces from IAM-HPLC set up.



Appendix Figure 3. Correlations of physicochemical properties for 57 unlabelled adenosine compounds. cLog D, cLog P, molecular weight (MW), number of hydrogen bond donor and acceptors, and Topological Polar Surface Area (TPSA) were generated using Chemicalize software. Log KIAM values were obtained experimentally in Chapter 4. Pearson's correlation analysis applied using GraphPad Prism as per methods Chapter.



Appendix Figure 4. Correlations of physicochemical properties for 57 unlabelled adenosine compounds and receptor-ligand kinetics. cLog D, cLog P, molecular weight (MW), number of hydrogen bond donor and acceptors, and Topological Polar Surface Area (TPSA) were generated using Chemicalize software. Log k_{on} , k_{off} and pK_d values were obtained experimentally in Chapter 3. Pearson's correlation analysis applied using GraphPad Prism as per methods Chapter.

